

**Theoretical Investigation of the Vibrational Spectroscopic
Signatures of Ion-water Clusters and Peptide-water Clusters**

Xijun Wang

A Thesis
In the Department Of
Chemistry and Biochemistry

Presented in Partial Fulfilment of the Requirements
For the Degree of
Doctor of Philosophy (Chemistry) at
Concordia University
Montreal, Quebec, Canada

January 2016

© Xijun Wang, 2016

Abstract

Theoretical Investigation of the Vibrational Spectroscopic Signatures of Ion-water Clusters and Peptide-water Clusters

Xijun Wang, Ph.D.

Concordia University, 2016

The aim of this work is to develop theoretical approaches to compute vibrational spectra beyond the harmonic approximation and to investigate the performance of the self-consistent-charge density-functional tight-binding model (SCC-DFTB) in studying the vibrational spectra of large systems. For this purpose, vibrational spectra of ion-water clusters and peptide-water clusters are computed from molecular dynamics (MD) simulations using the Fourier transform of the autocorrelation function of the dipole moment (FTACF). The performance of the SCC-DFTB model is evaluated by comparing computed spectra with available experimental results and ab initio or first-principles results. There are four distinct aspects to this work: **(1)** To demonstrate how the FTACF approach overcomes the limitations of the harmonic approximation, vibrational spectra of the “Zundel ion”, the protonated water dimer, are computed from ab initio MD simulations based on second-order Møller–Plesset (MP2) Perturbation Theory. The splitting of the band of the proton transfer mode is well reproduced, and its coupling with other modes is characterized by examining the correlation spectra of a combination of selected internal coordinates. Computed spectra at different temperatures further confirm the ability of the approach to unveil temperature-dependent features of vibrational modes coupling. **(2)** To confirm the spectral signature of “free water” at the surface of aqueous droplets seeded by sulfate ions proposed by experimentalists, theoretical vibrational spectra of sulfate-water clusters are generated using

the SCC-DFTB model. Computed spectra not only reproduce the spectral signature of free surface water molecules, hence confirming the hypothesis, but also reveal the distance within which the sulfate ion may affect the structure and dynamics of water molecules in the gas phase, within the accuracy of the approximate model employed and the possible limitations of conformational sampling. **(3)** To investigate the hydration effect on the CN stretch band of the guanidinium ion, vibrational spectra of guanidinium-water clusters are obtained with the SCC-DFTB model. Computed spectra reveal a redshift in the band position, in agreement with ab initio calculations of harmonic frequencies. The SCC-DFTB spectra are also in good agreement with those obtained from Car-Parrinello molecular dynamics (CPMD) simulations employing more rigorous density-functional theory (DFT). **(4)** To validate the suitability of the approach to describe the interactions and dynamics of peptide-water binary systems, vibrational spectra of several model clusters containing prototype peptides are generated from MD simulations at different temperatures, with the ultimate goal of gaining insight into solvation effects on the spectra of hydrated proteins. Computed spectra are in excellent agreement with available experimental results and reported theoretical results. Altogether, these findings not only shed light onto understanding the properties of ion-water and peptide-water clusters, but also validate an efficient approach to compute vibrational spectra of large systems with satisfactory performance and accuracy.

Acknowledgements

I would like to sincerely thank my supervisor, Dr. Gilles Peslherbe, for his guidance and support throughout this study, and especially for his confidence in me. I would also like to thank Drs. Ann English and Guillaume Lamoureux, the members of my research committee, for their insightful comments and advices. I wish to acknowledge the financial supports I received from Concordia University and Natural Sciences and Engineering Research Council of Canada as well as access to the computational resources from CalculQuebec.

Special thanks go to the Graduate Program Director, Dr. Heidi Muchall, and Graduate Program Assistant, Mrs. Maria Ciaramella, and Mrs. Miriam Posner, who have been helping me to go through many difficulties.

I also wish to thank my colleagues at the Centre for Research in Molecular Modeling, Soran Jahangiri, Mariya Shadrina, Esam Orabi, Bharat Sharma, Vinod Parmar, Chun Chi Mak, Bilkiss Issack and all the other members, for all the fun we have had in the past years.

I would like to dedicate this thesis to my parents and my dear wife, Congying Dai, for their endless love and encouragement.

Contribution of Authors

The work presented here has been performed and written by Xijun Wang and supervised and edited by Dr. Gilles Peslherbe.

Table of Contents

List of Figures	x
List of Tables	xii
List of Abbreviations and Acronyms	xiii
Chapter 1. Introduction	1
1.1. Preamble	2
1.2. Computational vibrational spectroscopy.....	4
1.3. Vibrational spectra of ion-water clusters and peptide-water clusters	7
1.4. SCC-DFTB models - theory and performance	8
1.5. Objective and outlines.....	10
Chapter 2. Coupling of Proton Transfer Mode and Temperature Effects in Vibrational Spectra of the Protonated Water Dimer Revisited with <i>ab initio</i> Molecular Dynamics Simulations	12
2.1. Introduction.....	13
2.2. Computational details	14
2.2.1. <i>ab initio</i> MD simulations	14
2.2.2. Computation of vibrational spectra.....	15
2.2.3. Time correlation spectra for specific modes	16
2.3. Results and discussions.....	20
2.3.1. Computed vibrational spectra: band assignment and anharmonic effects	20
2.3.2. Computed vibrational spectra of H_5O_2^+ : comparison with experimental results	22
2.3.3. Time correlation spectra: coupling of the proton transfer mode.....	26
2.4. Summary and conclusions	30
Chapter 3. Simulations of the Vibrational Spectra of Sulfate-Water Clusters: The OH stretch as a Signature of Water Binding.....	33
3.1. Introduction.....	34
3.2. Computational details	36
3.2.1. SCC-DFTB models.....	36

3.2.2. MD Simulations	38
3.2.3. Vibrational spectra	39
3.3. Results and discussions	41
3.3.1. Validation of DFTB Models	41
3.3.2. Structure and vibrational spectra of medium-size sulfate-water clusters.....	46
3.4. Summary and conclusions	51
Supporting information	53

Chapter 4. Vibrational Spectroscopy of Guanidinium-Water Clusters from First-Principles Molecular Dynamics Simulations **58**

4.1. Introduction.....	59
4.2. Computational details	61
4.3. Results and discussions.....	66
4.3.1. Molecular Geometry and harmonic frequencies.....	66
4.3.2. Simulated vibrational spectra.....	70
4.4. Summary and conclusions	79

Chapter 5. Simulation of the Vibrational Spectra of Biologically-Relevant Systems: The Amide Bands of Model Peptides **81**

5.1. Introduction.....	82
5.2. Computational details	85
5.2.1. Model systems	85
5.2.2. Quantum-chemistry calculation	87
5.2.3. SCC-DFTB model	87
5.2.5. MD simulations.....	88
5.2.6. Vibrational spectra	89
5.3. Results and discussions.....	90
5.3.1. Hydrogen bonding structures and interaction energies.....	90
5.3.2. Harmonic vibrational frequencies.....	91
5.3.3. Simulated Vibrational spectra: Averaging and band assignment	94
5.3.4. Vibrational spectra of NMA	96
5.3.5. Vibrational spectra of hydrated NMA complexes	98
5.3.6. Vibrational spectra of NMA dimer	102

5.3.7. Vibrational spectra of NMA-Na ⁺ complexes and (NMA) ₂ -Na ⁺	103
5.4. Summary and conclusions	105
Chapter 6. Conclusions and outlook	108
Bibliography	113

List of Figures

- Figure 2.1.** Combination of the internal coordinates used to compute time correlation spectra . 18
- Figure 2.2.** Calculated vibrational and correlation spectra for the Zundel ion H_5O_2^+ . **Top:** Simulated vibrational spectra at 10 K with MP2/aug-cc-pVDZ. **Middle 2:** time correlation spectra of terminal water stretch and bend modes. **Bottom:** harmonic spectra from normal mode analysis with MP2/aug-cc-pVDZ. 19
- Figure 2.3.** Experimental and simulated infrared spectra for the Zundel ion H_5O_2^+ . **(Left)** MP2/aug-cc-pVDZ results; **(Right)** B3LYP/aug-cc-pVDZ results. The top two panels display experimental infrared spectra from IRMPD and IRPD, respectively; the bottom three display simulated vibrational spectra from MD simulations at different temperatures. 23
- Figure 2.4.** Simulated MP2/aug-cc-pVDZ vibrational spectra of the Zundel ion H_5O_2^+ and time correlation spectra for the proton transfer mode at (a) 10K (b) 40K and (c) 80K. 27
- Figure 2.5.** Simulated B3LYP/aug-cc-pVDZ vibrational spectra of the Zundel ion H_5O_2^+ and time correlation spectra for the proton transfer mode at (a) 10K (b) 40K and (c) 80K. 28
- Figure 3.1.** Selected sulfate-water clusters $\text{SO}_4^{2-}(\text{H}_2\text{O})_n$ investigated in this work. 41
- Figure 3.2.** Vibrational spectra of sulfate water clusters, $\text{SO}_4^{2-}(\text{H}_2\text{O})_n$, $n=3, 4, 5, 6$. **(Left)** Experimental IRMPD results taken from ref. ²⁷ The temperature of the ion trap is reported to be 17K. **(Right)** Theoretical results obtained from MD simulations with DFTB3/OB at 20K. 44
- Figure 3.3.** Selected structural properties of for $\text{SO}_4^{2-}(\text{H}_2\text{O})_n$ clusters. **(Left)** Radial distribution function of the sulfate S atom distance from the O atoms of the water molecules. **(Right)** Radial distribution function of O-O distances in water molecules. 47
- Figure 3.4.** Radial distribution function of O-O atoms of pure water clusters and sulfate-water clusters at 120K. 48
- Figure 3.5.** Simulated spectra of sulfate-water clusters of varying size from MD simulations with DFTB3/OB. a) Vibrational spectra at $T=120, 150$ and 250K . b) Correlation spectra of an individual water molecule at the cluster surface at $T=120\text{K}$ 50
- Figure 4.1.** Molecular geometries of guanidinium (gmd^+), the guanidinium-chloride complex (gdm^+-Cl^-), and selected guanidinium-water clusters, $\text{gdm}^+(\text{H}_2\text{O})_n$ water clusters investigated in this study. Obtained from B3LYP/aug-cc-pVTZ calculation. 65
- Figure 4.2.** Vibrational features of deuterated guanidinium predicted by planewave BLYP **(Left)** and DFBT3/OB **(Right)** MD simulations at $\sim 50\text{K}$. The top panel shows the simulated vibrational spectra and the remaining ones time-correlation spectra corresponding to selected normal modes of vibration. 71

Figure 4.3. Vibrational spectra of guanidinium and its complexes with chloride (Left) and water (Right) predicted by planewave DFT (B3LYP, BLYP) and DFTB3/OB MD simulations at ~50K. DFTB spectra are averaged over 10 trajectories, while DFT spectra are based on a single trajectory. Band assignment is provided for the CN and NH(D) stretches.....	72
Figure 4.4. Simulated vibrational spectra of $\text{gdmH}^+(\text{H}_2\text{O})_n$, $n=1\sim 6$. The spectra are computed from constant-energy MD simulations at 50K with the DFTB3/OB model and are averaged over 10 trajectories.....	75
Figure 4.5. Computed vibrational spectra and radial distribution function of aqueous guanidinium droplet with DFTB. The spectra are computed from constant-energy MD simulations at 50K and are averaged over 10 trajectories.	78
Figure 5.1. Model clusters (with their abbreviation in square bracket) investigated in this work..	86
Figure 5.2. Simulated single-trajectory and averaged vibrational spectra from molecular dynamics simulations at 50K for <i>trans</i> -NMA (top) and <i>cis</i> -NMA (bottom), respectively. To highlight averaged spectral lines, their intensities are enlarged 5 times, and the lines of averaged spectra are thickened.	94
Figure 5.3. Simulated vibrational spectra of <i>trans</i> -NMA. The top panel shows the actual vibrational spectra. Remaining panels display time-correlation spectra of the localized modes in terms of specific internal coordinates or linear combination of coupled internal coordinates.	95
Figure 5.4. Vibrational spectra of NMA in the range 500-4000 cm^{-1} . Obtained from MD simulations with DFTB3 at 50K. The experimental FTIR results are taken from ref 128.	97
Figure 5.5. Vibrational spectra of NMA in the range 1000-1800 cm^{-1} . Top panel: experimental FTIR gas-phase spectrum; Lower panels: simulated spectra from molecular dynamics simulation with DFTB3 at various temperature for <i>trans</i> -NMA and <i>cis</i> -NMA.....	98
Figure 5.6. Simulated vibrational spectra of <i>trans</i> -NMA and <i>trans</i> -NMA-water complexes in the range 1200-1800 cm^{-1} (Left) and 3200-4000 cm^{-1} (Right), respectively. Obtained from molecular dynamics simulation with DFTB3 at 50K. In the NMA(CO)-H ₂ O complexes the water molecule is hydrogen bonded to the CO group of NMA.....	100
Figure 5.7. Simulated vibrational spectra of <i>trans</i> -NMA monomer and <i>trans</i> -NMA dimer in the range 1000-1800 cm^{-1} (Left) and 2600-3400 cm^{-1} (Right), respectively. Obtained from MD simulations with DFTB3 at different temperature.	101
Figure 5.8. Simulated vibrational spectra of <i>trans</i> -NMA, <i>trans</i> -NMA- Na^+ complex and <i>trans</i> -(NMA) ₂ - Na^+ complex in the range 1200-1800 cm^{-1} (Left) and 2700-3500 cm^{-1} (Right), respectively. Obtained from MD simulations at 50K with DFTB3 at 50K.	104
Figure 5.9. Vibrational spectra of (NMA) ₂ - Na^+ complex in the range 1200-1800 cm^{-1} . Top: experimental IRMPD spectra. ¹¹⁹ Bottom: Simulated spectra from MD simulations with DFTB3 at 50K and 300K. NMA molecules are in the <i>trans</i> form.....	105

List of Tables

Table 2.1 Vibrational frequencies and relative intensities (in parentheses) for Zundel H_5O_2^+	21
Table 3.1 Selected geometrical parameter of $\text{SO}_4^{2-}(\text{H}_2\text{O})_n$ calculated by various methods: Intermolecular sulfate-water distance $r_{\text{S-O}}$	42
Table 3.2. Selected $\text{SO}_4^{2-}(\text{H}_2\text{O})_n$ Cluster Binding Energies	43
Table 3.3. Vibrational frequencies of the OH stretch in $\text{SO}_4^{2-}(\text{H}_2\text{O})_n$, $n=1\sim 3$	53
Table 3.4. Vibrational frequencies of the H_2O bend in $\text{SO}_4^{2-}(\text{H}_2\text{O})_n$, $n=1\sim 6$	54
Table 3.5. Vibrational frequencies of the H_2O libration in $\text{SO}_4^{2-}(\text{H}_2\text{O})_n$, $n=1\sim 6$	55
Table 3.6. Vibrational frequencies of the SO_4 stretch in $\text{SO}_4^{2-}(\text{H}_2\text{O})_n$, $n=1\sim 6$	56
Table 3.7. Vibrational frequencies of the SO_4 bend in $\text{SO}_4^{2-}(\text{H}_2\text{O})_n$, $n=1\sim 6$	57
Table 4.1. Selected molecular geometry and harmonic frequencies of guanidinium calculated by various quantum-chemistry methods.	66
Table 4.2. Selected molecular geometry and harmonic frequencies of guanidinium calculated by various quantum-chemistry methods ^a	67
Table 4.3. Selected molecular geometry parameters and harmonic vibrational frequencies of (deuterated) guanidinium calculated by different implementations of DFT	68
Table 4.4. Selected molecular geometry parameters and harmonic vibrational frequencies guanidinium calculated by DFT and SCC-DFTB models.	69
Table 5.1. Selected geometric parameters for <i>trans</i> -N-methylacetamide (NMA) and its complexes. C, N, H atoms in the table are all from amide group.	90
Table 5.2. Binding energies of <i>trans</i> -N-methylacetamide (NMA) complexes.	91
Table 5.3. Vibrational frequencies of <i>trans</i> -NMA and <i>cis</i> -NMA.	92
Table 5.4. Vibrational frequencies of hydrated <i>trans</i> -NMA and <i>trans</i> -NMA- Na^+ complexes....	93

List of Abbreviations and Acronyms

BLYP	Beck's exchange plus Lee-Yang-Parr's correlation functional
B3LYP	Beck's three parameters nonlocal-exchange functional with the correlation functional of Lee-Yang-Parr
CPMD	Car-Parrinello molecular dynamics
NVE	constant-number-of-particles, constant-volume, constant-energy
NVT	constant-number-of-particles, constant-volume, constant-temperature
DFT	density functional theory
DFTB	density-functional tight-binding theory
FTACF	fourier transform of the autocorrelation function
gdmH ⁺	guanidinium cation with isotope of ¹ H
gdmD ⁺	guanidinium cation with isotope of ² H
IRMPD	infrared multiphoton dissociation
IRPD	infrared predissociation
MD	molecular dynamics
NMA	N-methylacetamide
NMA	normal mode analysis
PBE	Perdew, Burke, and Ernzerhof exchange-correlation functional
PCM	polarizable continuum model
RDF	radial distribution function
Ryd	Rydberg
MP2	second-order Møller-Plesset
DFTB2	second-order self-consistent-charge density-functional tight-binding theory
DFTB3	third-order self-consistent-charge density-functional tight-binding theory
VCI	vibrational configuration interaction
VDOS	vibrational density of states
VPT2	vibrational second-order perturbation theory
VSCF	vibrational self-consistent field

Chapter 1.

Introduction

1.1. Preamble

Computational vibrational spectroscopy is essential to aid the assignment and explanation of experimental spectroscopy.^{1, 2} Normal mode analysis under the harmonic approximation performed on a single molecule or small clusters is widely used to obtain vibrational modes, harmonic frequencies and relative intensities, which can be useful to determine the number of overlapping bands, the position of each individual band, and the vibrational mode relative contributions to the spectral bands. The normal modes can be easily visualized and characterized in internal coordinates. However, normal mode analysis is only effective when anharmonic effects and mode coupling are not very significant. Anharmonic effects could change the contribution of each internal degree of freedom, shift the band positions or relative order, and affect the relative intensities, thus introducing a possible source of error in the band assignment of experimental spectra.²

In this work, we investigate another approach of computing vibrational spectra, from the time correlation function of the dipole moment based on molecular dynamics (MD) simulations. This approach overcomes the limitations of the harmonic approximation and allows all modes to be coupled during the natural motion of the atoms. The broadened spectra are directly comparable to experimental ones, except that no combination or overtone are included since the MD simulations are performed on the vibrational and electronic ground states.^{3, 4} This approach has been proposed many decades ago,^{5, 6} but only became feasible in a realistic fashion with the development of quantum chemistry and increasing computational resources in recent decades. For instance, the approach has been used to generate vibrational spectra of pure bulk water,³ organic molecules in the gas phase and in aqueous solution,^{7, 8} and protonated peptides in the gas phase.^{1, 9, 10} However, the accuracy and efficiency of the simulations, the convergence of the band positions and shapes

with respect to sampling, and the band assignment of computed spectra still need to be validated and improved.^{8, 11}

In recent years, the development of Infrared multiphoton dissociation (IRMPD)^{12, 13} and infrared predissociation (IRPD)^{14, 15} techniques made it possible to compare computed and experimental vibrational spectra of small hydrated ion clusters and aqueous peptide clusters to validate the accuracy of the computed vibrational spectra. In this work, we take the protonated water dimer, sulfate water clusters, guanidinium water clusters, and small peptide complexes as models, and investigate the convergence of the simulated spectra, the band assignment and the efficiency of the computations. To obtain converged spectra, simulated spectra are averaged over at least 10 trajectories starting from a different initial distribution of atomic velocities.¹⁶ To resolve the nature of the vibrational bands of the computed spectra in terms of internal coordinates, the time correlation function of the dipole moment corresponding to selected internal coordinates motion is computed. To establish an efficient computational method, the recently developed first-principles-based but approximate self-consistent-charge density-functional-tight-binding model (SCC-DFTB) is selected and validated against high-level quantum chemistry calculations of molecular geometries, energetics and harmonic frequencies, and available experimental vibrational spectra data.

The goals of this work are not only to shed light on the observed features of IRMPD spectra of hydrated ions and model peptides, but also to advance our knowledge about the relative accuracy and efficiency of computational vibrational spectroscopy.

1.2. Computational vibrational spectroscopy

The computational approach to vibrational spectroscopy is derived from the Fermi Golden rule which takes the following form:^{3, 17}

$$I(\omega) = 3 \sum_i \sum_f \rho_i |\langle f | \hat{\mathbf{E}} \cdot \hat{\mathbf{M}} | i \rangle|^2 \delta(\omega_{fi} - \omega) \quad (1.1)$$

where $I(\omega)$ is the line shape function, $\hat{\mathbf{E}}$ is the external field vector, $\hat{\mathbf{M}}$ is the dipole moment vector of the whole molecular system, $|i\rangle$ and $|f\rangle$ are the initial and final vibrational states of the system, respectively, ρ_i is the density of the molecular system in the initial states, ω is the wave number, and ω_{fi} is the wave number associated with the transition between the initial and final vibrational states. Under the double harmonic approximation, i.e. the mechanical approximation and the electrical approximation, the above formula reduces to the normal modes analysis of the molecular system in its equilibrium geometry.¹¹

Within the linear response theory, which assumes that the coupling of the system and external field is weak, the line shape function can be rewritten as the Fourier transform of the autocorrelation function of the dipole moment of the whole system:¹¹

$$I(\omega) = \frac{4\pi^2\omega}{3\hbar c V n(\omega)} (1 - \exp[-\beta\hbar\omega]) \int_{-\infty}^{\infty} dt \langle \hat{\mathbf{M}}(t) \cdot \hat{\mathbf{M}}(0) \rangle e^{-i\omega t} \quad (1.2)$$

where $\beta = 1/kT$, c is the speed of light in vacuum, V is the volume (taken as 1 for a cluster system). \hbar is Planck reduced constant, $n(\omega)$ is the index of refraction, which is approximated as 1 in practice,. The angular brackets indicate a statistical average of the correlation of the dipole moment $\hat{\mathbf{M}}$ of the molecular system. The above formula (1.2) is directly derived for a quantum mechanical system, but in practice, classical MD simulations are performed to obtain the time-

series trajectory of the dipole moment. To reduce the formula to its classical limit, i.e. replacing the quantum operator $\hat{\mathbf{M}}$ with the classical vector \mathbf{M} , a quantum correction factor $Q(\omega)$ is introduced into the line shape function to correct for the different symmetry between the classical and quantum line shapes:

$$I^{cl}(\omega) = \frac{4\pi^2\omega}{3\hbar cVn(\omega)} (1 - \exp[-\beta\hbar\omega])Q(\omega) \int_{-\infty}^{\infty} dt \langle \mathbf{M}(t) \cdot \mathbf{M}(0) \rangle e^{-i\omega t} \quad (1.3)$$

where $I^{cl}(\omega)$ is the classical line shape function. In fact, $I^{cl}(\omega)$ is an even function of ω , i.e. $I^{cl}(-\omega) = I^{cl}(\omega)$, while its quantum counterpart satisfies the detailed balance condition in the frequency (or wave number) domain: $I(-\omega) = \exp[-\beta\hbar\omega]I(\omega)$. As shown in Ref. ¹¹, the Kubo correction factor, also referred to as the harmonic correction factor, has been widely used and proved to systematically improve the consistency between computed and experimental results. The Kubo correction factor takes the following form:¹⁸

$$Q(\omega) = \frac{\beta\hbar\omega}{1 - \exp[-\beta\hbar\omega]} \quad (1.4)$$

By applying the Kubo correction factor to equation (1.3), the classical line shape function reduces to:

$$I^{cl}(\omega) = \frac{2\pi\beta\omega^2}{3cVn(\omega)} \int_{-\infty}^{\infty} dt \langle M(t) \cdot M(0) \rangle e^{-i\omega t} \quad (1.5)$$

Equation (1.5) is used in this work to compute the line shape function based on the dipole moment obtained from MD simulations.

The two computational approaches mentioned above, i.e. normal mode analysis and time correlation analysis, have been used to compute vibrational spectra. In the former, the molecular system is taken as connected harmonic oscillators, and normal modes are the vibrational modes in

which all the atoms move at a given frequency. Harmonic frequencies are calculated from the second derivatives of the potential energy surface along each individual mode. The absorption intensity is proportional to the square of the induced dipole moment of the vibrational distortion of the molecular system. Such analysis requires the geometry of the molecular system optimized in the ground state, i.e. the global minimum or a local minimum on the potential energy surface, and thus it is a “static analysis” of the system. In the latter approach, all atoms are allowed to move subject to interatomic forces at finite temperature for a time sufficiently long to generate a trajectory of the dipole moment of the whole system, on which a time correlation analysis is performed to obtain the naturally broadened bands corresponding to all active vibrational modes. The relative intensity of the bands is proportional to the magnitude of the fluctuation of the dipole moment of the whole system. Thus, spectra are obtained through a dynamical simulation of the molecular system under thermal conditions, and this can be taken as a “dynamics analysis”.

The static analysis is good only for small molecules or clusters. It becomes impractical when the system is so large that there are many local minima to search for. It is not adequate for systems containing floppy molecules since anharmonic effects could cause large errors in frequencies and relative order of the spectral bands. Normal mode analysis provides clear vibrational modes that can be easily visualized, but such modes are different from actual vibrational modes because of the harmonic approximation. It yields only line spectra and the peak broadening is usually artificially introduced through convolution with a Gaussian or Lorentzian function.

The dynamics analysis is adequate for systems of any size, in particular condensed-phase systems for which periodic boundary conditions may be used. No harmonic approximation is made and the coupling between different modes is included. It yields naturally broadened bands by including temperature effects. However, MD simulations are usually performed classically, and

the model system is evolving in the vibrational ground state, and thus no overtone bands can be obtained in such a way, which might cause discrepancies when comparing computed and experimental spectra.

1.3. Vibrational spectra of ion-water clusters and peptide-water clusters

The hydration of ions has been the topic of intensive studies for decades due to its importance in establishing a modern theory of electrolyte solution, and understanding important phenomena such as the Hofmeister effect.^{19,20} The structure and dynamics of ionic hydration has been studied in bulk solution using X-ray dispersion and vibrational spectroscopy, but the coexistence of counter-ions makes it difficult to understand the results.^{21,22} In recent years, the development of IRMPD and IRPD techniques allowed the separation of the counter-ions and the detection of clusters of water with an individual ion. They were used to study the protonated water dimer, sulfate-water clusters, and peptide-water clusters, amongst other systems. These investigations disclosed some features of ion-water interactions.²³⁻²⁶

The protonated water dimer is a typical prototype for studying proton transfer. Both IRMPD^{12, 13, 23} and IRPD^{14, 15} were used to obtain vibrational spectra, but the inconsistencies between the reported experimental results have not been fully explained.¹² In this work, we compute vibrational spectra from ab initio MD simulations, and the band assignment is achieved by computing the time correlation spectra for vibrational modes involving selected relevant internal coordinates. Mode coupling and temperature effects are found to play an important role in the discrepancies between various sets of experimental results.

Sulfate is one of the strongest kosmotropic ions, which can bind water molecules tightly to form hydration shells in aqueous solution.^{27, 28} However, over what distance the sulfate ion may

affect the orientation and dynamics of water molecules remains an unresolved issue so far. Williams and co-workers investigated the question in the gas phase using the IRMPD technique.²⁹ A weak shoulder in the OH stretch band at around $\sim 3700\text{ cm}^{-1}$ was identified as a signature of “free water molecules” at the surface of aqueous droplets seeded by sulfate. In this work, we attempt to examine this hypothesis with computed spectra based on DFTB models.

The guanidinium ion is a powerful denaturant that can break down the secondary structure of proteins at moderate concentration.^{30, 31} The CN bond stretch of guanidinium might be used as a probe to detect the binding states of the ion. In this work, we investigate how hydration affects the band positions and shapes in the vibrational spectra of guanidinium water clusters.

Vibrational spectroscopy is widely used to detect secondary-structure changes of proteins.^{1, 32, 33} For large peptides with significant mode coupling, computed vibrational spectra from MD simulations could be a powerful tool to aid in the spectral band assignment. To establish an efficient first-principles-based method, we validate DFTB models against ab initio results and available experimental and theoretical vibrational spectra for several prototypical model peptides, peptide-water and peptide-ion complexes.

1.4. SCC-DFTB models - theory and performance

The DFTB model is an approximate quantum-chemistry method based on DFT and the tight-binding model.³⁴ In this method, the total energy is calculated by expanding the DFT total energy in terms of charge density fluctuations around the charge density of a reference state, which is usually the electron density of neutral atoms. The third-order expansion of the SCC-DFTB method, referred to as DFTB3³⁵ is formulated as

$$E^{DFTB3} = \sum_i^{OCC} n_i \varepsilon_i + E^{rep} + \frac{1}{2} \sum_{ab} \gamma_{ab} \Delta q_a \Delta q_b + \frac{1}{3} \sum_{ab} \Gamma_{ab} \Delta q_a^2 \Delta q_b \quad (1.6)$$

where the first term in the right-hand side sums up orbital energies, obtained with an Hamiltonian operator constructed on the basis of a given reference density and the single-electron wave functions are represented as linear combinations of Slater-type atomic orbitals. The second term describes the short-range repulsion potentials, and the last two terms involve the second-order and third-order expansions of the DFT energy with respect to the electron density of the reference state of the atoms, respectively. Δq_a and Δq_b are atomic charge fluctuations which are calculated using Mulliken's scheme in a self-consistent manner, γ_{ab} is a function that describes the "chemical hardness" of atoms and includes an extra term to correct for hydrogen bonding, and Γ_{ab} is the coefficient describing the fluctuation of γ_{ab} with atomic charge. A more detailed description of the SCC-DFTB model is provided in **Section 3.2.1** of **Chapter 3**.

DFTB has been widely validated for various systems and properties, including molecular geometries, binding energies and harmonic frequencies.³⁵⁻⁴⁰ DFTB models are found to be computationally efficient approximations to DFT that have been shown to give reliable structural and energetic properties for various systems; in particular, they were shown to properly account for the geometries, energetics, intermolecular polarization and harmonic vibrational frequencies of hydrogen-bonded ion-water clusters with 2~3 orders higher computational efficiency than DFT.^{41, 42} In this work, we further validate the performance of DFTB models in computing vibrational spectra from MD simulations. The computed spectra are compared to available experimental results, or high-level theoretical results.

1.5. Objective and outlines

The primary objectives of this work is two-fold: to explore computational vibrational spectroscopy beyond the harmonic approximation and to investigate the performance of the self-consistent-charge density-functional tight-binding (SCC-DFTB) model in computing the vibrational spectra of ion-water complexes and peptide-ion/water complexes. To this effect, 4 prototypical systems have been selected, covering a wide range of intermolecular interactions such as proton-water, anion-water, cation-water, cation-anion, amide-water and amide-ion interactions.

In Chapter 2 of this thesis, computed vibrational spectra of the protonated water dimer, i.e. the Zundel ion, are discussed. The spectra are generated from MD simulations with both ab initio (MP2)⁴³⁻⁴⁵ and DFT (Becke's 3-Parameter Exchange, Lee-Yang-Parr Correlation form, B3LYP).⁴⁶⁻⁴⁹ The MD simulations are performed at a broad range of temperatures from 40K to 160K to investigate temperature effects on the computed spectra.

In Chapter 3 of this thesis, the vibrational spectral signature of free water at the surface of aqueous droplets seeded by the sulfate ion is investigated. The vibrational spectra of sulfate-water clusters are obtained from MD simulations with DFTB models. Correlation spectra of individual water molecules at the surface of the droplets are examined to validate the hypothesis proposed in the literature.

In Chapter 4 of this thesis, the effects of hydration and ion association on the CN bond stretch band has been investigated. The DFTB model is validated against DFT for the prediction of molecular structure, harmonic frequencies and MD-simulation-derived vibrational spectra of small guanidinium-water clusters and guanidinium-chloride clusters. DFTB is then used to compute vibrational spectra of guanidinium-water clusters of different sizes, with a number of water

molecules ranging from 0 to 80. The structure of the guanidinium-water clusters are also investigated by examining radial probability distribution functions.

In Chapter 5 of this thesis, the performance of the DFTB model in computing vibrational spectra of peptides is validated against available experimental and theoretical results. Several typical interactions, including peptide-water, peptide-ion and peptide-peptide interactions are investigated.

In Chapter 6 of this thesis, the results are summarized and general conclusions on the primary objectives of this work are outlined.

Chapter 2.

**Coupling of Proton Transfer Mode and Temperature
Effects in Vibrational Spectra of the Protonated Water
Dimer Revisited with *ab initio* Molecular Dynamics
Simulations**

2.1. Introduction

The protonated water dimer, i.e. Zundel ion, is the simplest prototype model for studying proton transfer and is thus of high interest in chemistry and biochemistry.^{12, 14, 15} Developments of the infrared multiple photon dissociation (IRMPD) technique and inertia atom(s) tagged infrared predissociation (IRPD) technique opened the door to investigate the dynamics and internal vibrational relaxation (IVR) of ion-water clusters in the gas phase.^{12-15, 23, 24, 50} However, application of both techniques to the protonated water dimer painted very different pictures of the vibrational spectra. For example, the sawtooth pattern of the bands near 1000 cm^{-1} in the IRMPD spectra of bare $\text{H}_5\text{O}_2^{+12}$ is in contrast to the clean doublet split bands in the IRPD spectra of neon tagged H_5O_2^+ , which is assigned to the proton transfer mode.¹⁵ Intensive theoretical studies have been reported to attempt to provide a basis for the band assignment and for understanding these discrepancies,⁵¹⁻⁵⁹ particularly with respect to the proton transfer mode, due to its importance in understanding vibrational mode coupling in general.⁵⁵ In previous studies, it was concluded that lower-frequency modes such as the terminal water wag and torsion are coupled with the proton transfer mode.⁵¹⁻⁵⁵ However, a thorough understanding of the spectral signature and the associated dynamics remains to be achieved.⁵⁵

This work aims at investigating the vibrational spectral signature of the protonated water dimer. Temperature has been suggested to play an important role in possibly explaining the discrepancies between experimental spectra.^{23, 58} Therefore, ab initio molecular dynamics (MD) simulations are performed at different temperatures to investigate temperature effects on the vibrational spectra. In addition to previously reported MD simulations, such as quantum molecular dynamics (QMD) at 0K,⁵⁵ classical ab initio MD simulations at 1K,⁶⁰ 350K⁵⁸ and 360K,⁶⁰ our simulations are performed at moderate temperatures. Equilibrium temperatures of the constant-

energy simulations correspond to 10K, 40K, 80K for MP2-based simulations and 10K, 80K, 160K for B3LYP-based simulations.

In this work, vibrational spectra are computed from the Fourier transform of the autocorrelation of the total dipole moment calculated along MD trajectories. This method has been successfully applied in many cases^{7, 8, 11} to obtain vibrational spectra beyond the harmonic approximation as full mode coupling and anharmonicity effects are accounted for in the MD simulations.

To examine the coupling between vibrational modes, time-correlation spectra for modes involving motion along linear combinations of selected internal coordinates are also computed. This is shown in this work to be a powerful tool to unveil the coupling of the proton transfer mode with the other modes. Together with the careful choice of simulation temperatures, this analysis reveals details and new features of the coupling of the actual vibrational modes of the protonated water dimer.

This chapter is organized as follows. After the brief review of research progress on the topic presented in this section, details of the computational procedure employed to produce vibrational spectra are outlined in the next section. Results are presented in a third section, along with a discussion of the band assignment, comparison with experimental results, coupling of vibrational modes and temperature effects. As summary and conclusions follow in the last section.

2.2. Computational details

2.2.1. ab initio MD simulations

Classical *ab initio* constant-energy MD simulations of H_5O_2^+ and D_5O_2^+ were performed with the system energy and forces calculated using second-order Møller–Plesset (MP2) Perturbation Theory⁴³⁻⁴⁵ and the Becke’s 3-parameter exchange, Lee-Yang-Parr correlation form (B3LYP)^{46-49, 61-64} of density-functional theory (DFT) with the aug-cc-pVDZ basis set.⁶⁵ The equations of motion are integrated using the velocity Verlet algorithm.⁶⁶ Simulations are initiated at the ground-state geometry, and random velocities satisfying a Maxwell-Boltzmann distribution are generated for all atoms with a total kinetic energy set according to the target temperature. A timestep of 0.2 fs was found to be sufficiently small to maintain the conservation of the total energy to an acceptable level and was thus used for all simulations. The time span of each simulation is 10 ps (50000 steps), which was found long enough to achieve convergence of the computed vibrational spectra with a resolution of $\sim 7 \text{ cm}^{-1}$.

2.2.2. Computation of vibrational spectra

The computation of vibrational spectra as the Fourier transform of the autocorrelation function of the total dipole moment has been widely used and well documented in many reference articles.^{7, 8} In this work, the absorption coefficient is computed from the following formula,

$$\alpha(\omega)n(\omega) = \frac{2\pi\beta\omega^2}{3cV} \int_{-\infty}^{+\infty} dt \cdot e^{-i\omega t} \langle \boldsymbol{\mu}(0) \cdot \boldsymbol{\mu}(t) \rangle \quad (2.1)$$

in which $\alpha(\omega)$ is the absorption intensity with respect to the vibrational frequency or wavenumber ω , $n(\omega)$ is the frequency-dependent refractive index of the medium [$n(\omega) = 1$ is used in this work], c is the speed of light in vacuum, V is the volume (set to be 1 in this work), $\beta = 1/kT$ with T the average temperature And k the Boltzmann constant, $\boldsymbol{\mu}$ is the dipole moment, and the brackets indicate an ensemble average over the time span of the simulations. A quantum

correction factor is added to the above formula to take the effects of quantum nuclear motion on the band shape into account. Among various quantum correction factors proposed¹⁸, the factor often referred to as the “harmonic correction”¹⁸ factor satisfies both the detailed balance and the fluctuation-dissipation theorem, and takes the following form,

$$Q_{harmonic} = \frac{\beta \hbar \omega}{1 - e^{-\beta \hbar \omega}} \quad (2.2)$$

The spectra were then smoothed using a Gaussian smoothing scheme, i.e. by replacing each signal data with a Gaussian kernel function.⁶⁷ The full width at the half maximum of the Gaussian function is set to 20 cm⁻¹, which reduces the resolution of the spectra to obtain smoothed curves.

2.2.3. Time correlation spectra for specific modes

Effective vibrational modes can be represented as linear combinations of selected internal coordinates. Conjugated pairs of internal coordinates are usually linearly combined and are shared in many coupled vibrational modes. For example, for the Zundel ion, the symmetric stretch of a terminal water molecule is represented as r_1+r_2 , while the anti-symmetric stretch is represented as r_1-r_2 , with r_1 and r_2 the length of the two OH bonds. Similarly, the symmetric water bend and anti-symmetric water bend are represented as $\theta_1+\theta_2$ and $\theta_1-\theta_2$, respectively, with θ_1 the angle between OH bonds of one terminal water molecule, and θ_2 that of the other water molecule. **Figure 2.1** illustrates the definition of the combined internal coordinates used in this work. In the above definition, the coefficients of the linear combination are set to unity which might not always be true in actual cases. However, the simplification does not affect the frequencies of their autocorrelation function.

The calculation of the time-correlation spectra for modes described by combined internal coordinates is taking the following form:

$$C(\omega) = \frac{2\pi\beta\omega^2}{3cV} \int_{-\infty}^{+\infty} dt \cdot e^{-i\omega t} \langle \mathbf{R}(0) \cdot \mathbf{R}(t) \rangle \quad (2.3)$$

in which C is the correlation value with respect to the frequency or wave number ω , and \mathbf{R} is the linear combination of the selected internal coordinates. Other parameters have been defined above for equation 2.1.

Of particular interest is the proton transfer mode, i.e. the asymmetric OHO stretch denoted as $\nu(\text{OHO})_{\text{as}}$ and defined as $r_1 - r_2$, with r_1 and r_2 the distances of the central proton to the O atoms of the two terminal water molecules. This combination of internal coordinates defines the main feature of the proton transfer between the two terminal water molecules, and time correlation spectra for this mode includes important information such as the spectral position of the actual proton transfer mode vibration, and the spectral position of other vibrational modes that are coupled with the proton transfer mode.

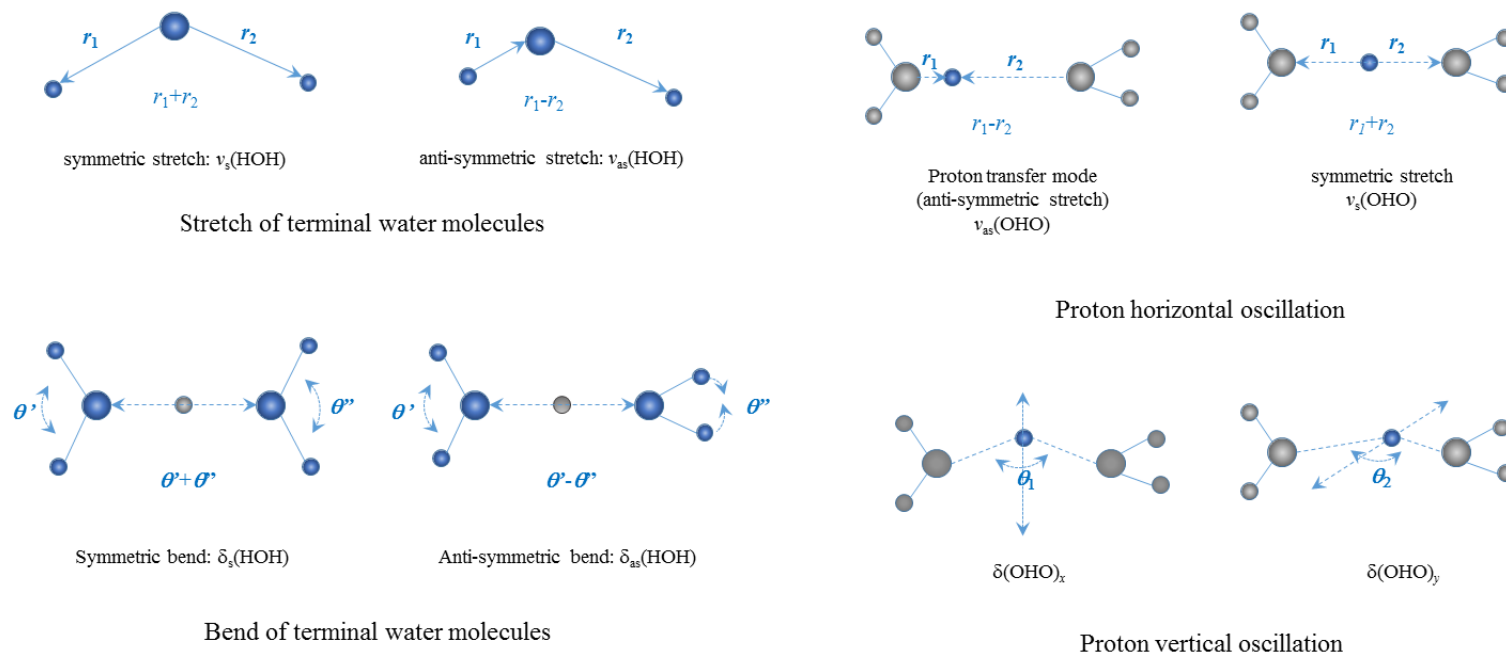


Figure 2.1. Combination of the internal coordinates used to compute time correlation spectra

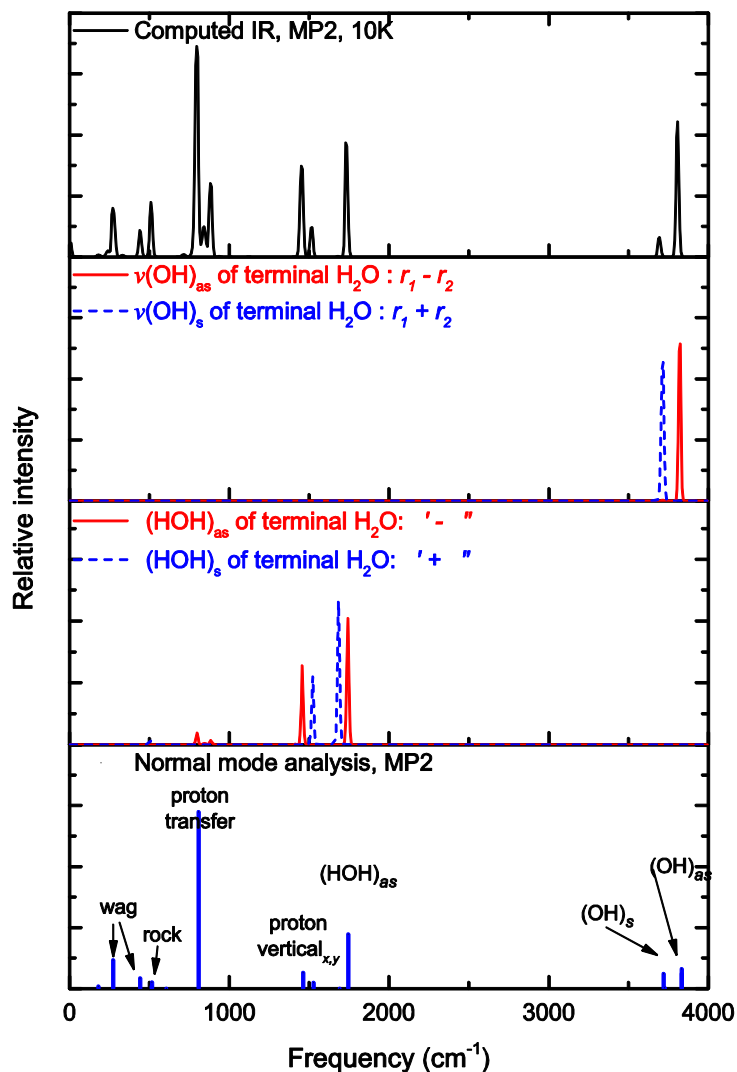


Figure 2.2. Calculated vibrational and correlation spectra for the Zundel ion H_5O_2^+ . **Top:** Simulated vibrational spectra at 10 K with MP2/aug-cc-pVDZ. **Middle 2:** time correlation spectra of terminal water stretch and bend modes. **Bottom:** harmonic spectra from normal mode analysis with MP2/aug-cc-pVDZ.

Figure 2.2 demonstrates how band assignment is performed using correlation spectra for modes involving linear combinations of selected internal coordinates on the basis of a few examples. The first example is the OH stretch of the terminal water molecules. Due to the C_2 symmetry of the Zundel ion, the two terminal water molecules are indistinguishable, and therefore

the symmetric and antisymmetric stretches can be defined with the bond lengths of the same water molecule. It can be seen that the two modes have clearly distinct vibrational frequencies. From this analysis, the bands at 3820 cm^{-1} and 3716 cm^{-1} are assigned to the asymmetric and symmetric OH stretches, respectively. The second example is the assignment of the bend of the terminal water molecules. The symmetric and antisymmetric bend modes of the terminal water molecules are defined as $\theta' + \theta''$ and $\theta' - \theta''$, and their time correlation spectra exhibit several intense bands. For example, three bands at 1742 , 1457 and 885 cm^{-1} are found in the time correlation spectra of the antisymmetric bend. We assign the most intense band at 1742 cm^{-1} to the actual mode, while the other two result from the coupling with other modes, the proton vertical oscillation (at 1457 cm^{-1}) and the proton transfer mode (at 885 cm^{-1}). It should be noted that the symmetric bend mode of the terminal water molecules is dipole forbidden, so that no corresponding band shows in the computed overall spectra.

2.3. Results and discussions

2.3.1. Computed vibrational spectra: band assignment and anharmonic effects

Band assignment. The bands in the computed spectra of the protonated water dimer in **Figure 2.2** are assigned using the method described in **Section 2.2.3**. For modes whose principal component is hard to define with a pair of internal coordinates, bands are assigned by comparison to the harmonic results. Since anharmonic effects do not seem to affect the relative positions of the bands for most modes in this case, and the bands are well separated from each other, the assignment is unambiguous. The frequencies and relative intensities of the assigned bands are summarized in **Table 2.1**, together with the harmonic results calculated from normal mode analysis with MP2 (MP2/aug-cc-pVDZ) and DFT (B3LYP/aug-cc-pVDZ), respectively.

Table 2.1 Vibrational frequencies and relative intensities (in parentheses) for Zundel H_5O_2^+ .

	MP2 ^a		B3LYP ^a		IRMPD ¹	IRMPD ²	IRPD (Ne) ³
	harmonic	MD (10K)	harmonic	MD (10K)	Asmis et al	Fridgen et al	Johnson et al
terminal water wag	275 (459)	273 (521)	288 (274)	280 (98)	--	--	--
	444 (166)	439 (281)	377 (248)	372 (25)	--	--	--
terminal water rock	514 (36)	511 (582)	484 (0)	492 (36)	--	--	--
	517 (98)		497 (19)		--	--	--
proton transfer	809 (2893)	796 (2244)	908 (2701)	895 (892)	1317	990	920
		842 (324)		948 (191)			
proton vertical oscillation	1463 (255)	1451 (969)	1436 (233)	1425 (1609)	921	1163	1392
	1527 (95)	1517 (314)	1484 (96)	1471 (922)	1043	1337	1455
terminal water bend	1691 (889)	1678 (5)	1660 (0)	1649 (5)	1741	1756	1760
	1746 (241)	1729 (1214)	1733 (1109)	1716 (2242)			1875
OH stretch of terminal water symmetric	3719 (241)	3695 (208)	3717 (234)	3695 (335)	--	--	3603
	3726 (9)		3725 (6)				
OH stretch of terminal water antisymmetric	3832 (238)	3807 (1438)	3816 (253)	3787 (2661)	--	--	3683
	3833 (316)		3817 (300)				

^a. Obtained from MP2 and B3LYP calculation with aug-cc-pVDZ basis set.

¹ from ref 12, ² from ref 23, ³ from ref 15

Unit: frequency in cm^{-1}

Anharmonic effects. Comparison of the frequencies and intensities between harmonic results and MD results unveils the consequences of anharmonic effects in the classical limit. The first noticeable feature of anharmonicity is the slight redshift down by about 10 cm^{-1} for all modes due to interactions with each other. The second effect is the splitting of the proton transfer band due to strong coupling with other modes. This coupling will be further discussed below in **Section 2.3.3**. The third one is the intensification of the band corresponding to the proton vertical oscillation mode, a feature probably due to the change of the oscillation direction of the proton leading to an increase in the transition dipole moment. The fourth one is the disappearance of the symmetric bend band for the terminal water molecules in the MP2 results and the increased intensity of the antisymmetric bend band for the terminal water molecules. The fifth one is the intensification of the antisymmetric OH stretch band for the terminal water molecules. These effects reflect differences between the harmonic normal modes and the actual vibrational modes, and the non-trivial coupling of actual vibrational modes.

2.3.2. Computed vibrational spectra of H_5O_2^+ : comparison with experimental results

This section is devoted to present the overall vibrational spectra in the region of $0\sim 2000\text{ cm}^{-1}$, and discuss the consistency between the computed spectra and the experimental spectra, including IRMPD^{12, 23} and IRPD^{14, 15} results, as shown in **Figure 2.3**. Such comparison also provides basis for evaluating the reliability of the method currently in use.

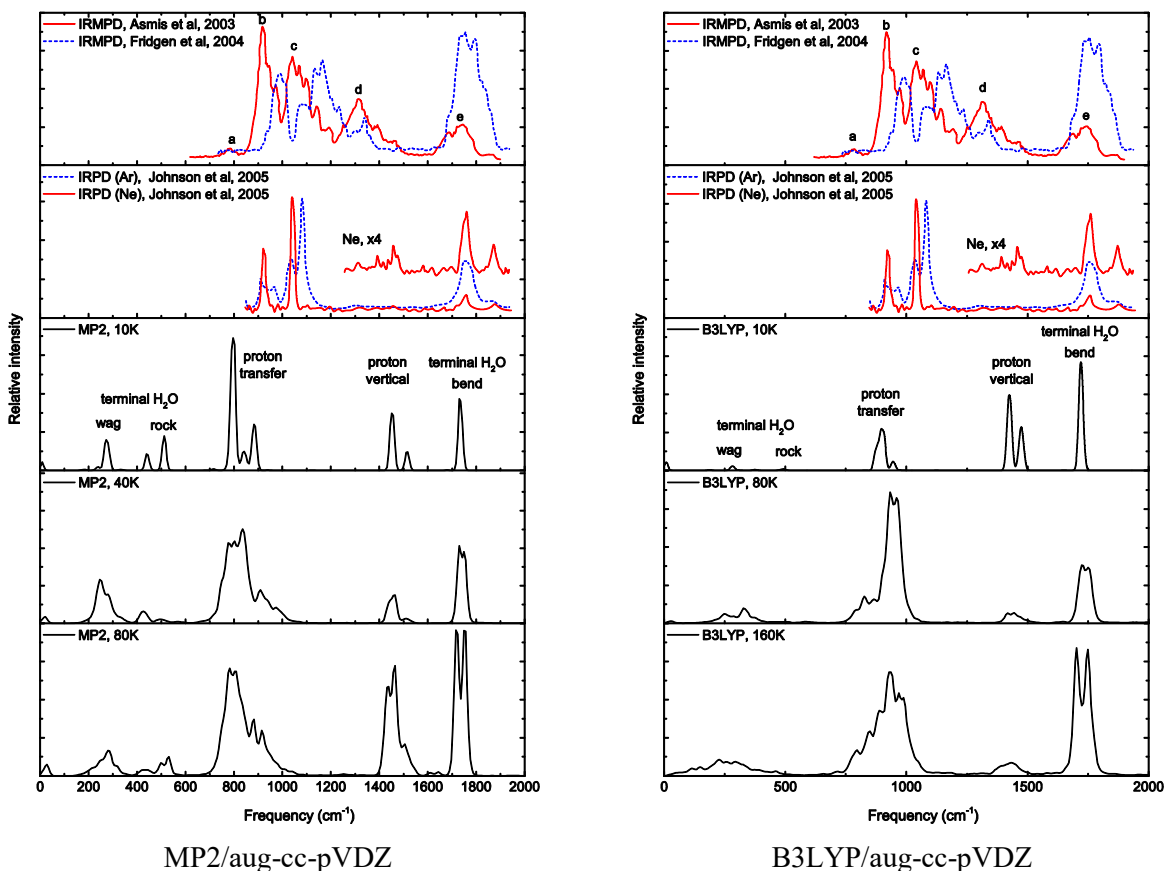


Figure 2.3. Experimental and simulated infrared spectra for the Zundel ion H_5O_2^+ . (**Left**) MP2/aug-cc-pVDZ results; (**Right**) B3LYP/aug-cc-pVDZ results. The top two panels display experimental infrared spectra from IRMPD and IRPD, respectively; the bottom three display simulated vibrational spectra from MD simulations at different temperatures.

Proton transfer bands. The bands within $600\sim 1200\text{ cm}^{-1}$ are assigned to be the proton transfer mode, also named as antisymmetric stretch of OHO, or noted as $\nu_{\text{as}}(\text{OHO})$. At low temperature (10K) the band is triple split, resembles to the multiple-split feature of IRPD.¹⁵ While at higher temperature (80K for MP2 and 160K for B3LYP), the band shape features the sawtooth pattern observed in the IRMPD spectra by Asmis and co-workers.¹² More specifically, in the 10K simulated spectra, the terminal water molecule bend mode shows as a single band and the bands associated with the proton transfer mode are multiple-split, consistent with the experimental IRPD spectra.¹⁵ In the simulated

80K MP2 spectra, the terminal water molecule bend mode band splits and that associated with the proton transfer mode broadens, with two significant shoulders on the right side, similar to the experimental IRMPD spectra of Asmis and coworkers.¹² We note a significant difference in the position of the shoulders in the bands associated with the proton transfer modes in the spectra calculated with MP2 and B3LYP. On the shoulders are found on the right side in MP2 spectra, in agreement with the experimental IRMPD results of Asmis and coworkers, but they are found on the left side in B3LYP spectra.

Proton vertical oscillation bands. The bands near 1500 cm^{-1} are assigned to the proton vertical oscillation modes, referring to the OHO bend and denoted as $\delta(\text{OHO})_x$ and $\delta(\text{OHO})_y$. In IRPD spectra,¹⁵ the modes show as double-split bands in this spectra region, while in IRMPD spectra of Asmis and coworker,¹² it is the two most intense bands b (921 cm^{-1}) and c (1043 cm^{-1}) that are assigned to the proton vertical oscillation based on a quantum anharmonic calculation including 4 fully coupled vibrational degree of freedom (quantum 4D), as shown in **Figure 2.3**. This assignment was later questioned by Fridgen and coworkers,²³ who assigned the bands at 1163 cm^{-1} and 1337 cm^{-1} to the proton transfer modes based on a normal mode analysis with B3LYP. This discrepancy is still unresolved due to the complex nature of the IRMPD process, but the present work supports the latter assignment by Fridgen and coworkers.

From the simulated spectra shown in **Figure 2.3**, the intensities of the proton vertical oscillation bands appear to weaken upon temperature increase. This trend is seen in the spectra calculated with both B3LYP and MP2, though an unexpected intensification of the bands is observed at 80K for MP2, probably due to over-coupling with the proton transfer mode which changes the direction of the proton oscillation leading to a larger transition dipole moment. Nevertheless, this trend is consistent with the low intensity of the proton vertical oscillation bands observed in the IRPD spectra and the fact that the bands do not even show in IRMPD spectra.

Terminal water bend bands. The bands near 1750 cm^{-1} are unambiguously assigned to the terminal water bend in all reports. The simulated spectra at low temperature (10K) accurately reproduce the singlet feature observed in the IRPD spectra, and those at higher temperatures (40K and 80K for MP2, 80K and 160K for B3LYP) the doublet feature observed in IRMPD spectra. The splitting of the terminal water bend bands is due to mode coupling with the proton transfer mode, as discussed below in **section 2.3.3**. The temperature dependence of the intensities of these bands found in our simulated spectra is in good agreement with the differences observed in the IRPD and IRMPD spectra.

Terminal water wag and rock bands. The bands below 600 cm^{-1} are assigned to the terminal water wag bands ($273, 438\text{ cm}^{-1}$) and rock bands (511 cm^{-1}), as shown in **Figure 2.3**. The broadening of the bands with temperature increase may reflect increased coupling of the modes, and with each other.

In summary, the simulated spectra at low temperature are found in overall very good agreement with the IRPD spectra, in particular the splitting of the proton transfer bands in the region of $700\sim 1200\text{ cm}^{-1}$ is well reproduced. The single band associated with the terminal water bend band in IRPD spectra, and its splitting in the higher-temperature IRMPD spectra, are features well captured by our simulated results at different temperatures. We note, however, a slight underestimation of the band positions, compared to the IRPD results, most likely due in part to the possible errors introduced by describing the potential energy surface by MP2 and B3LYP with only a medium-size basis set (aug-cc-pVDZ).

MP2 vs B3LYP. The simulated spectra at low temperature are found in overall very good agreement with the IRPD spectra, in particular the splitting of the proton transfer bands in the region of $700\sim 1200\text{ cm}^{-1}$ is well reproduced. The single band associated with the terminal water

bend band in IRPD spectra, and its splitting in the higher-temperature IRMPD spectra, are features well captured by our simulated results at different temperatures. We note, however, a slight underestimation of the band positions, compared to the IRPD results, most likely due in part to the possible errors introduced by describing the potential energy surface by MP2 and B3LYP with only a medium-size basis set (aug-cc-pVDZ).

2.3.3. Time correlation spectra: coupling of the proton transfer mode

The splitting of the band of the proton transfer mode near 800~1200 cm⁻¹ mentioned earlier is well known and typically results from anharmonic effects and mode coupling, features that captured by our MD simulations. Let us now turn our attention to the nature of mode coupling with the proton transfer mode and how it is affected by temperature.

The coupling of the proton transfer mode with other modes is investigated by examining the time correlation spectra of combined internal coordinates r_1 - r_2 , where r_1 and r_2 are the distances of the central proton to the O atoms of the two terminal water molecules. The bands in the time correlation spectra correspond to all the vibrational modes that include a contribution from the proton transfer motion. Vibrational modes interact with each other through collective atomic motion, and thus the coupling can be inferred from the time correlation spectra of modes involving shared combinations of internal coordinates. The simulated MP2 and B3LYP time correlation spectra along with overall vibrational spectra are shown in **Figures 2.4** and **2.5**, respectively.

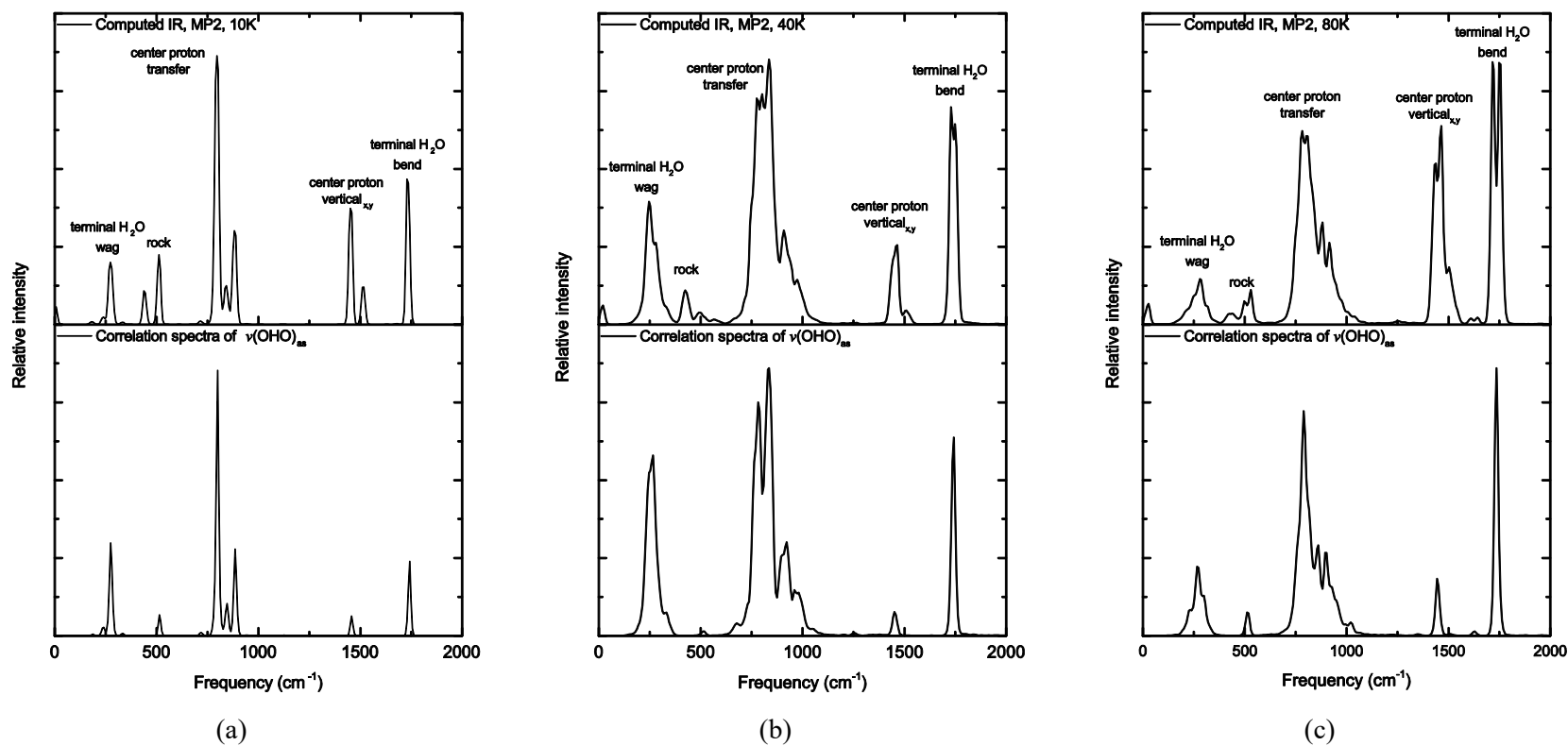


Figure 2.4. Simulated MP2/aug-cc-pVDZ vibrational spectra of the Zundel ion H_3O_2^+ and time correlation spectra for the proton transfer mode at (a) 10K (b) 40K and (c) 80K.

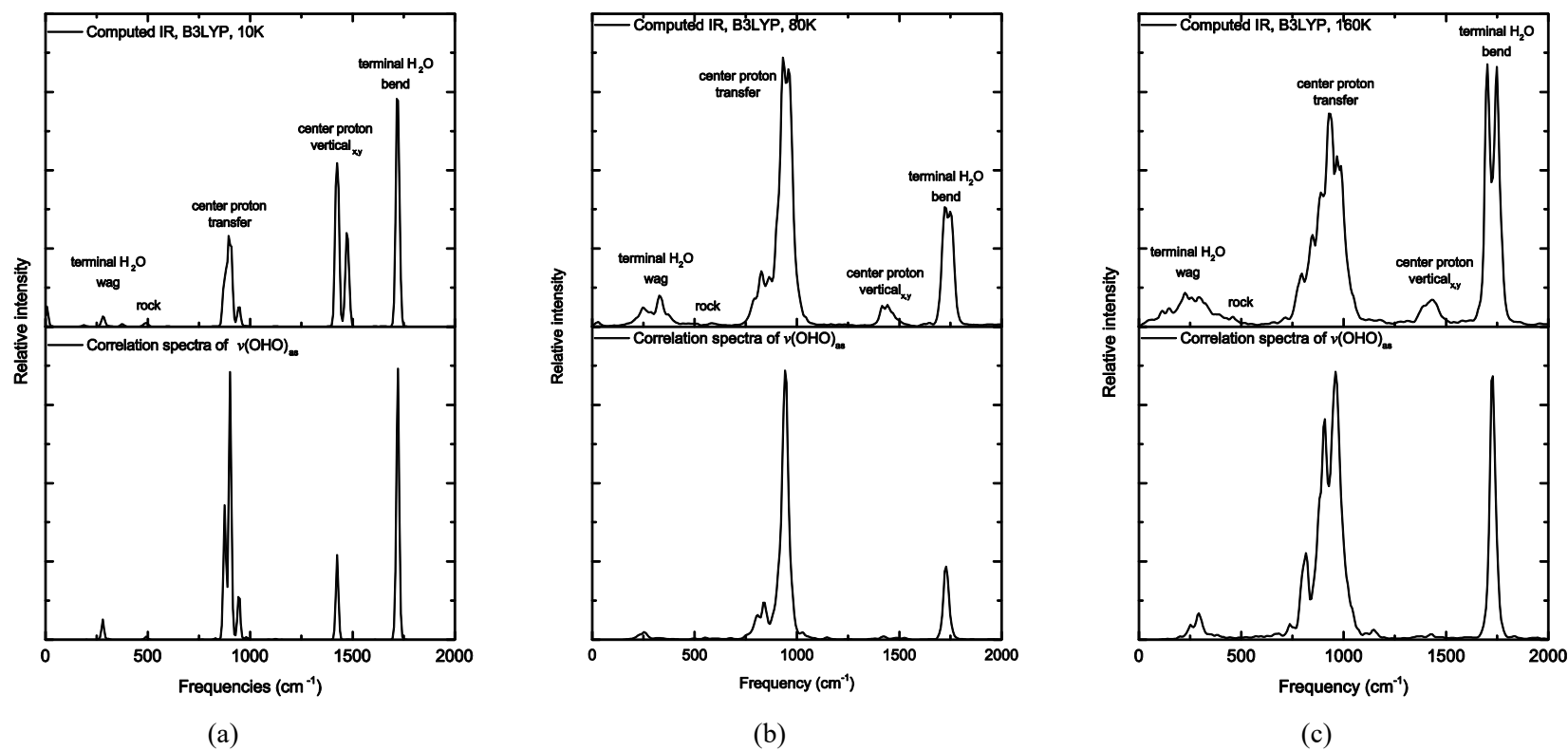


Figure 2.5. Simulated B3LYP/aug-cc-pVDZ vibrational spectra of the Zundel ion H_5O_2^+ and time correlation spectra for the proton transfer mode at (a) 10K (b) 40K and (c) 80K.

MP2, 10K. In simulated MP2 vibrational spectra of 10K, the band associated with the proton transfer mode near $800\sim 900\text{ cm}^{-1}$ splits into 5 distinguishable peaks due to its interaction with other modes, indicating that at least 4 other modes are involved into the coupling. These four bands are clearly present in the time correlation spectra of the proton transfer motion and correspond to coupling with the terminal water molecular wag, terminal water molecular rock, proton vertical oscillation and terminal water molecular bend. From the intensities of these bands, two of the modes (terminal water molecular wag and bend) appear to be strongly coupled, while the other two modes are relatively weakly coupled to the proton transfer mode. This finding is complementary to the previous report based on quantum MD results,⁵⁵ in which only the lower-frequency modes (terminal water molecular wag and rock) were deemed responsible for the splitting of the proton transfer band. This slight discrepancy might be due to temperature effects, since the latter are not accessible in quantum MD simulations (performed at 0K).

MP2, 40K and 80K (Temperature effects). Simulated spectra at higher temperatures (40K and 80K) reveal interesting temperature effects on the coupling of the proton transfer mode. The number of split peaks does not change with temperature except that at 80K the left weak shoulder merges with the major peak. Also, the bands greatly broaden indicating strengthening of the coupling between modes. The major peak, with the highest intensity, lies in the center of the band at 40K, but shifts to the left at 80K, indicating stronger coupling with the lower-frequency modes, and resulting into a slight redshift. The two shoulders on the right side, most likely caused by the coupling with the two higher-frequency modes, form a sawtooth pattern as typically observed in the IRMPD spectra of Asmis and coworkers. This indicates that the origin of the discrepancies observed in IRPD and IRMPD spectra may lie in temperature effects. Temperature effects also

results in the splitting of the bands associated with the terminal water molecular bend and the proton vertical oscillation, most likely a consequence of coupling with the proton transfer motion.

B3LYP vs MP2. The overall band shape and temperature-dependent broadening and splitting found in the simulated B3LYP spectra of **Figure 2.5** are very similar to their MP2 counterparts. However, two main differences are noticeable. First, B3LYP predicts sawtooth-form shoulders reflecting coupling with other modes on the left side of the proton transfer band, a feature that may be due to stronger coupling with the terminal water bend than with the lower-frequency modes such as terminal water wag and rock. Second, the coupling of the proton transfer mode with the proton vertical oscillation is weaker, as indicated in the time correlation spectra in **Figures 2.4** and **2.5**, suggesting weaker mode coupling and less efficient internal vibrational energy redistribution according to B3LYP.

2.4. Summary and conclusions

The protonated water dimer has long been a prototype model to investigate proton transfer. IRPD and IRMPD techniques open the door to characterize the vibrational dynamics and the internal vibrational energy relaxation in this process, while companion theoretical studies can be used to assist in the band assignment and provide a thorough interpretation of the spectra. However, discrepancies between various sets of reported experimental results and calculations for the protonated water dimer remain poorly understood.

In this work, we aim to provide a rigorous theoretical basis for shedding light on the discrepancies between reported IRMPD^{12,23} and IRPD^{14,15} spectra. Simulated spectra are obtained from the Fourier transform of the autocorrelation function of the total dipole moment computed from classical *ab initio* MD simulations which account for full anharmonicity and mode coupling.

Spectral bands are assigned based on a time correlation analysis of modes characterized by a set of linearly combined internal coordinates. Of particular interest is the proton transfer mode, which plays a key role in understanding the vibrational spectra of the protonated water dimer.

Simulated spectra at low temperature (10K) are in excellent agreement with experimental IRPD spectra, reproducing such features as the multiple splitting of the proton transfer band in the region of 800~1000 cm^{-1} , and the single band associated with the terminal water bend mode near 1700 cm^{-1} .¹⁵ On the other hand, simulated spectra at higher temperatures (40K to 160K) reproduce important features of the IRMPD spectra, such as the sawtooth pattern of the bands in the region 800~1200 cm^{-1} , and the splitting of the terminal water bend band near 1700 cm^{-1} .¹² This suggests that temperature effects are the main origin of the discrepancies between the reported experimental IRPD and IRMPD spectra.

The simulation results also suggest that the splitting and broadening of the proton transfer bands are caused by coupling with other modes, and further analysis of correlation spectra shows that the proton transfer mode is coupled with not only the lower-frequency modes (terminal water wag and rock), as reported earlier from quantum MD simulation results at 0K, but also the higher-frequency modes (terminal water bend and proton vertical oscillation).

Both MP2 and B3LYP have been used to characterize the interatomic interactions in the ab initio MD simulations, MP2 is found to generally outperform B3LYP in reproducing the temperature-dependent changes of band shapes and positions when compared to available experimental spectra. Compared with previous theoretical studies, the novel findings of the present work are enabled by the selection of moderate simulation temperatures and the use of correlation spectra for modes involving linear combinations of selected internal coordinates. Simulated spectra in the temperature region 10K - 200K provide a clearer and more detailed picture

than previously accessible from simulations performed at 0K⁵⁵, 1K⁵⁸, and 350K⁶⁰, 360K⁵⁸. As for time-correlation spectra, they provide powerful means of unambiguously assigning spectral bands and aid in the interpretation of convoluted vibrational spectra.

Chapter 3.

Simulations of the Vibrational Spectra of Sulfate-Water

Clusters: The OH stretch as a Signature of Water Binding

3.1. Introduction

Hydration of ions and space span of their effects. The hydration of ions has been a topic of extensive research in recent years due to its importance to modern molecular physical chemistry and biology related to such phenomena as the Hofmeister effect.^{19, 20, 68} In particular, the effects of ions on the structure of surrounding water molecules has gained increasing attention and a variety of experimental and theoretical investigations in the past decades have shown that the effects are only significant within a specific distance in dilute solution at moderate temperature,^{21, 22, 69, 70} even for one of the strongest kosmotropic ions, sulfate.^{29, 71-74} However, the debate over what distance the ions in aqueous solutions exert definite effects on the structure of water remains unsettled, due to the limitations of traditional experimental techniques regarding the detection of water structure, and the co-existence of counter-ions in aqueous solutions.^{21, 22}

Experimental investigation of sulfate-water clusters. Ion-water clusters lend themselves as an ideal model in order to provide key insight into the interactions of ions and water molecules. Williams and co-workers have investigated the effects of the sulfate ion on the hydrogen-bonded network of surrounding water molecules using the infrared multiphoton dissociation (IRMPD) technique developed in recent years.^{27-29, 71, 73, 75} With this technique, ion-water clusters of different size are generated using electrospray ionization, and then subjected to dissociation under excitation by an infrared laser. Products of dissociation at a given excitation frequency are counted and define the intensity of the absorption spectrum of the parent ions. It was found that a weak peak centered at around $\sim 3700\text{ cm}^{-1}$ in the OH stretch region emerge in the spectra for clusters containing over 43 water molecules.²⁹ This peak was assigned to the free OH stretch of water molecules at the surface of the nanodroplet. Even though a similar assignment has been employed in several similar studies,^{71, 74} this is one of the most unequivocal reports of vibrational spectroscopic evidence of

the spatial range of the effects of ions on the structure of surrounding water molecules in a gas-phase cluster.

Theoretical investigation of sulfate-water clusters. This study motivated in part our interest to explore suitable theoretical tools to model the structure and vibrational spectra of ion-water clusters. Obtaining vibrational spectra of large ion-water clusters from normal mode analysis (NMA) is a challenge due to the required computational cost, and has limitations due to anharmonic effects that cannot be addressed by usual NMA. Anharmonic corrections to NMA results are even more challenging for nanodroplets due to the drastically increased computational cost of typical correction methods.⁷⁶ Vibrational spectra can be evaluated beyond the harmonic approximation from molecular dynamics (MD) simulations,^{8, 11} where the relative intensity of the fundamental vibrational bands is computed from the Fourier transform of the autocorrelation function of the total dipole moment of the model system. Bands are naturally broadened due to inclusion of dynamical and thermal effects within the classical limit.

CPMD and SCC-DFTB. In recent years, Car-Parrinello molecular dynamics (CPMD) techniques based on density-functional theory (DFT) have been widely used to compute vibrational spectra of small molecular species in the gas phase and in aqueous solution.^{8, 9, 11, 77-79} The reliability and accuracy of the vibrational spectra obtained with this scheme have been shown to be satisfactory. However, the computational requirements increase drastically for nanodroplets in the gas phase when traditional, popular planewave basis sets are used for such studies. In contrast, methods based on semi-empirical or approximate first-principles quantum chemistry can achieve a better compromise between accuracy and computational requirements. To investigate sulfate-water clusters of small to medium size using a consistent and practical method, we explore the use of approximate DFT models, such as the self-consistent charge density-functional tight-

binding (SCC-DFTB) method, which has been shown to be 2~3 orders of magnitude more efficient than more rigorous DFT while still yielding acceptable predictions.^{35, 38, 80} In fact, a recent study has shown that DFTB models could be a good choice for investigating large seeded water droplets.⁴²

Objectives, method and outcomes of this work. The main objective of this work is to investigate the structure and vibrational spectra of sulfate-water clusters with SCC-DFTB models. The SCC-DFTB model must first be validated against DFT and experimental results on the basis of molecular geometries, interaction energies and vibrational frequencies of small sulfate-water clusters, $\text{SO}_4^{2-}(\text{H}_2\text{O})_n$, $n=1\sim 6$. Then MD simulations of larger nanodroplets, $\text{SO}_4^{2-}(\text{H}_2\text{O})_n$, $n=20\sim 108$, are performed at temperatures of 120K, 150K, 250K to obtain structural features and vibrational spectra. This article is organized as follows. The simulations procedure of vibrational spectra based on MD simulations with SCC-DFTB is outlined in the next section. Validation results of the SCC-DFTB model and simulation results of sulfate-water nanodroplets represented in a third section, while conclusions follow in the last section.

3.2. Computational details

3.2.1. SCC-DFTB models

The SCC-DFTB model is an approximate quantum-chemistry method based on DFT and the tight-binding model.³⁴ Latest versions of the model involve an expansion of the DFT total energy in terms of charge density fluctuations around the charge density of a reference state, which is usually the electron density of neutral atoms, and the second-order expansion of the SCC-DFTB model, referred to as DFTB2,⁸¹ is formulated as

$$E^{DFTB3} = \sum_i^{OCC} \langle \psi_i | \hat{H} | \psi_i \rangle + E^{rep} + \frac{1}{2} \sum_{ab} \gamma_{ab} \Delta q_a \Delta q_b \quad (3.1)$$

while the third-order expansion of the SCC-DFTB model, referred to as DFTB3,³⁵ is formulated as

$$E^{DFTB3} = \sum_i^{OCC} \langle \psi_i | \hat{H} | \psi_i \rangle + E^{rep} + \frac{1}{2} \sum_{ab} \gamma_{ab} \Delta q_a \Delta q_b + \frac{1}{3} \sum_{ab} \Gamma_{ab} \Delta q_a^2 \Delta q_b \quad (3.2)$$

where the first term in the right-hand side sums up orbital energies, obtained with an Hamiltonian operator constructed on the basis of a given reference density and the single-electron wave functions ψ_i are represented as linear combinations of Slater-type atomic orbitals.

The second term, E^{rep} , describes the short-range repulsion potential and is defined as

$$E^{rep} = \frac{1}{2} \sum_{ab} V_{ab}^{rep} [\rho_a^0, \rho_b^0, r_{ab}]$$

where V_{ab}^{rep} is the repulsion potential between atoms a and b , ρ_a^0 and ρ_b^0 are the reference densities of atoms a and b , respectively, and r_{ab} is the distance between atoms a and b .

The third term represents the second-order expansion of the total energy with respect to the atomic charge fluctuation, where $\Delta q_a = q_a - q_a^0$ and $\Delta q_b = q_b - q_b^0$ are atomic charge fluctuations calculated using Mulliken's scheme in a self-consistent manner. γ_{ab} is the "chemical hardness" of atoms, defined as

$$\gamma_{ab} = \frac{1}{r_{ab}} - S_{ab} \times f_{ab}, f_{ab}$$

$$= \begin{cases} \exp \left[- \left(\frac{U_a + U_b}{2} \right)^\zeta r_{ab}^2 \right], & \text{if } (a \text{ or } b = H) \\ 1, & \text{else} \end{cases}$$

where S_{ab} is an exponentially decaying short-range function. f_{ab} is the dumping function introduced to correct the hydrogen-bonding interaction. U_a and U_b are the atomic Hubbard parameters of atoms a and b , respectively. Further details are described in detail in ref 81.

The fourth term is the third-order expansion of the total energy with respect to the atomic charge fluctuation. Γ_{ab} is the coefficient describing the change of γ_{ab} with respect to atomic charge variation, which is defined as the derivatives of γ_{ab} function with respect to atomic charges.

The DFTB model is an approximation model to DFT according to the following simplification strategies. First, only valence electrons are considered in the energy calculation and core electrons are represented via an effective potential. Secondly, a minimal number of Slater-type orbitals is used to represent the location of valence electrons. Thirdly, the computation of orbital energies is simplified by using the Slater and Koster formalism with tabulated matrix elements over orbitals. In this work, the 3OB set of Slater-Koster parameters, which has been designed for typical organic and biological compounds,^{82, 83} is used. Other relevant parameters such as the atomic Hubbard parameters or hydrogen bonding correction for DFTB2 and DFTB3 are taken from ref 83.

3.2.2. MD Simulations

To generate the trajectories necessary for the computation of vibrational spectra, MD simulations based on DFTB3/3OB are performed. The simulated systems include $\text{SO}_4^{2-}(\text{H}_2\text{O})_n$, $n=1\sim 6, 20, 36, 48, 60, 80, 100$ in the gas phase. Initial cluster configurations were prepared by keeping the sulfate ion in the center of the cluster and adding water molecules in a sequential

manner to the surface of the cluster with their hydrogen atoms pointing to the nearest water molecule oxygen atoms to form hydrogen bonds. All simulations involve an equilibration stage with a thermostat, followed by a production run at constant energy. At the equilibration stage, the system is relaxed until the total potential energy and temperature are fluctuating around a stable value, which normally happens within the span of 50 ps. In the production run, simulations are performed for another 50 ps to generate the trajectories of the total dipole moment. In all of the simulations, a timestep of 20 atomic unit (~ 0.48 fs) is used since it was found sufficiently small to maintain the stability of the simulations (based for instance on total energy conservation). Moreover, this value is much smaller than the timescale of the highest-frequency atomic vibration in the system, i.e. the OH stretch of the water molecules at 3700 cm^{-1} (~ 10 fs). The velocity Verlet algorithm⁶⁶ is employed to integrate the equations of motion, together with the Andersen thermostat scheme⁸⁴ when needed. All MD simulations are performed with the code DFTB+.⁸⁵

3.2.3. *Vibrational spectra*

The absorption coefficient is computed from the Fourier transform of the autocorrelation function of the total dipole moment⁸⁶, which takes the following form:

$$\alpha(\omega)n(\omega) = \frac{2\pi\beta\omega^2}{3cV} \int_{-\infty}^{+\infty} dt \cdot e^{-i\omega t} \langle \boldsymbol{\mu}(0) \cdot \boldsymbol{\mu}(t) \rangle \quad (3.3)$$

in which $\alpha(\omega)$ is the absorption intensity with respect to the vibrational frequency or wavenumber ω , $n(\omega)$ is the frequency-dependent refractive index of the medium ($n(\omega) = 1$ is used in this work), c is the speed of light in vacuum, V is the volume (set to be 1 in this work) $\beta = 1/kT$ with T the average temperature and k the Boltzmann constant, $\boldsymbol{\mu}$ is the dipole moment, and the brackets indicate an ensemble average over the time span of the simulations.

The resolution of the spectra is determined by the time span of the conformational sampling. In this work, the last 20 ps of the trajectories of the dipole moment are used to compute the spectra, which gives a resolution of 1.65 cm^{-1} . To reduce noise in computed spectra, trajectories are split into 2 sets and spectra are taken as the average of the resulting spectra from both data sets, with a resolution of 3.3 cm^{-1} , which is sufficient for the purpose of our investigation.

A quantum correction factor is added to the above formula to take the effects of quantum nuclear motion on the band shape into account. Among various quantum correction factors proposed¹⁸, the factor often referred to as the “harmonic correction”¹⁸ factor satisfies both the detailed balance and the fluctuation-dissipation theorem, and takes the following form,

$$Q_{\text{harmonic}} = \frac{\beta \hbar \omega}{1 - e^{-\beta \hbar \omega}} \quad (3.4)$$

The spectra were then smoothed using a Gaussian smoothing scheme, i.e. by replacing each signal data with a Gaussian kernel function.⁶⁷ Each data point is multiplied by a Gaussian kernel function

$$g(\omega) = \frac{1}{\sigma \sqrt{2\pi}} e^{-(\omega - \omega_0)^2 / 2\sigma^2} \quad (3.5)$$

in which ω is the frequency, σ is the full width at the half maximum (FWHM) of the distribution. In this work, σ is set to 20 cm^{-1} .

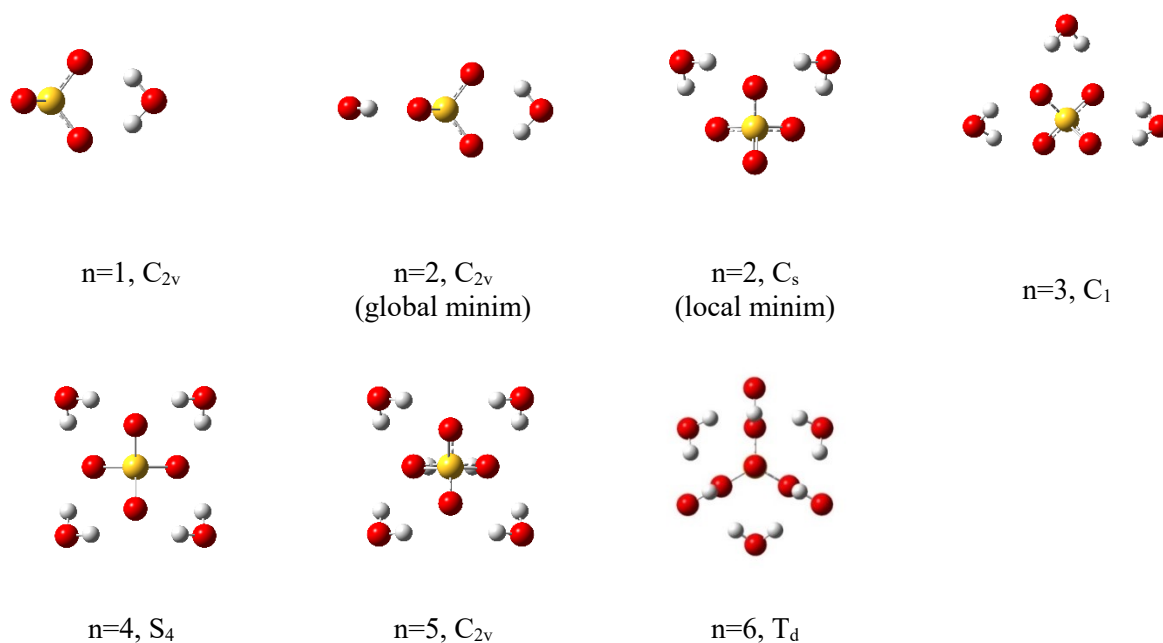


Figure 3.1. Selected sulfate-water clusters $SO_4^{2-}(H_2O)_n$ investigated in this work.

3.3. Results and discussions

3.3.1. Validation of DFTB Models

To validate the reliability of DFTB models in describing the interaction between the sulfate ion and water molecules, molecular geometries, binding energies and vibrational frequencies predicted by DFTB for selected $SO_4^{2-}(H_2O)_n$ clusters ($n=1, 2, 3, 6$) are compared to those obtained from high-level *ab initio* quantum chemistry.

3.3.1.1. Molecular Geometries

Selected intermolecular geometrical parameters, i.e. the distance between the S atom of the sulfate ion and the O atom of the water molecules, are collected in **Table 3.1**. All DFTB models

satisfactorily reproduce not only the symmetry of the ground-state cluster structure but also the distance between sulfate and water molecules. The largest average deviation is only -4% for DFTB3/MIO, while that for DFTB2/MIO and DFTB3/OB is only -3%. This systematic underestimation of intermolecular distances is consistent with previous reports.⁴²

3.3.1.2. Binding Energies

Total cluster binding energies, calculated as the energy difference between the whole cluster and its individual constituent species are listed in **Table 3.2** for selected clusters. Compared to MP2 results, all DFTB models overestimate the binding between sulfate and water molecule(s). Again, DFTB3/MIO gives the largest error, as high as 15%, while DFTB2/MIO and DFTB3/OB results exhibit average deviations of only 5% and 7%, respectively.

Table 3.1 Selected geometrical parameter of $\text{SO}_4^{2-}(\text{H}_2\text{O})_n$ calculated by various methods: Intermolecular sulfate-water distance $r_{\text{S-O}}$

		MP2/aug-cc-pVDZ	DFTB2/MIO	DFTB3/MIO	DFTB3/OB
n=1	C_{2v}	3.376	3.284	3.261	3.277
n=2	D_{2d}	3.384	3.382	3.261	3.283
	C_s	3.399	3.290	3.270	3.296
n=3	C_2	3.409	3.292	3.267	3.305
		3.428	3.304	3.283	3.324
n=6	T_d	3.491	3.339	3.317	3.365
Average Deviation From MP2 results			-3%	-4%	-3%

Unit: Å

3.3.1.3. Vibrational Spectra and Frequencies

The performance of DFTB models in predicting vibrational properties of sulfate-water clusters is examined on the basis of harmonic frequencies of selected clusters from normal modes analysis and comparison to those from high-level ab initio results. Vibrational spectra are also obtained from MD simulations, and the frequencies of all modes are compared to ab initio anharmonic results (CC-VSCF with MP2/TZP) and experimental IRMPD results. Frequencies are listed in supplementary Table S1~S5 for selected active modes (OH stretch, bend, and libration of water molecules, SO₄ stretch, SO₄ bend), while comparison of experimental and simulated spectra in the region of 500~1800 cm⁻¹ is provided in **Figure 3.2**.

OH stretch. Calculated reference frequencies of the OH stretch are in the region of 3600~3700 cm⁻¹, with a slight blueshift upon cluster size increase. Significant anharmonic effects are revealed for these modes by CC-VSCF calculations, resulting in a typical ~200 cm⁻¹ decrease in frequencies. DFTB models predict a similar distribution of frequencies but in a lower and broader region, 3200~3500 cm⁻¹. According to MD simulation results, anharmonicity typically

Table 3.2. Selected SO₄²⁻(H₂O)_n Cluster Binding Energies

		MP2/aug-cc-pVDZ		DFTB2/MIO	DFTB3/MIO	DFTB3/OB
		No BSSE	BSSE			
n=1	C _{2v}	29.5	27.3	29.0	32.1	29.7
n=2	D _{2d}	56.4	52.3	54.7	59.9	56.0
	C _s	56.0	51.8	54.7	60.0	55.9
n=3	C ₂	80.3	74.3	77.6	84.6	79.4
n=6	T _d	140.2	128.8	134.1	143.6	137.0
Average Deviation				5%	15%	7%

Unit: kcal/mol

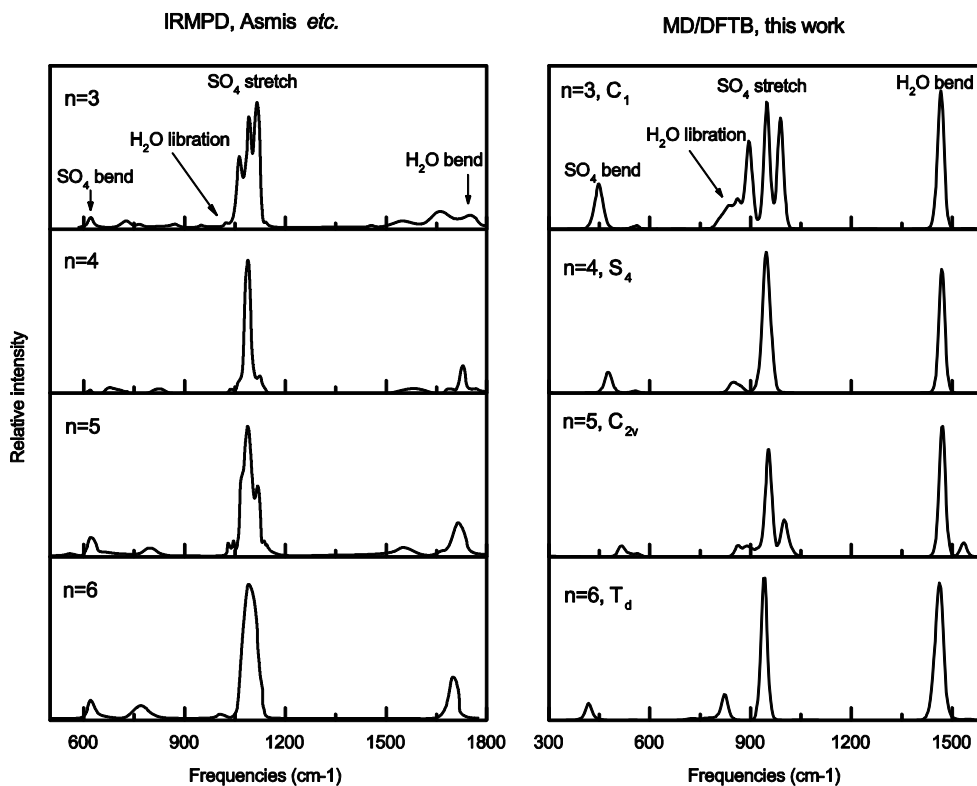


Figure 3.2. Vibrational spectra of sulfate water clusters, $\text{SO}_4^{2-}(\text{H}_2\text{O})_n$, $n=3, 4, 5, 6$. **(Left)** Experimental IRMPD results taken from ref. ²⁷ The temperature of the ion trap is reported to be 17K. **(Right)** Theoretical results obtained from MD simulations with DFTB3/OB at 20K.

lowers frequencies by $\sim 150 \text{ cm}^{-1}$. DFTB3 seems to exhibit the best performance in this region since DFTB2 frequencies are even lower by $\sim 100 \text{ cm}^{-1}$. We note that DFTB models predict frequencies of asymmetric modes typically larger than those of symmetric modes by 150 cm^{-1} , while the relative order is reversed in the reference ab initio data and the difference in frequencies is much smaller, typically $\sim 20 \text{ cm}^{-1}$.

H₂O bend. Experimental results and reference calculations show that the bend frequencies are near 1700 cm^{-1} , with a slight but definite redshift upon cluster size increase. The anharmonic

correction revealed by CC-VSCF calculations lowers the frequencies by 30cm^{-1} . A similar redshift upon cluster size increase is reproduced by DFTB models, with very close amplitude. Anharmonic corrections calculated from MD simulations also agree with those inferred from reference data. However, DFTB models underestimate the frequencies by about 230 cm^{-1} , with values centered at $\sim 1470\text{ cm}^{-1}$. DFTB2 performs slightly better for these modes.

H₂O libration. Libration of water molecules in selected clusters show up as weak and broad bands near $770\sim 860\text{ cm}^{-1}$. Ab initio harmonic frequencies exhibit a redshift upon cluster size increase. Anharmonic effects revealed by CC-VSCF calculations are significant in the larger clusters and result in higher frequencies due to coupling with the SO₄ stretch. DFTB models successfully reproduce all the above features with negligible absolute error.

SO₄ stretch. The SO₄ stretch bands near 1090 cm^{-1} are the most intense bands in the spectral region of interest and are deemed as the signature of different cluster conformers.⁷⁵ According to reference ab initio data, the position of the band is insensitive to cluster size and anharmonic effects are not significant. DFTB3 achieves excellent agreement with ab initio predictions, with a moderate underestimation of the frequencies by $\sim 100\text{ cm}^{-1}$. However, the DFTB2 model predicts very poor frequencies, underestimated by as much as $\sim 400\text{ cm}^{-1}$, likely due to an inadequate parameterization of the S-O atom pair interaction for the system of interest.

SO₄ bend. Frequencies of the SO₄ bend modes centered at 630 cm^{-1} provide another indication of the success of DFTB models. The redshift upon cluster size increase and negligible anharmonic effects are reproduced by both DFTB models. Frequencies are found to be underestimated with an average absolute error of $\sim 80\text{ cm}^{-1}$.

Band shape. Inspection of **Figure 3.2** reveals that DFTB3 successfully reproduces several key features of the experimental spectra. It predicts four well-defined bands in the proper order, and the features of the SO₄ stretch signature bands, i.e. the triplet for n=3, singlet for n=4, doublet for n=5, and singlet for n=6. The H₂O bend bands are incorrectly predicted to be too intense, possibly due to an excess electrons transfer for bend mode.

3.3.2. Structure and vibrational spectra of medium-size sulfate-water clusters

To investigate the effect of the central ion on the structure and dynamics of the surrounding water molecules, MD simulations of medium-size sulfate-water droplets were performed with DFTB3/OB. The cluster sizes for SO₄²⁻(H₂O)_n were selected to be n = 20, 36, 48, 60, 80, 100, based on the balance between sufficient conformational sampling and computational cost. Clusters of these sizes have been investigated experimentally by Williams and co-workers using the IRMPD technique,²⁹ which enables a thorough comparison between experimental and simulated spectra. Finally, temperature effects have also been considered, by performing simulations at three different temperatures, 120K, 150K, and 250K. The melting temperature of ion-water clusters is thought to lie near 200K, though variations may be found for different ionic species and cluster sizes.⁸⁷ The above selection of temperatures would thus cover the “frozen” and “melted” region.

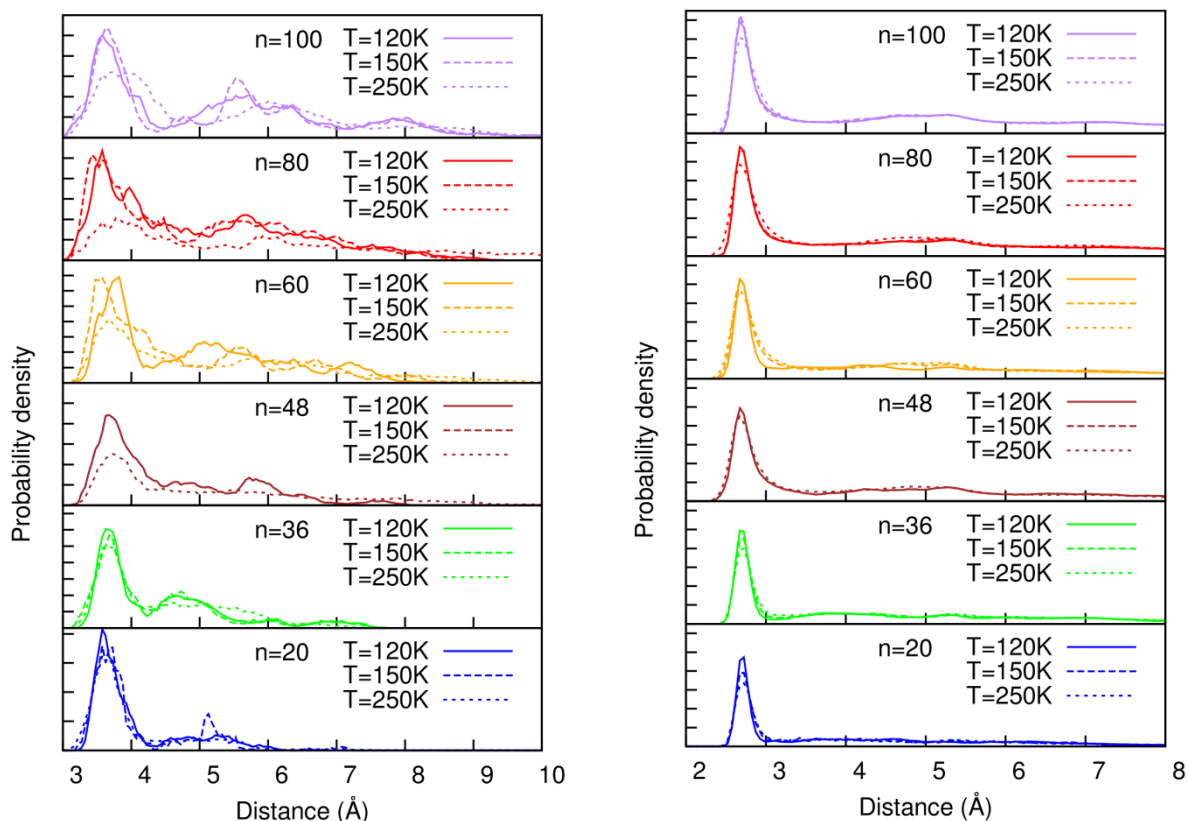


Figure 3.3. Selected structural properties of for $\text{SO}_4^{2-}(\text{H}_2\text{O})_n$ clusters. **(Left)** Radial distribution function of the sulfate S atom distance from the O atoms of the water molecules. **(Right)** Radial distribution function of O-O distances in water molecules.

3.3.2.1 Cluster Structural Properties

Radial distribution functions (RDFs) of the ion-water and water-water coordinates in sulfate-water clusters of varying size are shown in **Figure 3.3**. The former RDF clearly suggest a hydration shell structure in clusters of all sizes. The first peak in the RDF identifies the first hydration shell, at an average position of 3.6 Å (**Figure 3.3 - left panel**). A weak peak at 4.8 Å is found for $n=20$, 36, 48, indicating that the number of water molecules may not be sufficient to form a second hydration shell. For $n=80$ and 100, the second hydration shell seems to be complete and centered at ~ 5.7 Å, while ending at ~ 7 Å. For $n=60$, the position of the second hydration shell varies with

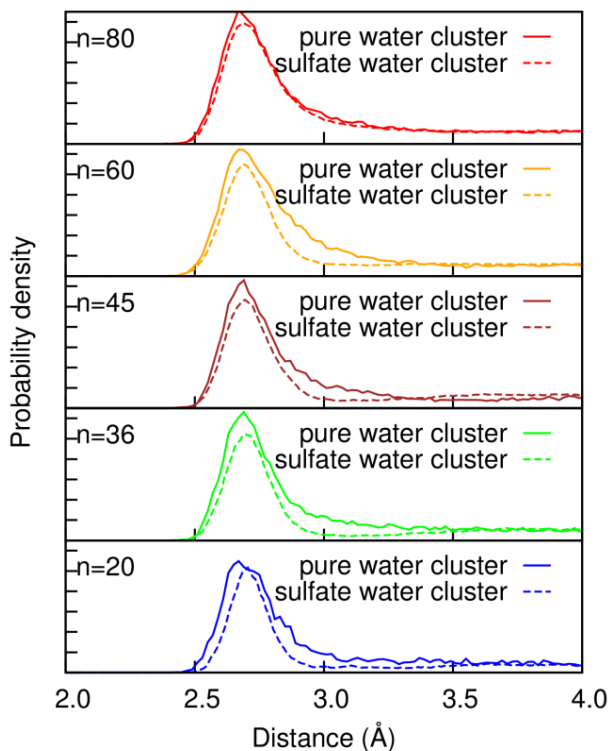


Figure 3.4. Radial distribution function of O-O atoms of pure water clusters and sulfate-water clusters at 120K.

temperature, but a clear peak centered at 5.2 Å can be determined at the low temperature $T=120\text{K}$. As temperature increases, the hydrations shells are much broader, with less pronounced peaks, especially for clusters whose size is larger than 48 at 250K, indicative of gradual melting. In comparison, no melting is observed for clusters of size $n=20$ and 36 at the temperatures investigated.

The intermolecular water-water RDFs shown in **Figure 3.3 - right** panel describe the structure of the water molecules surrounding the central ion. For all simulated systems, only one significant peak can be distinguished, reflecting the hydrogen-bond network structure of the solvent. The peak appears to slightly broaden and shift to large values with cluster size increase, suggesting that the hydrogen-bond network becomes slightly less structured due to the complex

interaction between an increasing numbers of molecules. Finally, to further investigate the effects of the ion on the hydrogen-bond network, the water-water RDFs of sulfate-water clusters and pure water clusters of the same size at T=120K are compared in **Figure 3.4**. The first peaks in the sulfate-water cluster RDFs are all lower than that of the pure-water clusters because that the presence of the sulfate ion decrease the density of the water molecules. However, they are narrower than those for pure water clusters, suggesting that the presence of the sulfate ion causes the hydrogen-bond networks to be more structured, and providing evidence of the “structure-making” effect of the central ion, as described in the literature.^{22, 69}

3.3.2.2. Vibrational spectra

The vibrational spectra obtained from MD simulations of sulfate-water clusters with DFTB3/OB are shown in Figure 5, with particular emphasis on the OH stretch region (3000-4000 cm^{-1}) for comparison with experimental results reported by Williams and co-workers. The correlation spectra of single water molecules located at the surface and buried in the droplet are also shown for perspective and discussion of the “free” water molecule OH stretch band previously hypothesized.

The OH stretch region is characterized by a broad band ranging from 3000 to 3800 cm^{-1} in the simulated spectra of $\text{SO}_4^{2-}(\text{H}_2\text{O})_n$ at all cluster sizes, which corresponds to the symmetric and asymmetric stretches of the OH bonds of water molecules. There is a slight discrepancy in the band position, with a band centered at around 3500 cm^{-1} in the simulated spectra while the band is centered at 3420 cm^{-1} in the experimental spectra. The discrepancy is not too surprising due to the approximate form of the DFTB models and is certainly within the error bars on frequencies reported in the validation section.

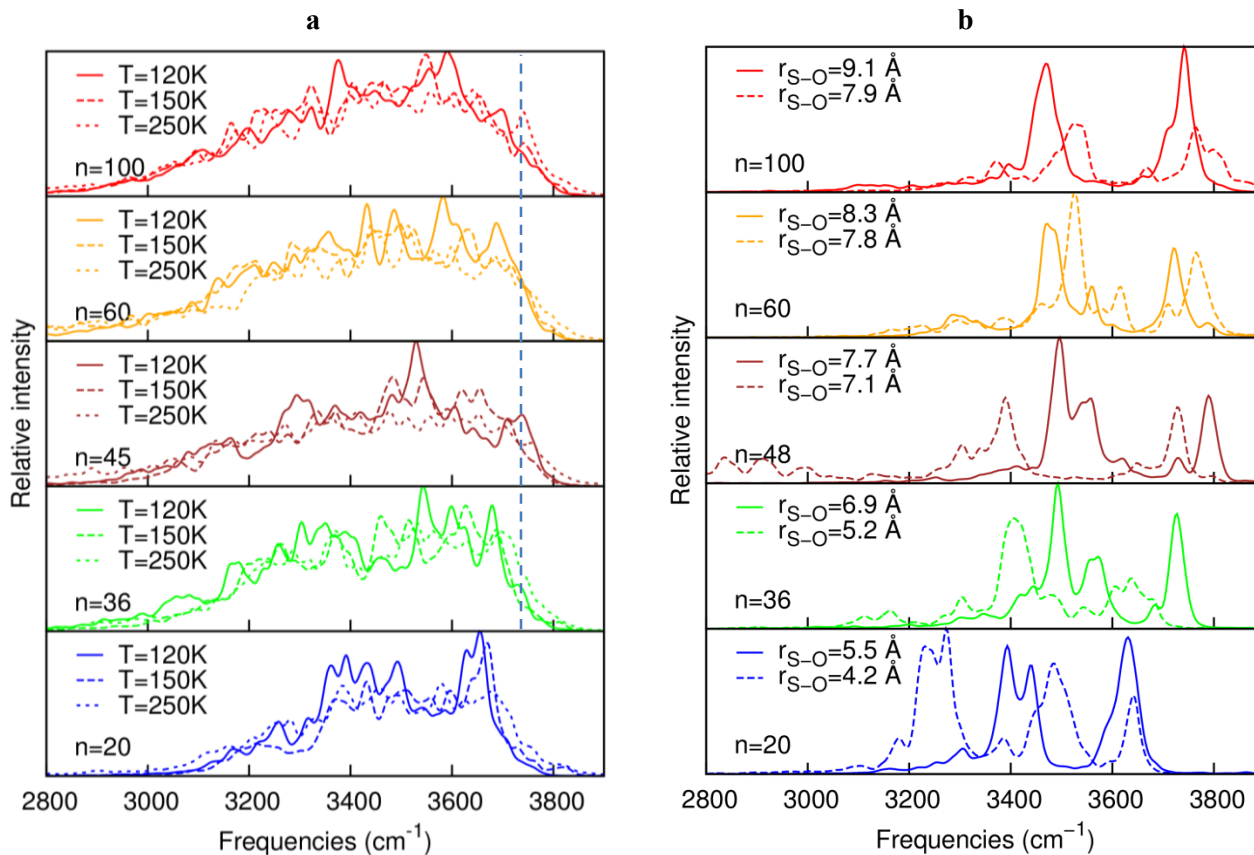


Figure 3.5. Simulated spectra of sulfate-water clusters of varying size from MD simulations with DFTB3/OB. a) Vibrational spectra at T=120, 150 and 250K. b) Correlation spectra of an individual water molecule at the cluster surface at T=120K.

The simulated band shape is in excellent agreement with experimental results, reproducing in particular the following features: (1) the intense shoulder near 3650 cm⁻¹ is consistent with the shoulder at 3550 cm⁻¹ observed in the experimental spectra, which is assigned to the asymmetric stretch mode of water molecules; (2) there are several bands centered near 3400 cm⁻¹, which can be assigned to the symmetric stretch mode of the water molecules and become more intense upon cluster size increase, a trend also found in experimental spectra; (3) a weak band emerges near 3720 cm⁻¹ in simulated spectra for n=45, 60, 100, a band that can be assigned to the free OH stretch of water molecules at the surface of the droplet and is analogous to that found in experimental

spectra near 3700 cm^{-1} for cluster sizes larger than 47. In summary, the computed spectra reproduce all the major features of the experimental spectra.

Vibrational correlation spectra of selected water molecules (Figure 5b) clearly show that the OH stretch band shifts to higher frequencies with cluster size increase ($n>36$). Furthermore, the outer right branch of the OH stretch reach 3720 cm^{-1} as water molecules locate towards the surface of the sulfate-water cluster, consistent with the assignment of the band to the free OH stretch modes of water molecules in the simulated and experimental spectra. In particular, the outer right branch of the band shifts over to 3720 cm^{-1} only for water molecules with S-O distances larger than 7 \AA , indicating that water molecules at the surface can be considered “free” of the ion influence only when they are beyond this distance from the central ion. This threshold distance of 7 \AA is also consistent with the RDFs of Figure 3, which do not exhibit significant structural features beyond 7 \AA . Thus the effects of the sulfate ion on the structure and dynamics of water are confined to a distance of 7 \AA in the sulfate-water droplets investigated, which corresponds roughly to two hydration shells.

3.4. Summary and conclusions

The structure and vibrational dynamics of sulfate ion seeded aqueous droplet has been investigated by first-principles-based simulations. The reliability and performance of the DFTB3 model combined with the OB2 parameter set has been shown to be satisfactory when compared to the results of high level *ab initio* quantum-chemistry data and available experimental results, DFTB models are able to reproduce the main geometric features of small $\text{SO}_4^{2-}(\text{H}_2\text{O})_n$ clusters, $n=1\sim 6$, with an average deviation smaller than 5%. Binding energies are also well reproduced, with an average error within 10%. For vibrational frequencies obtained from both normal mode

analysis and MD simulations, the DFTB models successfully reproduce cluster size-dependent effects and anharmonic effects, with an acceptable absolute error. This is consistent with previous validation of the model based on a systematic evaluation of small water clusters containing polyatomic anions of the Hofmeister series.⁴²

The DFTB model is then used to investigate the structure and vibrational dynamics of medium size sulfate-water droplets with a number of water molecules ranging from 20 to 100. The simulated vibrational spectra are consistent with those reported from IRMPD experiments by Williams and co-workers. The OH stretch region is of particular interest due to the reported size-dependent signature of the free OH band in experimental spectra. Comparison of simulated vibrational spectra and correlation spectra of specific water molecules at the surface of the cluster allows to demonstrate unambiguously how OH bands of water molecules blueshift upon increase of their distance from the central sulfate ion and how the outer right OH stretch feature that emerges upon cluster size increase can indeed be assigned to the OH stretch of free water molecules at the surface of larger droplet, as speculated before

Comparison of the radial distribution functions of sulfate-water clusters and pure water clusters reveals a clear “structure making” effect, i.e. effects as a kosmotropic ion. Finally, combined analysis of both structural properties and vibrational dynamics suggests that the effects of the sulfate-water interaction on the structure of the water molecules surrounding the central ion is confined to a distance of 7 Å, i.e. roughly two hydration shells. This work further demonstrates that approximate first-principles-based simulation methods such as MD with DFTB models, once properly validated, are a promising tool to investigate complex and fluxional systems such as seeded aqueous droplets, their structural and thermodynamic properties, as well as their spectroscopic features for crucial connection with experiment.

Supporting information

Calculated vibrational frequencies for selected sulfate-water clusters.

Table 3.3. Vibrational frequencies of the OH stretch in $\text{SO}_4^{2-}(\text{H}_2\text{O})_n$, $n=1\sim 3$

		Harmonic*	Anharmonic*	Harmonic	Harmonic	MD
		MP2/TZP	CC-VSCF	DFTB2/MIO	DFTB3/OB	DFTB3/OB
n=1, C_{2v}	OH stretch, sym.	3592	3286	2997	3333	2981
	OH stretch, asym.	3541	3039	3213	3153	3064
n=2, D_{2d}	OH Stretch, sym.	3641	3291	3108	3212	3070
	OH Stretch, asym.	3617	3118	3358	3422	3430
	OH Stretch, asym.	3617	3118	3358	3422	3250
n=2, C_s	OH Stretch, sym.	3654	3367	3171	3262	3381
	OH Stretch, sym.	3644	3382	3123	3225	3197
	OH Stretch, asym.	3625	3348	3382	3452	3232
	OH Stretch, asym.	3617	3332	3365	3431	3287
n=3, C_1	OH stretch, sym.	3698	3414	3258	3336	
	OH stretch, asym.	3691	3396	3461	3524	3287
	OH stretch, sym.	3687	3545	3200	3292	
	OH stretch, sym.	3683	3463	3196	3285	3411
	OH stretch, asym.	3679	3380	3442	3505	
	OH stretch, asym.	3675	3410	3451	3498	

* Taken from Ref 75

Unit: cm^{-1}

Table 3.4. Vibrational frequencies of the H₂O bend in SO₄²⁻(H₂O)_n, n=1~6

		Harmonic*	Anharmonic*	Harmonic	Harmonic	MD
	EXP	MP2/TZP	CC-VSCF	DFTB2/MIO	DFTB3/OB	DFTB3/OB
n=1, C _{2v}	--	1765	1701	1491	1494	1492
n=2, D _{2d}	--	1764	1712	1570	1509	1470
	--	1753	1705	1511	1475	1470
n=2, C _s	--	1771	1722	1584	1520	1519
	--	1747	1706	1516	1470	1455
n=3, C ₁		1770	1727	1609	1531	
	1735	1746	1711	1530	1478	1471
		1738	1699	1528	1468	
n=4, S ₄	1714	1768	--	--	1477	1470
n=5, C _{2v}		1732	--	--	1478	1467
	1705	1732	--	--	1473	1465
n=5, C _s		1732	--	--	1473	1465
n=6, T _d	1700	1700	--	--	1474	1462

* Taken from Ref 75

Unit: cm⁻¹

Table 3.5. Vibrational frequencies of the H₂O libration in SO₄²⁻(H₂O)_n, n=1~6

		Harmonic*	Anharmonic*	Harmonic	Harmonic	MD
	EXP	MP2/TZP	CC-VSCF	DFTB2/MIO	DFTB3/OB	DFTB3/OB
n=1, C _{2v}	--	932	930	924	915	945
n=2, D _{2d}	--	891	924	886	867	908
	--	891	924	886	867	
n=2, C _s	--	898	932	902	877	885
	--	878	929	867	862	
n=3, C ₁	862	869	936	874	847	862
		852	913	850	830	
		833	905	823	811	
n=4, S ₄	819	814	--	--	824	849
n=5, C _{2v}	792	782	--	--	792	863
		782	--	--	785	826
n=6, T _d	770	734	--	--	737	730

* Taken from Ref 75

Unit: cm⁻¹

Table 3.6. Vibrational frequencies of the SO₄ stretch in SO₄²⁻(H₂O)_n, n=1~6

	EXP	Harmonic* MP2/TZP	Anharmonic* CC-VSCF	Harmonic DFTB2/MIO	Harmonic DFTB3/OB	MD DFTB3/OB
n=1, C _{2v}	--	1095	1078	579	1002	1003
	--	1060	1045	600	935	945
	--	1003	986	564	880	860
n=2, D _{2d}	--	1064	1051	522	951	1122
	--	1049	1032	557	947	984
	--	1049	1032	567	927	942
n=2, C _s	--	1056	1037	512	1000	1037
	--	997	981	517	960	970
	--	907	925	857	900	821
n=3, C ₁	1102	1094	1076	559	977	996
	1079	1058	1043	521	940	956
	1052	1016	1000	513	900	950
n=4, S ₄		1061	--	--	940	
	1078	1046	--	--	937	945
		1061	--	--	932	
n=5, C _{2v}		1090	--	--	963	988
		1054	--	--	935	948
	1081	1029	--	--	896	897
n=5, C _s		1080	--	--	964	987
		1041	--	--	945	987
		1061	--	--	912	952
n=6, T _d	1090	1014	--	--	938	942
		1014	--	--	930	942

* Taken from Ref 75

Unit: cm⁻¹

Table 3.7. Vibrational frequencies of the SO₄ bend in SO₄²⁻(H₂O)_n, n=1~6

	EXP	Harmonic* MP2/TZP	Anharmonic* CC-VSCF	Harmonic DFTB2/MIO	Harmonic DFTB3/OB	MD DFTB3/OB
n=1, C _{2v}	--	585	580	495	576	646
	--	580	575	485	572	642
	--	569	566	512	555	552
n=2, D _{2d}	--	591	586	590	581	577
	--	573	569	458	561	561
	--	573	569	445	560	536
n=2, C _s	--	585	580	592	590	578
	--	583	578	536	580	578
	--	567	565	569	552	552
n=3, C ₁		589	585	594	583	563
	613	580	576	567	567	513
		567	565	567	552	513
n=4, S ₄		586	--	--	574	506
	631	586	--	--	568	476
		565	--	--	551	470
n=5, C _{2v}		574	--	--	571	561
		572	--	--	555	543
	628	451	--	--	552	448
n=5, C _s		601	--	--	586	572
		577	--	--	557	513
		572	--	--	554	460
n=6, T _d	626	547	--	--	557	549

* Taken from Ref 75.

Unit: cm⁻¹.

Chapter 4.

**Vibrational Spectroscopy of Guanidinium-Water Clusters
from First-Principles Molecular Dynamics Simulations**

4.1. Introduction

Importance of guanidinium. Guanidinium is a prototypical organic cation that mimics important functional groups present in many biological systems,⁸⁸ organic materials⁸⁹ and ionic liquids⁹⁰. For example, guanidinium salts are powerful protein denaturants, which break down the secondary structure of proteins at moderate concentration. Vibrational spectroscopy is one of the most widely used techniques in probing protein denaturation. The CN stretch of guanidinium is very often taken as a vibrational spectral signature to detect changes of binding states of molecules containing guanidinium groups.^{30, 31, 91, 92}

Issues in vibrational spectroscopic study of protein denaturation. Issues may arise in vibrational spectroscopic studies of protein denaturation as the CN stretch band of the guanidinium cation near 1670 cm^{-1} and that of deuterated guanidinium near 1600 cm^{-1} are very close to the broad amide bands of proteins, such as the amide I near 1650 cm^{-1} and amide II near 1550 cm^{-1} . Overlapping of these bands may cause confusion in the band assignment and spectral interpretation, warranting a complete understanding of the vibrational spectroscopy of guanidinium.

Experimental and theoretical studies. Both experimental and theoretical studies have been reported regarding the solvated states of guanidinium,^{93, 94} guanidinium-protein binding,^{95, 96} and the harmonic frequencies of guanidinium,^{91, 92} unveiling important structural and dynamical information about guanidinium and its interaction with proteins. However, computational vibrational spectroscopy based on normal mode analysis (NMA) of isolated molecules in their ground state is limited in helping interpret experimental spectra. In this work, we develop a technique to compute vibrational spectra from MD simulations and the Fourier transform of the autocorrelation function (FTACF) of the dipole moment. Compared to NMA, the FTACF of the

dipole moment produce broad-band vibrational spectra with appropriate temperature effects beyond the harmonic approximation. However, before applying this method to complicated systems and problems such as chemical denaturation of proteins by guanidinium salts, the accuracy and efficiency of the method must be properly benchmarked.

Selection of models. The Car-Parrinello molecular dynamics (CPMD) method based on planewave DFT has been shown to be a valuable tool in simulating vibrational spectra of aqueous solutions of a number of chemical species.^{1, 10} However, such first-principles approach is limited to a few hundred atoms due to the extensive computational cost associated with the simulations. Alternative models that allow simulations of medium to large-size systems in a more economical fashion are thus desirable.

It has been pointed out that an accurate description of polarizability and many-body effects is crucial in obtaining reliable simulated vibrational spectra.⁹⁷ Thus the non-polarizable classical force fields widely used in simulations of solvated proteins and electrolytes are not suitable to generate vibrational spectra. Polarizable force fields are obviously a better choice, but they are rarely used in computational vibrational spectra due to inherent difficulties in parameterization, tedious validation, questionable transferability and in general their inability to describe possible chemical reactions. On the other hand, first-principles-like simulation methods based on approximate DFT and/or semi-empirical quantum chemistry may provide a very good balance between efficiency and accuracy. Of particular interest is the self-consistent-charge density-functional tight-binding (SCC-DFTB) model, which has been found to be 2~3 orders of magnitude faster than DFT, with only marginal errors in molecular geometries and acceptable errors in

interaction energies.^{38,98} SCC-DFTB harmonic frequencies of hydrated ions were also found to be in good agreement with DFT and ab initio quantum chemistry results.^{41,42}

Objectives of current study and rationalization. In this work, we focus on the vibrational spectral signatures of guanidinium upon hydration and ion association. DFT-based CPMD and DFTB-based Born-Oppenheimer MD⁹⁹ simulation techniques are used to compute vibrational spectra, following a brief validation on the basis of molecular geometries, energetic properties and harmonic frequencies for small complexes. Our aim is not only to evaluate the performance of DFT and DFTB simulations in computing vibrational spectra of systems containing the guanidinium cation, but also to produce converged spectra of guanidinium in aqueous droplets along with an unambiguous and reliable assignment of spectral bands.

4.2. Computational details

Computation of structure and harmonic frequencies. Ground-state structures of small complexes are determined by quantum chemistry calculations, employing either *second-order* Møller–Plesset (MP2) perturbation theory⁴³⁻⁴⁵ or DFT with the Becke-3 parameter Lee-Yang-Parr (B3LYP)⁴⁶⁻⁴⁹ functional together with the 6-311++g(d,p) Gaussian-type basis set.¹⁰⁰ Harmonic frequencies are then calculated through a standard normal mode analysis (NMA). The solvation effects are modeled with a polarizable continuum model (PCM).¹⁰¹ Since semi-local functional such as BLYP^{46,102} and PBE⁶¹⁻⁶³ are widely used in planewave DFT computation, we also put results of this flavor of DFT into comparison. All calculations are performed with the Gaussian 09 software.¹⁰³

DFTB models. DFTB models have been well documented in the literature.^{35, 37, 81, 98} In this work, the SCC-DFTB model based on a third-order expansion of the DFT total energy around a reference density³⁵ is employed together with a parameter set developed and tested against organic and biological systems (3OB),⁴⁰ as the model is hereafter referred to as DFTB3/OB. Born-Oppenheimer MD simulations based on DFTB3/OB are performed to generate trajectories of atomic positions and dipole moment to compute vibrational spectra. Model systems are initially optimized in the ground state, and equilibrated in constant-temperature (NVT) simulations thermostated at the target temperature. From the equilibration run provides initial sets of atomic coordinates and velocities to perform constant-energy (NVE) simulations to produce the desired trajectories of coordinates and dipole moments. The dipole moment is directly computed from atomic charges determined with a Mulliken scheme.¹⁰⁴ For charged species, the contribution of the net charge to the total dipole moment is subtracted. The timestep used in the above simulations is 10 atomic units (~0.24 fs), and the number of steps in the NVT simulations is 10,000 (~2.4 ps), and that in the NVE simulations is 100,000 (~24 ps).

For complexes in the gas phase, internal relaxation of kinetic energy is slow and the simulation time needed to reach a fully equilibrated state is beyond the time span used in this work. Therefore, following the suggestion of Hornicek and co-workers,¹⁶ 10 distinct trajectories are generated for each complex, with each trajectory initiated with a different distribution of atomic velocities sampled randomly with a Box-Muller generator¹⁰⁵ according to a Maxwell-Boltzmann distribution. All MD simulations using DFTB are performed with the DFTB+ code.⁸⁵

Car-Parrinello MD simulations. Vibrational spectra were also obtained from CPMD simulations based on planewave pseudopotential DFT. Several generalized gradient

approximation (GGA) functionals were tested, including Becke's exchange plus Lee-Yang-Parr's correlation functional (BLYP),^{46,99} Becke's hybrid three-parameter nonlocal-exchange functional with the Lee-Yang-Parr correlation functional (B3LYP),⁴⁶⁻⁴⁹ and the Perdew, Burke, and Ernzerhof exchange-correlation functional (PBE).⁶¹⁻⁶³

The simulation protocol is the same as that outlined previously for DFTB. The molecular complexes are optimized in their ground state, equilibrated in NVT simulations maintained at the target temperature by a Nose-Hoover chain thermostat, to finally yield initial conditions for the NVE production runs. The dipole moment along the trajectories is calculated using the Berry Phase scheme.^{106, 107}

The convergence of the energy and harmonic frequencies with respect to planewave cutoff and box size was first examined. For example, for guanidinium, a planewave cutoff of 100 Rydberg, with a 12x12x12 Å cubic box and Tuckerman's Poisson solver,¹⁰⁸ was found to be sufficient to eliminate the interaction between the model system and its periodic images, and obtain converged results. For the guanidinium-chloride and guanidinium-water complexes, the same cutoff could be used with a 13x13x13 Å cubic box. The simulation timestep was set to 4 atomic units (0.096 fs), and the number of steps in the NVT and NVE simulations are 2,000 (~0.2 ps) and 50,000 (~5 ps), respectively. All CPMD simulations as well as geometry optimizations and harmonic frequencies calculations based on planewave DFT are performed with the CPMD software package.¹⁰⁹

Vibrational spectra and averaging, smoothing. Vibrational spectra are computed as the Fourier transform of the autocorrelation function of the total dipole moment as derived from the Fermi golden rule within linear response theory:^{3, 11, 17}

$$\alpha(\omega)n(\omega) = \frac{2\pi\beta\omega^2}{3cV} \int_{-\infty}^{+\infty} dt \cdot e^{-i\omega t} \langle \boldsymbol{\mu}(0) \cdot \boldsymbol{\mu}(t) \rangle \quad (4.1)$$

in which $\alpha(\omega)$ is the absorption intensity with respect to the vibrational frequency or wave number ω , $n(\omega)$ is the frequency-dependent refractive index of the medium [$n(\omega) = 1$ is used in this work], c is the speed of light in vacuum, V is the volume (set to be 1 in this work), $\beta = 1/kT$ with T the average temperature and k the Boltzmann constant, $\boldsymbol{\mu}$ is the dipole moment, and the brackets indicate an ensemble average over the time span of the simulations. To correct for the error in band shape introduced by replacing the quantum time-correlation function with its classical counterpart, a quantum correction factor of the form $\beta\hbar\omega/(1 - \exp(-\beta\hbar\omega))$ is added to the formalism of equation (4.1), which was shown by Gaigeot and co-workers to give the most accurate computed intensities. Quantum correction factors have been discussed thoroughly elsewhere.^{18, 110}

Averaging. To obtain converged spectra, 10 trajectories are generated for each molecule or complex, with different distributions of initial atomic velocities, and the reported spectra are evaluated as the average of the 10 individual spectra generated from the distinct trajectories. Only the simulated DFTB spectra are obtained this way, while CPMD spectra are the result of a single trajectory given the computational cost associated with this approach.

Band assignment. Spectral band assignment is facilitated by computation of the time correlation spectra of modes involving specific internal coordinates or a combination of such coordinates. The calculation of time correlation spectra use the same formula as equation (4.1), but with the dipole moment replaced by the (combined) internal coordinates.

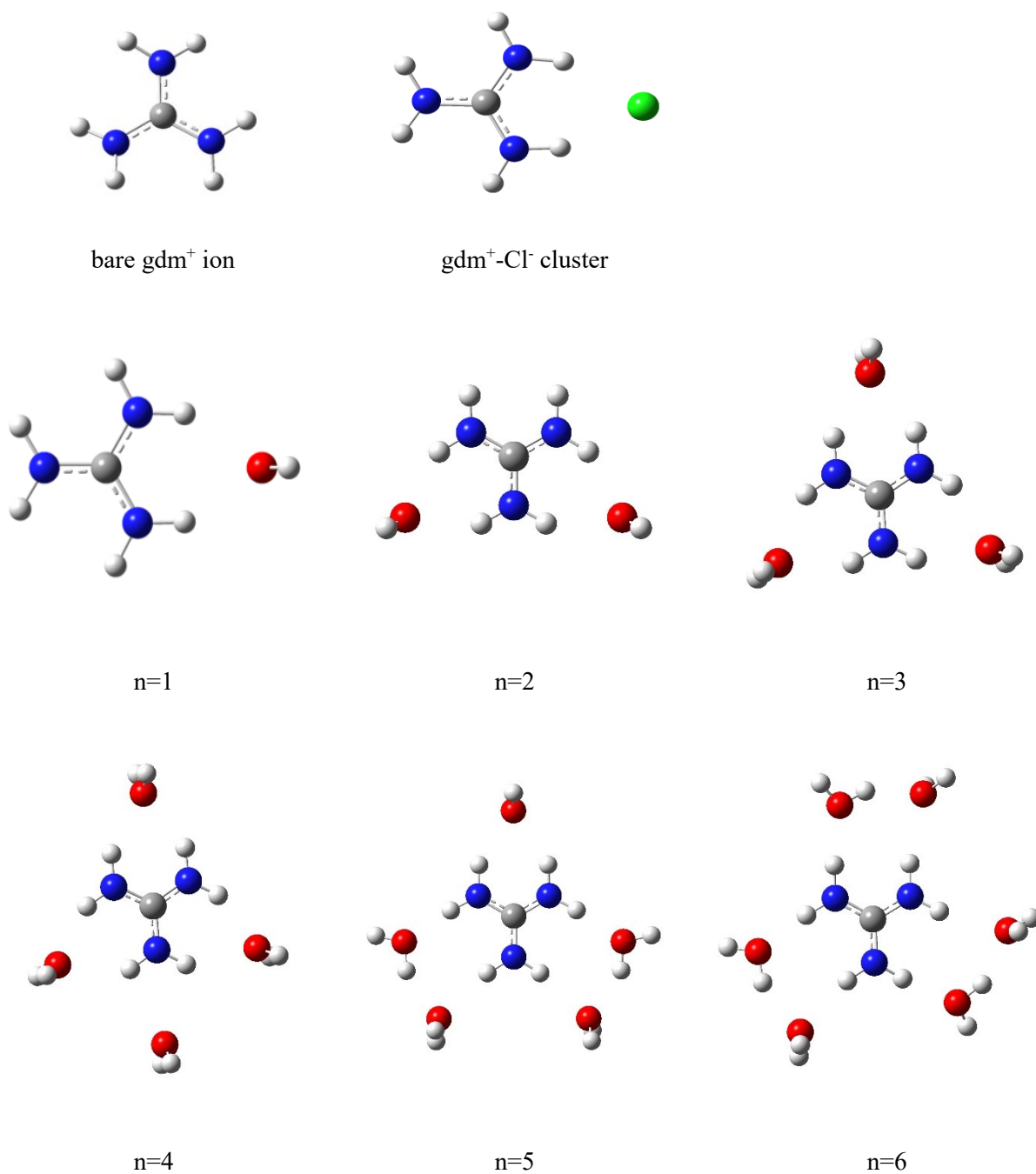


Figure 4.1. Molecular geometries of guanidinium (gdm^+), the guanidinium-chloride complex ($\text{gdm}^+\text{-Cl}^-$), and selected guanidinium-water clusters, $\text{gdm}^+\text{-(H}_2\text{O)}_n$ water clusters investigated in this study. Obtained from B3LYP/aug-cc-pVTZ calculation.

4.3. Results and discussions

4.3.1. Molecular Geometry and harmonic frequencies.

Computed molecular geometry. The molecular geometry and infrared spectra from normal mode analysis have been investigated previously with ab initio quantum chemistry³⁰ and DFT^{31, 91} methods, and guanidinium was reported to be quasi-planar with the H atoms slightly distorted from the molecular plane. The symmetry of the ion optimized geometries was found to vary from C₁ to D_{3h} depending on the model chemistry employed.^{30, 31, 91} Selected geometric parameters and harmonic vibrational frequencies of guanidinium calculated with MP2 and B3LYP with different basis sets are listed in **Table 4.1**. MP2 with a triple-split basis set predicts a highly distorted C₂ planar geometry with an H-N-C-N dihedral angle of 16°, while DFT predicts geometries closer to planar, with an H-N-C-N dihedral angle of 8°.

Table 4.1. Selected molecular geometry and harmonic frequencies of guanidinium calculated by various quantum-chemistry methods.

	B3LYP					MP2		
	3-21G	6-31G	6-31+G(d)	6-31++G(d,p)	6-311++G(d,p)	aug-cc-pVDZ	aug-cc-pVTZ	aug-cc-pVTZ
Symmetry	C ₂	C ₂	C ₁	C ₂	D ₃	C ₁	C ₂	C ₁
dihedral (H-N-C-N)	12.6	13.0	14.0	12.6	12.6	5.0	8.0	16.0
$\nu(\text{CN})$	1614	1654	1646	1640	1630	1634	1628	1670
$\nu(\text{NH})$	2546	2605	2590	2598	2590	2588	2589	2615
$\nu(\text{NH})$	2691	2760	2741	2758	2745	2747	2744	2783

Unit: bond length in Å; vibrational frequency in cm⁻¹.

From the use of basis sets of increasing size, it is seen from **Table 4.1** that a triple-zeta basis set such as aug-cc-pVTZ or 6-311++G(d,p) is needed to obtain converged (B3LYP) harmonic vibrational frequencies. Accordingly, the results calculated with this type of model chemistry are used as reference data hereafter.

Theoretical vs experimental results. Selected geometric and vibrational features of normal and deuterated guanidinium converged with respect to the choice of model chemistry are listed in

Table 4.2. Selected molecular geometry and harmonic frequencies of guanidinium calculated by various quantum-chemistry methods^a

	EXP (aq.)	MP2/Gaussian		DFT/Gaussian			
		MP2	MP2/PCM	hybrid		semi-local	
				B3LYP	B3LYP/PCM	BLYP	PBE
Symmetry		C ₂	C ₁	D ₃	C ₂	C ₁	C ₁
r(C-N)		1.334	1.335	1.335	1.334	1.347	1.341
dihedral (H-N-C-N)		~15.8	10~16	13	~6.7	~15.5	~15.8
gdnH ⁺ v(CN)	1670	1732 (500)	1702 (700)	1702 (467)	1673 (680)	1646 (400)	1663 (430)
v(NH)		3617 (264)	3620 (290)	3583 (230)	3597 (280)	3487 (208)	3512 (218)
		3749 (187)	3746 (216)	3700 (170)	3714 (220)	3600 (145)	3630 (154)
Symmetry		C ₂	C ₁	D ₃	C ₁	C ₁	C ₁
r(C-N)		1.334	1.335	1.335	1.334	1.347	1.341
dihedral(H-N-C-N)		~15.8	10~15	12.6	~6.5	~15.5	~15.7
gdnD ⁺ v(CN)	1600	1670 (403)	1631 (650)	1630 (377)	1602 (623)	1572 (333)	1605 (327)
v(NH)		2615 (211)	2615 (240)	2590 (185)	2600 (230)	2520 (165)	2540 (173)
		2783 (103)	2778 (120)	2745 (94)	2756 (125)	2670 (80)	26924)

^a All calculations are performed with the 6-311++G(d,p) basis set. Intensities of harmonic vibrations are given in parentheses.

Unit: bond length in Å; vibrational frequency in cm⁻¹.

Table 4.2, along with available experimental data Excellent agreement is found between the B3LYP calculated values of 1673 and 1600 cm^{-1} (including solvation) and the experimental ones of 1670 and 1602 cm^{-1} for the CN stretch of normal and deuterated guanidinium, , respectively. In contrast we note that MP2 overestimates these frequencies by ca. 30 cm^{-1} , i.e. 1702 vs 1670 cm^{-1} , and 1631 vs 1600 cm^{-1} . Finally, all semi-local DFT (BLYP, PBE) harmonic frequencies are systematically lower than their hybrid counterparts, but by only 2-3%.

Planewave vs Gaussian DFT. Selected geometric and vibrational features of guanidinium calculated with different implementations of DFT (planewave vs atom-centered Gaussian basis set) are listed in **Table 4.3**. Calculated geometries are in good general agreement, except for the symmetry point group described with the hybrid functional, for which planewave DFT predicts a lower symmetry of C_1 , as opposed to D_3 according to B3LYP/6-311++G(d,p); however, negligible

Table 4.3. Selected molecular geometry parameters and harmonic vibrational frequencies of (deuterated) guanidinium calculated by different implementations of DFT

	DFT/Gaussian			DFT/Planewave		
	hybrid	semi-local		hybrid	semi-local	
	B3LYP	BLYP	PBE	B3LYP	BLYP	PBE
Symmetry	D_3	C_1	C_1	C_1	C_1	C_2
r(C-N)	1.335	1.347	1.341	1.335	1.344	1.339
dihedral(H-N-C-N)	12.6	~15.5	~15.7	~11.3	~11.4	~11.4
$\nu(\text{CN})$	1630 (377)	1572 (333)	1605 (327)	1603 (227)	1552 (216)	1596 (215)
$\nu(\text{NH})$	2590 (185)	2520 (165)	2540 (173)	2583 (98)	2522 (94)	2544 (96)
$\nu(\text{NH})$	2745 (94)	2670 (80)	2692 (84)	2737 (60)	2672 (60)	2697 (60)

Unit: bond length in Å; vibrational frequency in cm^{-1} .

differences are found in the CN bond length. As for harmonic vibrational frequencies, planewave and Gaussian basis set DFT produce highly consistent results, with an average absolute error of only 10 cm⁻¹. Relative intensities are also in very good agreement.

DFTB vs DFT. Selected geometric and vibrational features of guanidinium predicted by DFT and several DFTB models are listed in **Table 4.4**. Inspection of the data reveals that: (1) calculated DFTB geometries are close to their B3LYP counterparts, with a slight overestimation of bond lengths; (2) the calculated CN and NH stretch harmonic vibrational frequencies are also

Table 4.4. Selected molecular geometry parameters and harmonic vibrational frequencies guanidinium calculated by DFT and SCC-DFTB models.

		DFT/gauss		SCC-DFTB	
		B3LYP	DFTB2/MIO	DFTB3/MIO	DFTB3/3OB
		NMA	NMA	NMA	NMA
gdnH ⁺	Symmetry	D ₃	C _{3v}	C _{3v}	C _{3v}
	r(C-N)	1.335	1.345	1.345	1.354
	Dihydral (H-N-C-N)	13	0.03	0.03	0.03
	$\nu_{as}(\text{CN})$	1702 (467)	1703 (153)	1703 (170)	1674 (160)
	$\nu(\text{NH})$	3583 (230)	3542 (3)	3540 (3)	3307 (4)
		3700 (170)	3711 (2)	3706 (3)	3566 (3)
gdnD ⁺	Symmetry	D ₃	C _{3v}	C _{3v}	C _{3v}
	r(C-N)	1.335	1.345	1.345	1.354
	Dihydral (H-N-C-N)	12.6	0.03	0.03	0.03
	$\nu_{as}(\text{CN})$	1630(377)	1643(313)	1644(350)	1609(330)
	$\nu(\text{NH})$	2590(185)	2563(10)	2562(10)	2400(13)
		2745(94)	2750(5)	2746(4)	2571(6)

Unit: bond length in Å; vibrational frequency in cm⁻¹.

in good agreement, except that DFTB3 with the 3OB parameter set systematically underestimates the frequencies (we note that the H/D ratio of frequencies with the 3OB parameter set is as good as for the MIO parameter set); (3) The influence of parameter set on the geometric and vibrational properties is more significant than that of the charge-expansion order of the DFTB model, with the MIO parameter set performing better in this case.

4.3.2. Simulated vibrational spectra

Band assignment. The simulated vibrational spectra of deuterated guanidinium shown **Figure 4.2** will serve as a reference and as a benchmark for our band assignment approach. Both planewave BLYP DFT and DFTB/3OB spectra exhibit 3 intense bands with different relative intensities. To aid in the band assignment, time-correlation spectra of several vibrational modes are also shown in **Figure 4.2**. The time-correlation spectra for the symmetric CN stretch $\nu(\text{CN})_s$, is calculated for the combination of internal coordinates $r_{\text{CN1}}+r_{\text{CN2}}+r_{\text{CN3}}$, where r_{CN1} , r_{CN2} and r_{CN3} are the bond lengths of the three CN bonds of guanidinium, respectively; that for the antisymmetric CN stretch, $\nu(\text{CN})_{\text{as}}$, is obtained as the average of three time-correlation spectra calculated for the combinations $r_{\text{CN1}}-r_{\text{CN2}}$, $r_{\text{CN2}}-r_{\text{CN3}}$ and $r_{\text{CN3}}-r_{\text{CN1}}$; that for the symmetric NH stretch, $\nu(\text{NH})_s$, is obtained as the average of three time-correlation spectra calculated for the combinations $r_{\text{NH1}}+r_{\text{NH2}}$, $r_{\text{NH3}}+r_{\text{NH4}}$ and $r_{\text{NH5}}+r_{\text{NH6}}$, where $r_{\text{NH1-6}}$ are the bond lengths of the three pairs of NH bonds; that for the antisymmetric NH stretch, $\nu(\text{NH})_{\text{as}}$, is obtained as the average of three time correlation spectra calculated for the combinations $r_{\text{NH1}}-r_{\text{NH2}}$, $r_{\text{NH3}}-r_{\text{NH4}}$ and $r_{\text{NH5}}-r_{\text{NH6}}$.

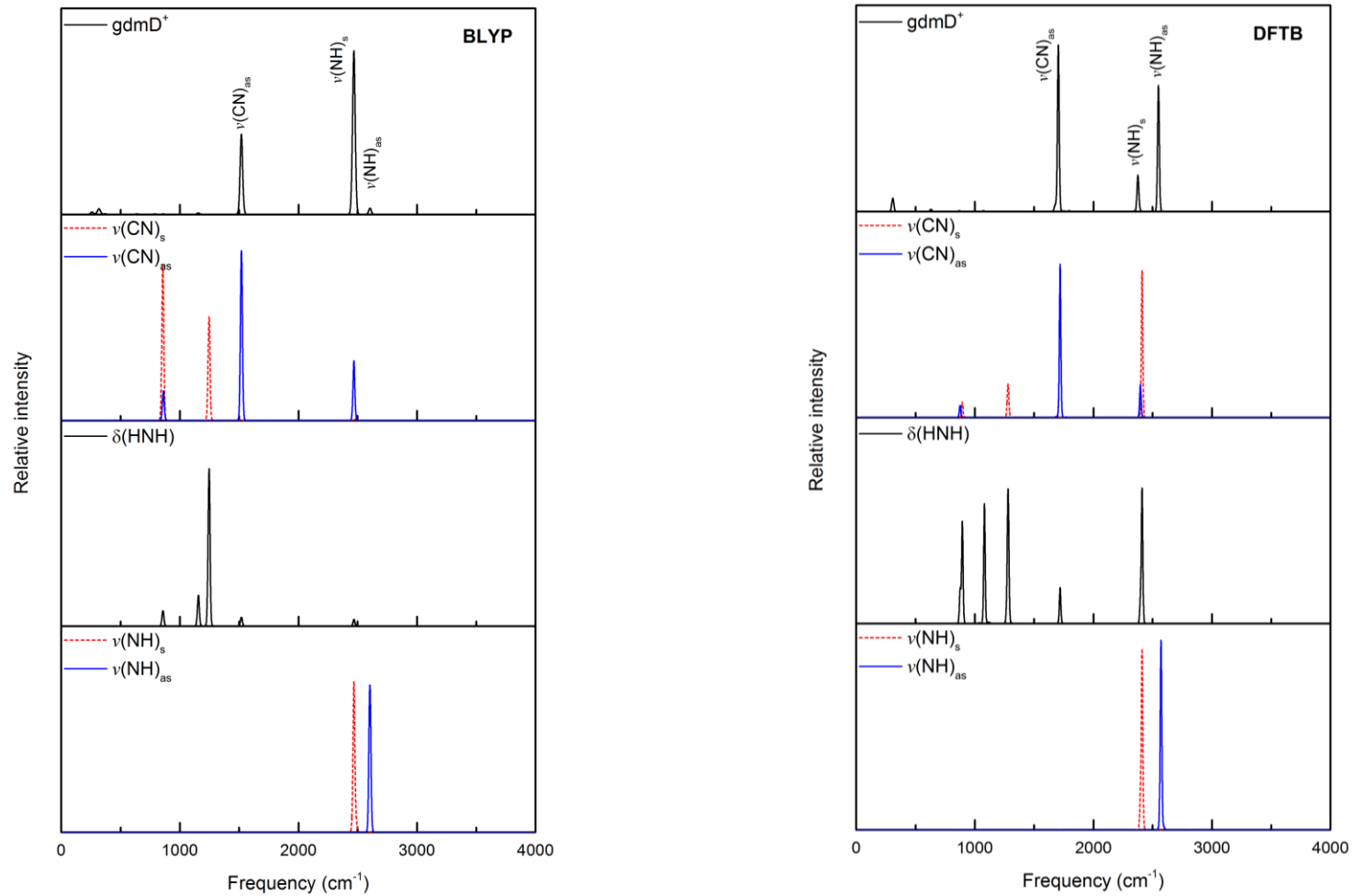


Figure 4.2. Vibrational features of deuterated guanidinium predicted by planewave BLYP (**Left**) and DFTB3/OB (**Right**) MD simulations at $\sim 50\text{K}$. The top panel shows the simulated vibrational spectra and the remaining ones time-correlation spectra corresponding to selected normal modes of vibration.

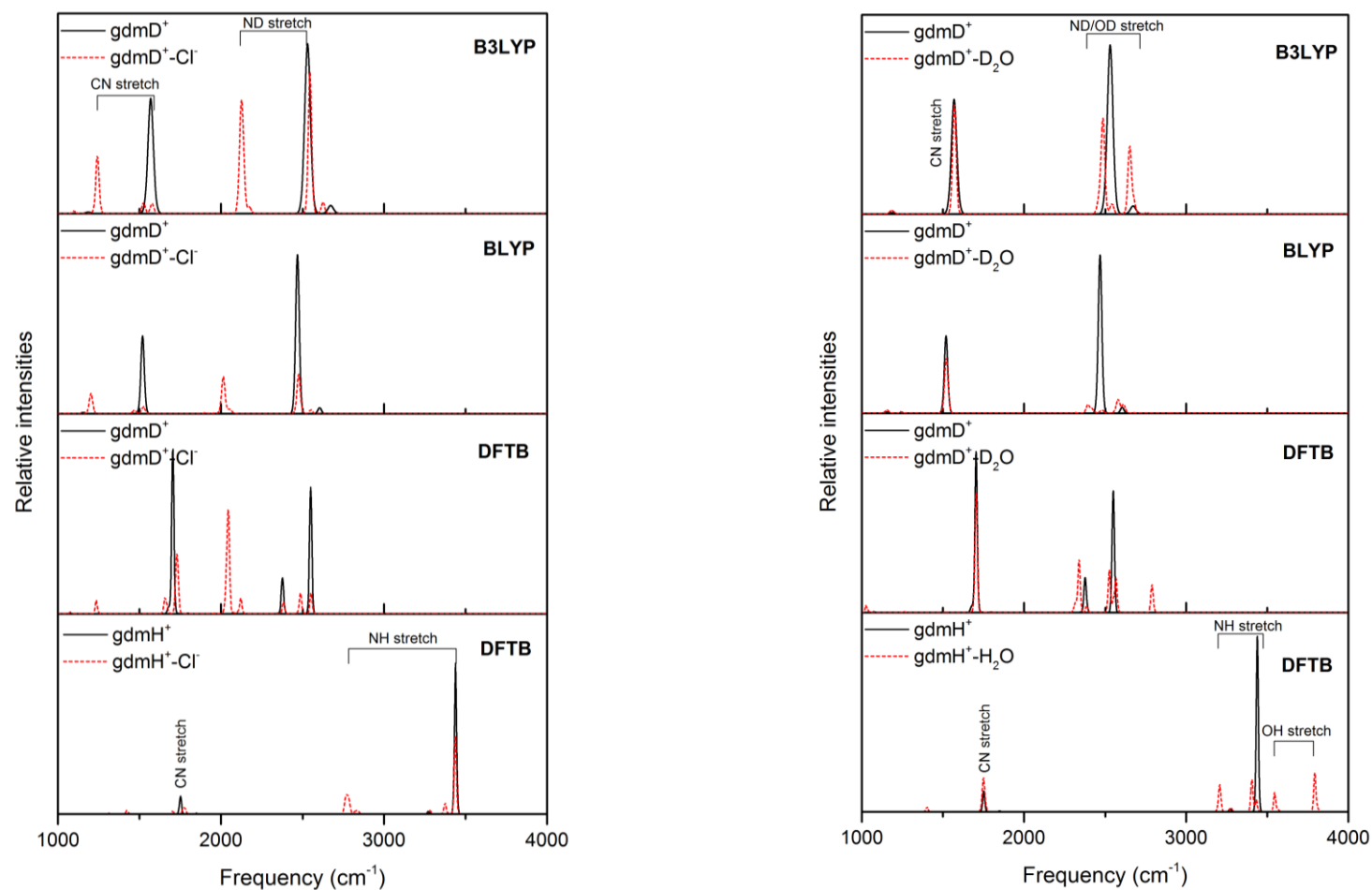


Figure 4.3. Vibrational spectra of guanidinium and its complexes with chloride (**Left**) and water (**Right**) predicted by planewave DFT (B3LYP, BLYP) and DFBT3/OB MD simulations at $\sim 50\text{K}$. DFTB spectra are averaged over 10 trajectories, while DFT spectra are based on a single trajectory. Band assignment is provided for the CN and NH(D) stretches.

The DFT band at 1515 cm^{-1} (**Figure 4.2 – left panel**) corresponds to the antisymmetric CN stretch and a small contribution of the HNH bend, and it is thus assigned to the antisymmetric CN stretch. Similarly, the other two bands at 2470 and 2605 cm^{-1} are assigned to the symmetric and antisymmetric NH stretches, respectively. The HNH bending mode manifests itself as a weak band at 1157 cm^{-1} in the vibrational spectra. The DFTB frequencies (**Figure 4.2-right panel**) for the antisymmetric CN stretch, symmetric and antisymmetric NH stretches differ a bit from their DFT counterparts, as 1704 , 2376 and 2550 cm^{-1} , respectively. The frequency of the CN stretch predicted by semi-local DFT (1515 cm^{-1}) is smaller than its harmonic counterpart (1572 cm^{-1}), a typical consequence of anharmonic effects. However, the experimental value for hydrated guanidinium lying at 1600 cm^{-1} , BLYP CPMD simulations appear to significantly underestimate vibrational frequencies, consistent with the previously reported and discussed 5~10% underestimation of frequencies by BLYP.^{7,8} The frequency of the CN stretch predicted by DFTB, 1704 cm^{-1} , is therefore as reasonable.

Effects of ion association. The effects of ion association with chloride and hydration on the vibrational spectra of guanidinium are illustrated in **Figure 4.3**. Ion association with chloride breaks the molecular symmetry of guanidinium and causes band splitting for both the CN and ND stretches (**Figure 4.3 – top left panel**). In B3LYP spectra of $\text{gdmD}^+\text{-Cl}^-$, new bands arise at 1241 cm^{-1} and 2124 cm^{-1} , which are assigned to the CN and ND stretches, respectively. BLYP spectra exhibit similar band splitting, with band positions downshifted by around 50 cm^{-1} . DFTB spectra reproduce the features of their B3LYP counterpart, with relatively larger gaps between split bands, suggesting a stronger effect of ion association on the vibrational dynamics of guanidinium, and some inconsistencies in the relative intensities of the bands. These subtle differences may be due to various levels of approximation in the characterization of the electronic structure. We note that

DFTB and B3LYP are in better agreement when it comes to the vibrational spectra of the $\text{gdmH}^+\text{--Cl}^-$ complex, both in terms of the relative intensities of the CN and NH stretches and band positions, with the CN stretch band at 1750 cm^{-1} and the two NH stretch bands at 3440 cm^{-1} .

Effects of hydration with water molecule. Upon association with a single water molecule, the guanidinium terminal NHs form two hydrogen “bonds” with the water molecule (**Figure 4.1**). The vibrational features of the guanidinium-water complex are shown in **Figure 4.3 – right panel**. According to the B3LYP vibrational spectra, the ion-water interaction has negligible effects on the CN stretch, while it splits the HD/OD stretch bands and weakens the relative intensities of the ND/OD bands. BLYP spectra paint a similar picture, with all band positions downshifted by around 50 cm^{-1} and even weaker relative intensities of the ND/OD stretch bands.

As for DFTB, it predicts that the CN stretch bands are also relatively unaffected by a single water molecule binding and that the NH stretch bands split into 4 bands with relative larger gaps, perhaps indicating an overestimation of hydrogen-bonding effects. Again better agreement in relative intensities between DFT and DFTB is observed in the gdmH^+ spectra.

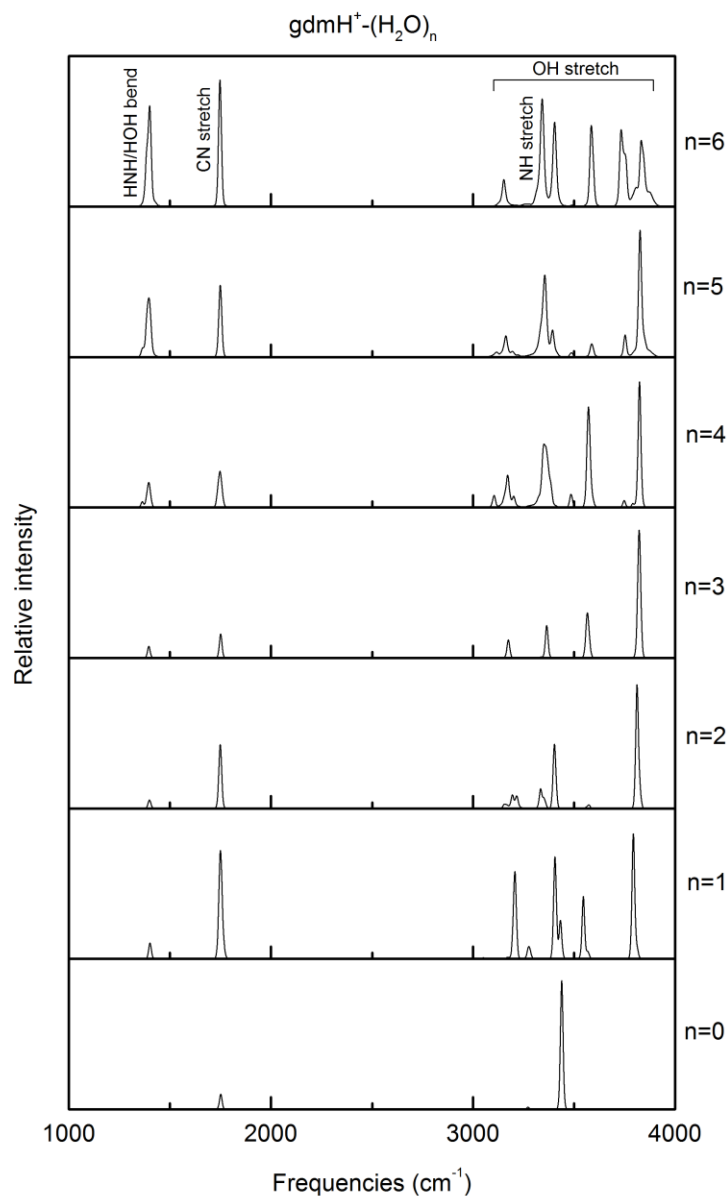


Figure 4.4. Simulated vibrational spectra of $\text{gdmH}^+(\text{H}_2\text{O})_n$, $n=1\sim 6$. The spectra are computed from constant-energy MD simulations at 50K with the DFTB3/OB model and are averaged over 10 trajectories.

Hydration with 1~6 water molecules. The hydration of guanidinium with 1~6 water molecules is further investigated with the computationally efficient DFTB, and simulated vibrational spectra are displayed in **Figure 4.4. CN stretch**. The position of the CN stretch band does not appear to shift upon hydration with up to 6 water molecules. However, upon cluster size

increase, the intensity of the band first decreases up to $n=3$ and then goes back up. This can perhaps be explained as an effect of the hydrogen bonding interaction on the transition dipole moment of the antisymmetric stretch mode of the CN bonds. With only one water molecule, the C_2 geometry of the complex favors the antisymmetric stretch of the CN bonds since the transition dipole moment is perpendicular to the direction of hydrogen bonding, leading to a relatively stronger intensity. With two or three water molecules, hydrogen atoms bonding to the amino groups (**Figure 4.1**) hinder the motion of the N atoms, resulting in smaller transition dipole moments. Upon addition of more water molecules, the hydrogen bonding interaction between water molecules themselves starts playing a role and perhaps reduces the impediment on N atom motion, making the antisymmetric stretch mode become more intense.

HNH/HOH bend. The HNH bend band is close to the HOH bend bands, and being much weaker, it manifests itself as a weak left shoulder of the HOH bend bands near 1400 cm^{-1} . These bands become more and more intense upon cluster size increase due to the increasing number of HOH bending vibrations that contribute to the band intensity. The OH/NH stretch bands are found in the spectral region between 3000 and 4000 cm^{-1} . Upon increasing the number of water molecules, the bands broaden and overlap with each other. The simulated spectra feature different patterns for cluster different sizes, which might be used as experimental probes.

Aqueous droplets of guanidinium. Finally, DFTB is employed to simulate larger aqueous droplets containing a guanidinium ion, with a number of water molecules of 20, 40, 60, and 80. The simulated radial distribution functions (RDFs) and vibrational spectra are shown in **Figure 4.5**. The first peak in the O-O RDF is much higher than that in the N-O RDF, suggesting more water structure and reflecting stronger collective water-water interactions relative to the

guanidinium-water interaction, consistent with the known chaotropic nature of guanidinium. The weak interaction between guanidinium and water molecules does not affect the CN stretch band position of guanidinium at 1750 cm^{-1} , with a redshift of only around 15 cm^{-1} observed by increasing the droplet size from 20 to 60. The trend is consistent with the hydration effects inferred from quantum chemistry calculations with and without the polarizable continuum model (**Table 4.2**), but with a slightly smaller shift. The relative intensity of the band naturally decreases upon droplet size increase, as the overall relative contribution of the ion vibrations to the vibrational spectra decreases and that of water molecules increases.

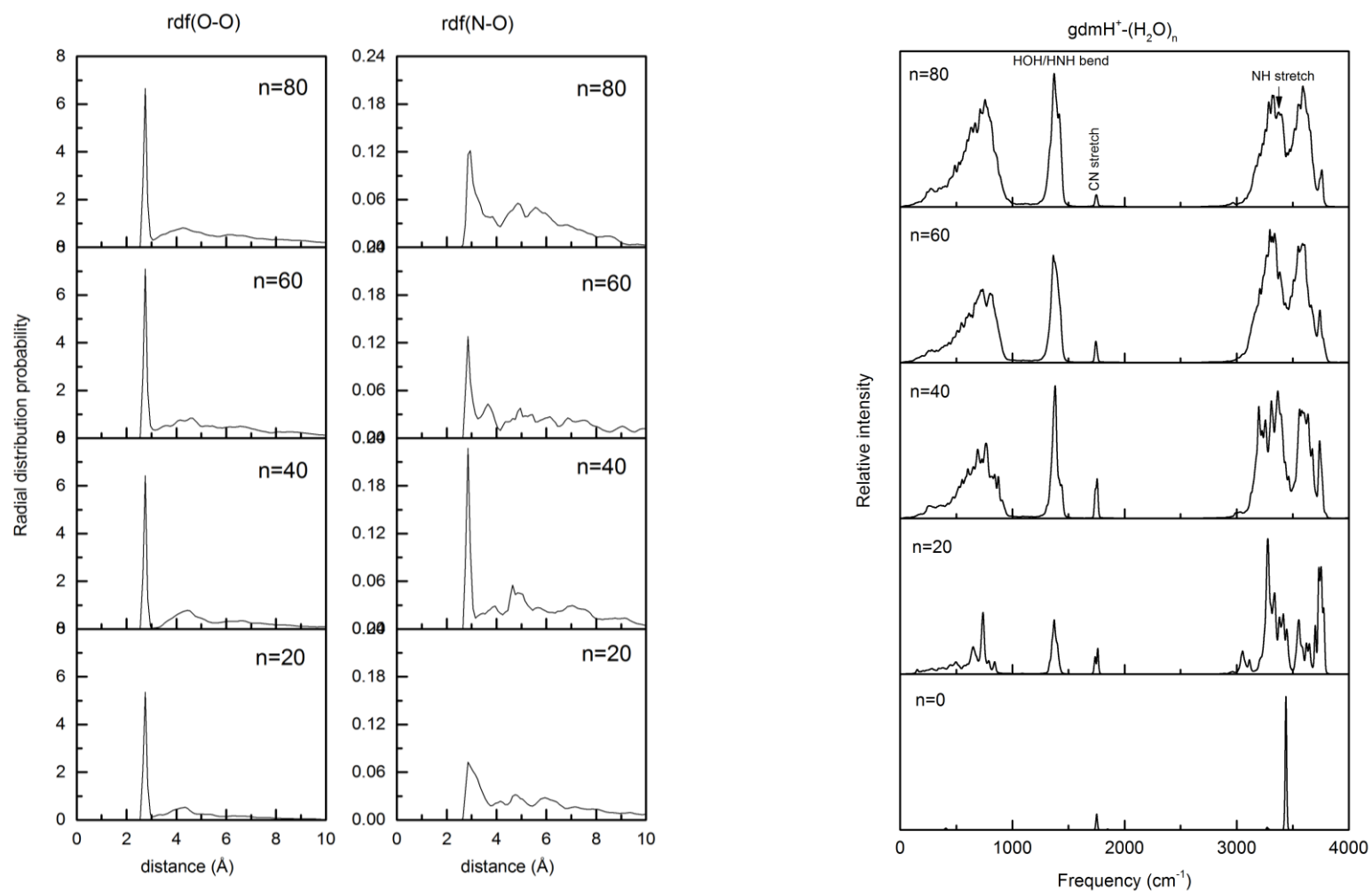


Figure 4.5. Computed vibrational spectra and radial distribution function of aqueous guanidinium droplet with DFTB. The spectra are computed from constant-energy MD simulations at 50K and are averaged over 10 trajectories.

4.4. Summary and conclusions

In this work, the vibrational spectroscopy of guanidinium, a widely used organic cation and a good model for a variety of functional groups, and its complexes with an anion and water molecules is investigated from first principles.

Hybrid DFT predicts very reasonable harmonic vibrational frequencies without any scaling. By including hydration effects via the polarizable continuum model, the calculated harmonic frequency of the CN stretch is in excellent agreement with that measured experimentally for the guanidinium ion in aqueous solution. Semi-local DFT systematically underestimate the frequencies, but within an acceptable range of error outweighed by the much higher computational efficiency. The planewave implementation of DFT widely used in simulations of condensed-phase systems produces results in agreement with atom-center Gaussian basis set DFT, provided a sufficiently high planewave cutoff (100 Ryd.) and sufficiently large periodic box are used. Frequencies tend to be slightly underestimated by planewave DFT though.

The simulation of vibrational spectra of guanidinium and its complexes further served as a benchmark to validate DFTB against planewave hybrid DFT as reference. The high computational efficiency of the DFTB, an approximate DFT model 2-3 orders of magnitude faster than DFT, allows to achieve larger simulation length and time scales. As a result, DFTB spectra can be simulated in a routine fashion for very large systems and spectra can be averaged over multiple trajectories to ensure convergence in band intensities. DFTB is able to reproduce all the spectral signatures of guanidinium upon hydration and ion association revealed by hybrid DFT.

The computational efficiency and reliability of DFTB made possible simulations of the vibrational spectra of small guanidinium-water clusters and aqueous droplets of guanidinium. The predicted spectra for small clusters could be used as an experimental probe. The main effect of hydration is confirmed to manifest itself in a slight redshift of the frequency of the CN stretch, which is consistent with quantum chemistry calculations.

This work confirms that DFTB is very promising, not only in predicting structural and energetic properties, but also in simulating vibrational spectra for very large systems, such as aqueous droplets containing a guanidinium ion or similar functional groups. The results obtained are generally comparable to those of hybrid DFT, but with a computational efficiency gain of 2~3 orders of magnitude.

Chapter 5.

**Simulation of the Vibrational Spectra of Biologically-
Relevant Systems: The Amide Bands of Model Peptides**

5.1. Introduction

Vibrational spectroscopy in biological study and amide bands. Vibrational spectroscopy has been widely used to probe the signature of molecular structure for a long time,^{111, 112} particularly to detect the 3D structure of proteins and polypeptides in aqueous solution thanks to the sensitivity of the amide modes to the conformation of the backbone and the structure of the side chains.^{113, 114} To be more specific, the amide I mode, involving stretching of the C=O bond, the amide II mode, involving wagging of the N-H bond, the amide A mode, involving the stretching of the N-H bond, have all been found to provide a fingerprint to distinguish between secondary structure motifs in proteins such as alpha-helices, beta-sheets and extended strands.¹¹³ While linear infrared and Raman vibrational spectroscopy has been well established for investigations in the condensed phase, several experimental approaches to probe the structure and dynamics of small molecular species in the gas phase, including polypeptides, have been developed in recent years,¹ such as for example infrared multi-photon dissociation (IRMPD)^{23, 115,}¹¹⁶ and infrared predissociation (IRPD)^{26, 117, 118}. These techniques make use of mass spectrometry for mass selection of small ionized molecular species, or messenger-tagged species. Selected species are further excited by infrared photon(s) and the count of dissociation products provides a measure of the absorption intensity. Such techniques opened the doors to studies of the fundamental physical and chemical properties of small model clusters in the gas phase, particularly when combined with quantum chemistry calculation or molecular simulations.^{23, 25}

The theoretical vibrational spectra: from Normal mode analysis to MD simulation. Computational vibrational spectroscopy, i.e. the computation of vibrational spectra through normal mode analysis (NMA), or as the Fourier transform of the autocorrelation function (FTACF) of the total dipole moment obtained from molecular dynamics (MD) simulations have been found

essential in helping provide a thorough interpretation of experimental results.¹ As widely accepted, normal mode analysis based on first-principles quantum chemistry in the double harmonic approximation is accurate enough to give acceptable vibrational spectra for many molecular species, though scaling factors are usually needed to correct the computed frequencies, in part because of the neglect of mode coupling.¹¹⁹ Interaction between modes could be very important for flexible molecules as those often found in biological or solvated systems. The vibrational self-consistent-field (VSCF) method and its higher level expansion such as the second-order correction under the perturbation theory framework (VPT2), as well as the vibrational configuration interaction (VCI) approach, are able to take anharmonic effect into account, but these techniques are all computationally demanding and are thus limited to small-size systems.¹ To overcome the harmonic approximation, and account for temperature effects and the influence of the environment on the vibrational dynamics that are typically present in condensed phase or large-size clusters, the FTACF of the total dipole moment based on MD simulations is increasingly employed in the modern modeling of vibrational spectra.^{1, 120} In this method, vibrational modes are allowed to interact with each other through internal energy relaxation. The success of the method has been illustrated by the successful computation of vibrational spectra of many systems from bulk aqueous solution to gas-phase clusters, such as liquid water,^{3, 121} aqueous solution,^{7, 72, 122} protonated water clusters,^{58, 123} peptides,^{8, 11, 124} to name a few.

Band Assignment. Band assignment is a challenge for understanding experimental vibrational spectra. Normal mode analysis provides a simple solution with clearly defined vibrational modes, but for large and flexible molecules that are typically encountered in biological systems, anharmonic effects make it difficult to rely solely on normal mode analysis. For dynamical spectra obtained through the FTACF method, interpretation of the infrared active bands may be achieved through vibrational densities of states (VDOS), calculated for each atom type as the Fourier transform of the autocorrelation function of the atomic

velocities. VDOS spectra allows one to connect a vibrational band to different atom types, and make conclusions on which atom type contributes to the band of interest. However, vibrational mode information is hardly conclusive using such method for complicated systems where delocalized vibrations take place through several groups of atoms, or diverse atomic motions are strongly coupled. Gaigeot and co-workers^{11, 125} have proposed a more generalized method allowing to construct localized vibrational modes as linear combinations of natural coordinates with the power spectrum of the mode as localized as possible in frequency. Other methods, such as plotting time-correlation spectra of the dipole moment of a group of atoms, or the time-correlation spectra of modes along specific internal coordinates or linear combination of conjugated internal coordinates provide a fast and convenient way to determine which atomic groups or internal coordinates are involved in the active modes. In this work, we take the last scheme to assign all bands

Theoretical spectroscopy towards medium-to-large-size biological system. Typical biological model systems usually consists of thousands to millions of atoms, which is far beyond the size that first-principles methods can handle.^{1, 119} Approximate density-functional theory (DFT) approaches such density-functional tight-binding (DFTB) could be the most promising model based on first principles,^{38, 41} as they suffer much less from the transferability issue than empirical models. DFTB is typically 2~3 orders of magnitude faster than DFT, while retaining an accuracy far superior to semiempirical quantum chemistry models.^{34, 38, 42, 80} The stored parameters describing atomic orbitals and repulsive potentials are fitted from high-level quantum chemistry results and the transferability of the parameters is far superior to that of classical force fields. The third-order expansion of the self-consistent charge version of DFTB, commonly referred to as DFTB3, has achieved great success in describing biological structures, ion hydration, proton transfer reactions, with a significant overall better performance than most of the semiempirical

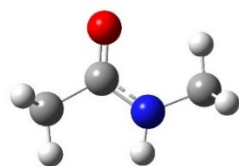
methods.^{35, 39, 42, 80, 98} However, its application in computational vibrational spectroscopy has not been fully examined and validated.

This work: motivation, aims, computation and organization. This work is motivated by the promising perspective of the application of DFTB to the computation of vibrational spectra for large-size biological systems in complicated environments. The DFTB model is first validated for prototypical peptide species, N-methylacetamide (NMA) and its complexes with water, itself and Na⁺, which involve a wide range of interactions from hydrogen bonding interaction to ionic interactions. The effects of complexation on the positions and shapes of the amide bands are investigated and simulated spectra are compared to available experimental results or first-principles data. In the last section, simulations of several minimum-size polypeptides that exhibit specific secondary structures on the simulation time span are performed to investigate differences in the frequencies of the C=O and N-H bond stretches, which constitute the core of the vibrational amide I/II/III and A modes. Comparison with empirical spectroscopic rules may further help assess the reliability and usefulness of the SCC-DFTB simulation results.

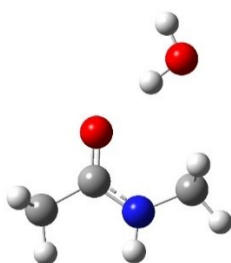
5.2. Computational details

5.2.1. Model systems

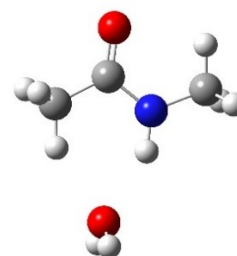
Amide bands in the vibrational spectra of proteins provide abundant information about their 3D structure and their environment due to the sensitivity of the amide I/II/III/A bands to the conformation of the backbone, side chains, and the environment in solution. *N*-methylacetamide (NMA) is the smallest molecular species possessing an amide group. Thus, NMA and its complexes are chosen as model peptides in this work. Since the aim of this work is to explore the applicability of the DFTB model in modeling peptides in their *in vivo* state, several typical



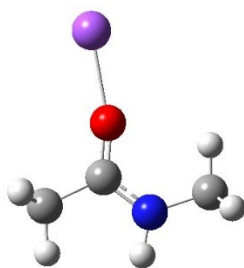
a. N-methylacetamide (NMA)



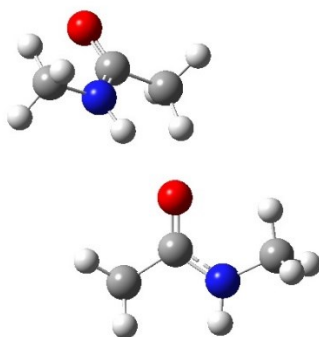
b. NMA-water complex with water binding to CO group
(NMA(CO)-H₂O)



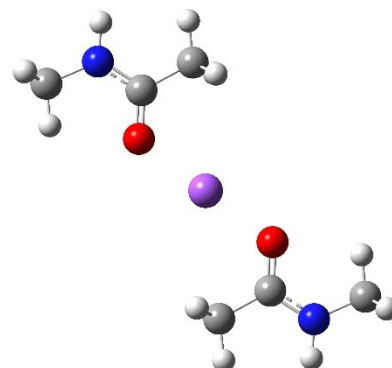
c. NMA-water complex with water binding to NH group
(NMA(NH)-H₂O)



d. NMA-Na⁺ complex



e. NMA dimer



f. (NMA)₂-Na⁺ complex

Figure 5.1. Model clusters (with their abbreviation in square bracket) investigated in this work.

interactions are considered in selecting model systems; in order to account for hydration of NMA, NMA dimerization and ion association, the 5 complexes shown in **Figure 5.1** are selected in this work.

5.2.2. Quantum-chemistry calculation

To provide first-principles reference data, the molecular geometries, binding energies and harmonic vibrational frequencies of all complexes are computed using second-order Møller–Plesset (MP2) perturbation theory⁴³⁻⁴⁵ with the aug-cc-pVTZ basis set⁶⁵ and DFT with the Becke-3 parameter Lyy-Yang-Parr (B3LYP)⁴⁶⁻⁴⁹ functional and the aug-cc-pVDZ basis set. All calculations were carried out with the Gaussian 09 software.¹⁰³ Harmonic vibrational frequencies are computed through normal mode analysis for the ground-state molecular species geometry optimized with the default route and convergence criteria. Binding energies are defined as the difference between the potential energy of the complex and that of each individual species.

5.2.3. SCC-DFTB model

The DFTB model is an approximate quantum-chemistry method based on DFT and the tight-binding model. The theory of DFTB and its SCC-DFTB3 extension (referred to as DFTB3 for brevity) has been well documented in the literature;^{35, 38, 80, 98} for a recent review, see ref 40, 83. Here, we briefly outline the formalism of DFTB3, according to which the total energies expressed as:

$$E^{DFTB3} = \sum_i^{OCC} \langle \psi_i | \hat{H} | \psi_i \rangle + E^{rep} + \frac{1}{2} \sum_{ab} \gamma_{ab} \Delta q_a \Delta q_b + \frac{1}{3} \sum_{ab} \Gamma_{ab} \Delta q_a^2 \Delta q_b \quad (5.1)$$

where the first term in the right-hand side is a sum over orbital energies, in which the Hamiltonian operator is constructed on the basis of a given reference density and single-electron wave function are expanded in Slater-type atomic orbitals. The second term is the summation of the short-range repulsion potentials, which are parameterized by fitting the potential energy surface of the reference atom pairs. The last two terms represent the second-order and the third-order expansion of the DFT total energy with respect to the electron density of the reference state of the atoms,

respectively, with Δq_a and Δq_b the atomic charge fluctuations which are calculated using Mulliken's scheme¹⁰⁴ in a self-consistent manner. γ_{ab} is a function that describes the "chemical hardness" (Hubbard parameter) of an atom, and also includes an extra hydrogen-bonding term to correct for interactions involving hydrogen atoms. Γ_{ab} is the higher-order coefficient describing the "hardness" of γ_{ab} .

Fully third order expansion was used in this work.⁸³ The atomic Hubbard parameter for DFTB3 model were set as -0.1492 -0.1857, -0.1575, -0.1535 for C, H, O and N, respectively.⁸³ The ξ parameter in the hydrogen-corrected function was set to 4.0. The parameter set, containing the electron parameters and two-center repulsive potential parameters, used in this work is 3OB, which is optimized for organic and biological applications and DFTB3. The parameters are obtained by fitting experimental or quantum chemistry data for atomization energies, molecular geometries and vibrational frequencies of model molecules. The accuracy of the DFTB3/OB model has been well established,^{40, 83} and was even shown to outperform DFT methods with small basis set in geometric properties and binding energies.

5.2.5. MD simulations

Molecular dynamics (MD) simulation are performed to generate the time-series data of the total dipole moment of the clusters needed to compute vibrational spectra, or the time-series data for motion along specific internal coordinates to compute time correlation spectra for the purpose of band assignment.

The dipole moment is calculated from the Mulliken charges, with the artificial contribution of the net charge to the total dipole moment subtracted for non-neutral species. To overcome the slow internal vibrational energy relaxation in isolated molecules pointed out by Hornicek and co-

workers,¹²⁶ multiple trajectories initiated with different random velocities are propagated and the vibrational spectra are obtained as the average over individual spectra calculated for each trajectory. For each simulation, the constant-energy ensemble is chosen to avoid the rescaling effects of the thermostat on the integration time. The timestep is chosen as 0.2 fs and the total time span of each trajectory is 20 ps (100,000 steps). Large fluctuations in the calculated intensities in the single-trajectory spectra were observed, and thus averaging over 10 trajectories is confirmed to be essential in obtaining converged spectra for the systems investigated here.

The initial configuration is chosen as the optimized molecular geometry, and random atomic velocities are generated according to a Maxwell-Boltzmann distribution using the Box-Muller algorithm,¹⁰⁵ with the total kinetic energy dictated by the target temperature. The model systems were then equilibrated with 20,000-step constant-temperature simulations thermostated at the target temperature with a Nose-Hoover-chain thermostat¹²⁷ and a timestep of 0.5 fs. The atomic Cartesian coordinates and velocities of the last frame were taken as initial conditions for the constant-energy production run employed to compute spectra. All MD simulations were performed with the DFTB+ code.⁸⁵

5.2.6. *Vibrational spectra*

Theorem and formula. Vibrational spectra are computed as the Fourier transform of the autocorrelation function of the total dipole moment as derived from the Fermi golden rule within linear response theory:^{3, 11, 17}

$$\alpha(\omega)n(\omega) = \frac{2\pi\omega(1 - \exp(-\beta\hbar\omega))}{3cV\hbar} \int_{-\infty}^{+\infty} dt \cdot \exp(-i\omega t) \langle \boldsymbol{\mu}(0) \cdot \boldsymbol{\mu}(t) \rangle \quad (5.2)$$

in which $\alpha(\omega)$ is the absorption intensity with respect to the vibrational frequency or wave number ω , $n(\omega)$ is the frequency-dependent refractive index of the medium [$n(\omega) = 1$ is used in

this work], c is the speed of light in vacuum, V is the volume (set to be 1 in this work) $\beta = 1/kT$ with T the average temperature and k the Boltzmann constant, μ is the dipole moment, and the brackets indicate an ensemble average over the time span of the simulations. To correct for the error in band shape introduced by replacing the quantum time-correlation function with its classical counterpart, a quantum correction factor of the form $\beta\hbar\omega/(1 - \exp(-\beta\hbar\omega))$ is included in equation (5.2), which was shown by Gaigeot and co-workers to give the most accurate computed intensities. Quantum correction factors have been discussed thoroughly elsewhere.^{18, 110}

5.3. Results and discussions

5.3.1. Hydrogen bonding structures and interaction energies

Table 5.1. Selected geometric parameters for *trans*-N-methylacetamide (NMA) and its complexes. C, N, H atoms in the table are all from amide group.

		MP2	DFTB3
NMA	C=O	1.226	1.233
	N-H	1.004	1.015
	C-N	1.362	1.382
	O-C-N	122.8	121.9
NMA(CO)-H ₂ O	C=O	1.234	1.244
	N-H	1.004	1.016
	O--H	1.852	1.800
NMA(NH)-H ₂ O	C=O	1.229	1.237
	N-H	1.009	1.019
	O--H	2.035	2.093
NMA-Na ⁺	C=O	1.252	1.267
	N-H	1.007	1.018
	O--Na ⁺	2.156	2.156
	C-O-Na ⁺	165.3	135.1
	N-C-O-Na ⁺	180.0	180.0

Unit: bond length in Angstrom, bond angle and dihedral angle in degree. Basis set for MP2 calculations: aug-cc-pVTZ.

For geometric properties, it is found that the performance of DFTB3 model is excellent, as listed in **Table 5.1**, in which only geometry of amide group and the intermolecular distance are selected. The relative error of DFTB3 with respect to the reference values are within 3% except the bond angle O-Na⁺ in NMA-Na⁺ complex, which is underestimated by 30 degree. The variation of the bond length of C=O and N-H upon Hydrogen bonding with water molecule and Na⁺ is in excellent agreement with the reference values.

For interaction energies, it is well known that DFTB systematically underestimate the hydrogen bonding energies by about 1~2 kcal/mol.^{38, 80} In the case of NMA complexes, the error is relative larger. The root of mean square deviation of the interaction energies for the 4 complexes is 3.4 kcal/mol. However, the root of mean square deviation for the other two popular semi-empirical ab initio methods PM6 and AM1 are 5.7 and 8.0 kcal/mol, respectively. The largest absolute error of DFTB3 interaction energy comes from NMA dimer, indicating that it is difficult to describe the hydrogen bonding between two flexible molecules with minimum number of basis functions.

5.3.2. Harmonic vibrational frequencies

Table 5.2. Binding energies of *trans*-N-methylacetamide (NMA) complexes.

	MP2	DFTB3	PM6	AM1
NMA(NH)-H ₂ O	6.7	3.8	4.0	3.5
NMA(CO)-H ₂ O	8.5	7.2	6.1	4.2
NMA-NMA	11.7	5.8	5.8	4.3
NMA-Na ⁺	44.1	42.6	35.0	57.3

Unit: kcal/mol. Basis set for MP2 calculation: aug-cc-pVTZ.

To validate the accuracy of the second derivatives of the potential energy surface, we compare the harmonic frequencies of the NMA and its complexes calculated with DFTB model and high level quantum chemistry. The frequencies are obtained through standard normal mode analysis. All computed frequencies are not scaled. **Table 5.3** shows comparison of *trans*-NMA and *cis*-NMA, and **Table 5.4** shows hydrated NMA and NMA-Na⁺ complex.

In **Table 5.3**, the first thing noted is that both MP2 and DFT overestimate the experimental values in a systematical way, by 4% for MP2, and 3% for DFT, respectively. In contrast to MP2 and DFT, DFTB3 model underestimates the harmonic frequencies of amide A and amide I by -150 cm⁻¹, while for amide II and III, the error is negligible. Though the absolute error of DFTB3 model is even smaller than MP2 and DFT, our focus is the frequency shift of amide modes upon isomerization, hydrogen bonding or ion association of NMA.

Upon hydration and ion association, the variation of amide I, II, III and A given by DFTB3 are in excellent consistence with those given by MP2 and DFT. The mean square deviation (MSD)

Table 5.3. Vibrational frequencies of *trans*-NMA and *cis*-NMA.

		EXP ^a	Harmonic			MD
			MP2 ^b	DFT ^c	DFTB3	DFTB3 ^d
<i>trans</i> -NMA	amide A	3457, 3485	3680	3639	3349	3310
	amide I	1713-1731	1746	1732	1561	1702
	amide II	1500	1573	1560	1486	1536
	amide III	1225	1282	1265	1225	1246
<i>cis</i> -NMA	amide A	3433	3623	3644	3356	3312
	amide I	1515	1733	1741	1564	1705
	amide II	1432	1459	1436	1488	1487
	amide III	1325	1400	1388	1267	1311

^a Experimental IR spectra of *cis*-NMA in an argon matrix¹²⁸; ^b basis set: aug-cc-pVTZ; ^c B3LYP functional with basis set: aug-cc-pVDZ; ^d SCC-DFTB3 with 3OB parameter set. Unit: cm⁻¹

between DFT and MP2 are 6 cm^{-1} , and the MSD between DFTB3 and DFT is 43 cm^{-1} . It is notable that almost all the sign of errors are the same, except for amide I and II of NMA- Na^+ . MP2 and DFT indicate a blueshift in amide I and II, but DFTB3 gives a redshift. However, the frequencies of the dynamics simulation correct the error, and gives proper sign of shift.

When looking at the NMA isomerizing from *trans*- to *cis*- isomer, MP2 and DFT give different sign of shift for amide A and I. DFTB3's results including harmonic frequencies and frequencies from dynamics simulation, are in consistence with DFT.

From the above discussion, we conclude that DFTB3 achieves an overall good consistence with high-level quantum-chemistry calculations. Such conclusion is in consistent with previous report on the performance of DFTB model in describing hydrogen bonded anionic-water clusters.⁴²

Table 5.4. Vibrational frequencies of hydrated *trans*-NMA and *trans*-NMA- Na^+ complexes.

		Harmonic			MD
		MP2 ^a	DFT ^b	DFTB3 ^c	DFTB3 ^c
NMA(CO)-H ₂ O	amide A	3685	3650	3339	3317
	amide I	1726	1710	1551	1672
	amide II	1572	1560	1483	1563
	amide III	1302	1288	1252	1267
NMA(NH)-H ₂ O	amide A	3610	3576	3314	3296
	amide I	1739	1724	1550	1688
	amide II	1595	1585	1483	1540
	amide III	1305	1285	1235	1252
NMA- Na^+	amide A	3658	3628	3332	3314
	amide I	1695	1670	1616	1685
	amide II	1608	1595	1443	1580
	amide III	1332	1319	1282	1295

^a basis set: aug-cc-pVTZ; ^b B3LYP functional with basis set: aug-cc-pVDZ; ^c SCC-DFTB3 with 3OB parameter set; Unit: cm^{-1}

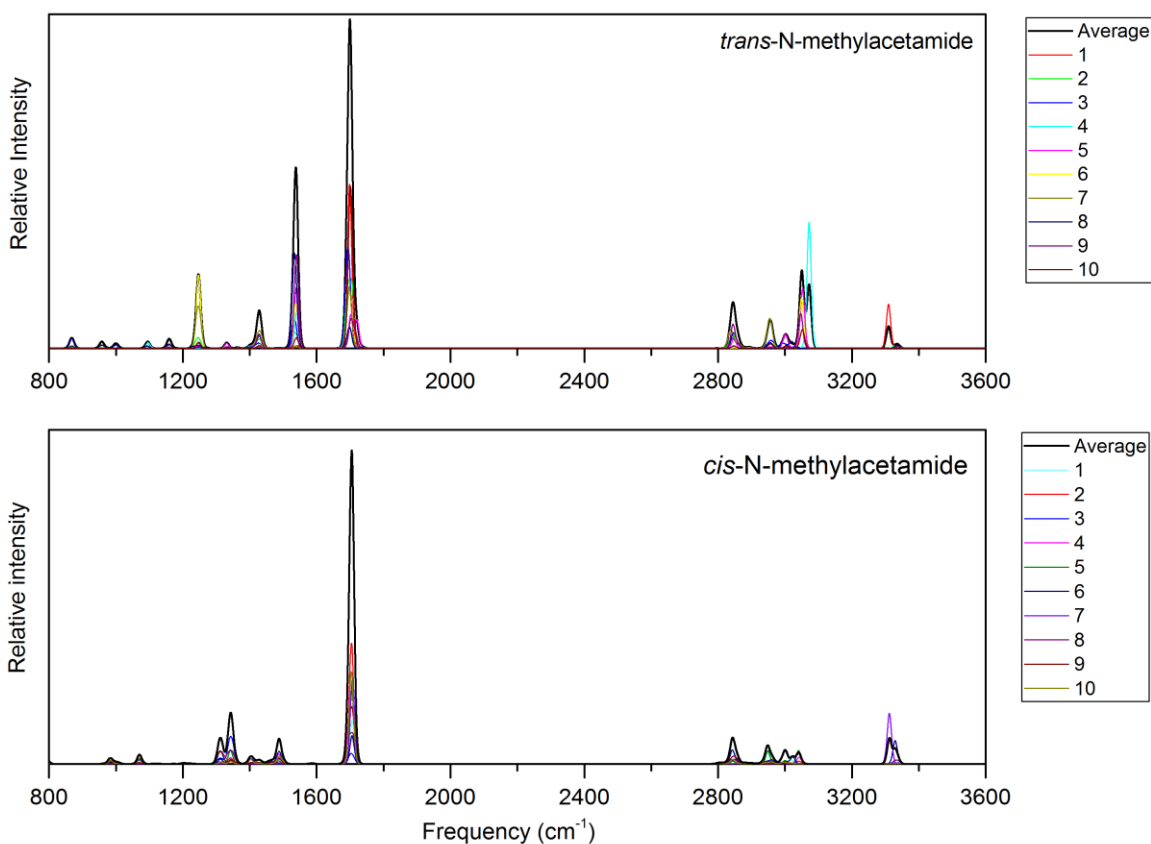


Figure 5.2. Simulated single-trajectory and averaged vibrational spectra from molecular dynamics simulations at 50K for *trans*-NMA (top) and *cis*-NMA (bottom), respectively. To highlight averaged spectral lines, their intensities are enlarged 5 times, and the lines of averaged spectra are thickened.

5.3.3. Simulated Vibrational spectra: Averaging and band assignment

Averaging. Uneven energy distribution among the vibrational degree of freedom may make the computed spectral intensities difficult to converge, particularly for the molecular species in gas phase. As it had been shown by J. Hornicek and co-workers,¹²⁶ the development of the energy distribution towards equilibrium $\bar{\epsilon} = kT$ is very slow. The time needed to achieve equilibrium is usually far beyond 20 ps, which is the typical time span used to generate a single sample of the spectra. Fortunately, averaging over several independent MD trajectories provides converged

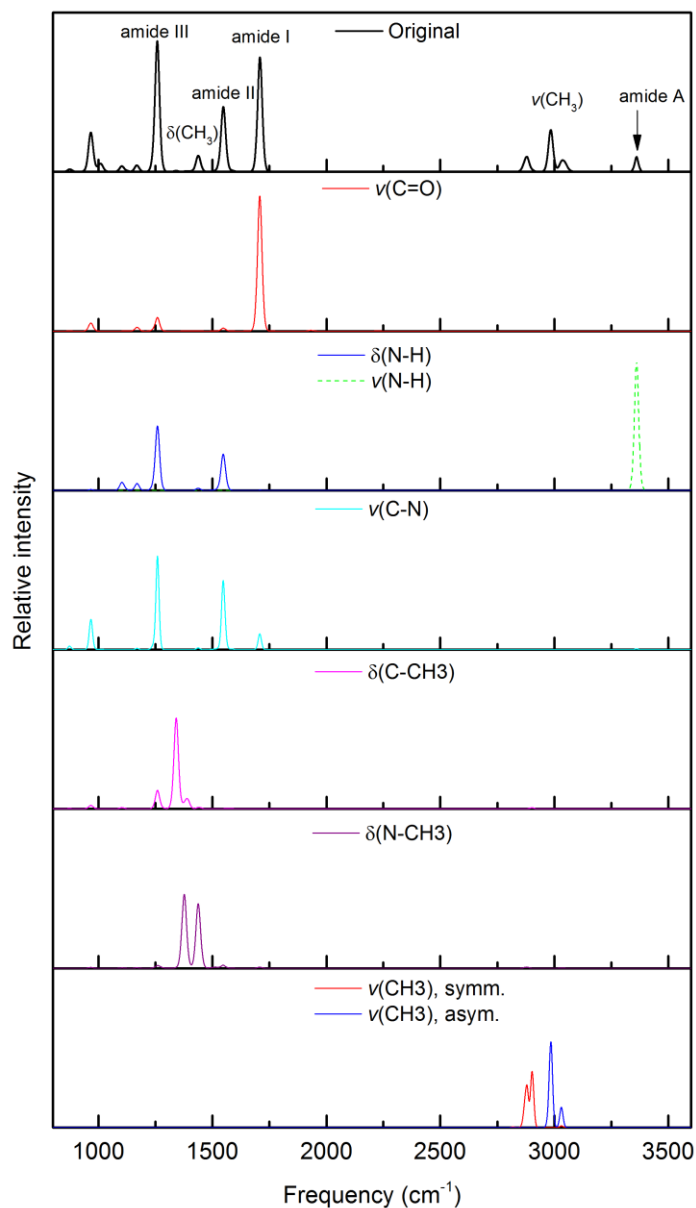


Figure 5.3. Simulated vibrational spectra of *trans*-NMA. The top panel shows the actual vibrational spectra. Remaining panels display time-correlation spectra of the localized modes in terms of specific internal coordinates or linear combination of coupled internal coordinates.

spectral intensities.^{1, 126} Therefore, all vibrational spectra in this work are computed by taking the average of 10 trajectories. **Figure 5.2** shows an example of the averaging from 10 simulations, which are the spectra of *trans*-NMA and *cis*-NMA.

Band assignment. Figure 5.3 displays simulated spectra for *trans*-NMA to illustrate the assignment of bands in vibrational spectra on the basis of time-correlation spectra for specific vibrational modes.. The band at 1702 cm^{-1} in the vibrational spectra is assigned to the amide I since it corresponds to the main band in the time-correlation spectra of the C=O bond stretch, $\nu(\text{C}=\text{O})$. Similarly, the amide II band is assigned according to the peaks observed in the N-H wagging and skeleton C-N stretching time-correlation spectra, the amide III band on the basis of the time-correlation spectra for N-H wagging and skeleton C-N stretching, and a slight contribution from C=O stretching, and the amide A band assigned according to the peaks observed in the time-correlation spectra of pure N-H stretching. Such assignment is in excellent agreement with empirical information regarding amide bands.

5.3.4. *Vibrational spectra of NMA*

Figure 5.4 shows computed vibrational spectra of NMA from molecular dynamics simulation at 50K with DFTB3 model, and the experimental infrared spectra at low temperature.¹²⁸ An excellent agreement in band shape is observed between the computed *trans*-NMA and the experimental results, which is reasonable considering that the energy barrier of the inversion from *trans*-NMA to *cis*-NMA is as high as 89 kJ/mol, and the relative potential energy is 5-8 kJ/mol.³³

The main discrepancies are the relative positions, or the frequencies of amide I, II and A, with errors of -20, 36 and -170 cm^{-1} , respectively. However, the error in frequencies is within a reasonable range, and the relative order is consistent.

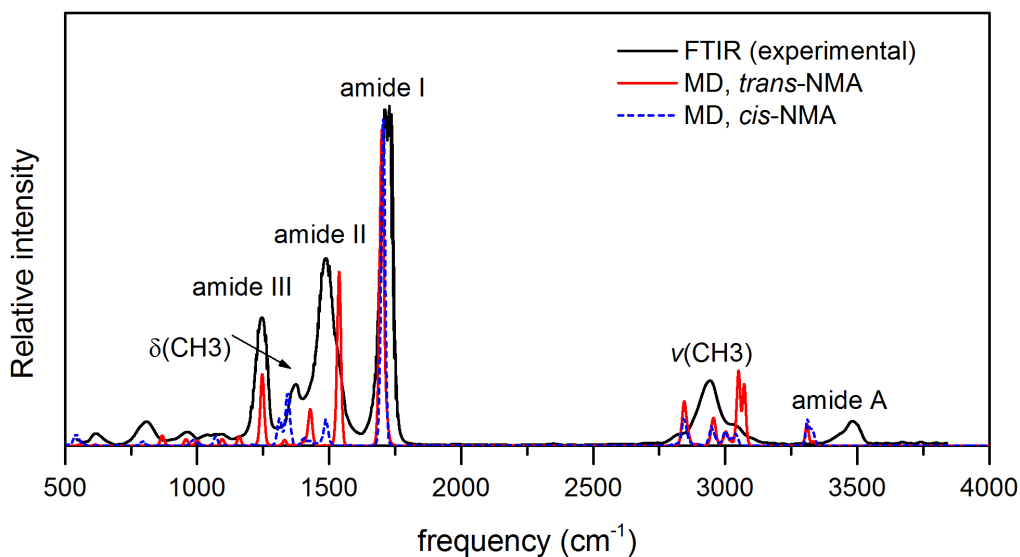


Figure 5.4. Vibrational spectra of NMA in the range 500-4000 cm^{-1} . Obtained from MD simulations with DFTB3 at 50K. The experimental FTIR results are taken from ref 128.

An important feature of the experimental spectra of NMA is the doublet of the amide I, as it had been reported.^{128, 129} The doublet might be feature of the spectra at high temperature. We have also investigated the temperature effects on amide I band of *trans*-NMA with the DFTB model. Molecular dynamics simulations are performed at 50K, 300K and 400K, respectively. The final averaged spectra are given in **Figure 5.5**. The broadening and splitting of the amide I band are well reproduced. The band position of amide I shifts down by 20 cm^{-1} upon increasing the temperature from 50K to 400K, consistent with reported value discovered by a study with polarizable molecular dynamics simulation.¹¹⁹ The agreement of the position and shape of amide II and III is even remarkable. The band position of amide II, a mode related to N-H wagging, significantly redshifts by 40 cm^{-1} , and achieve much better agreement with the experimental spectra.

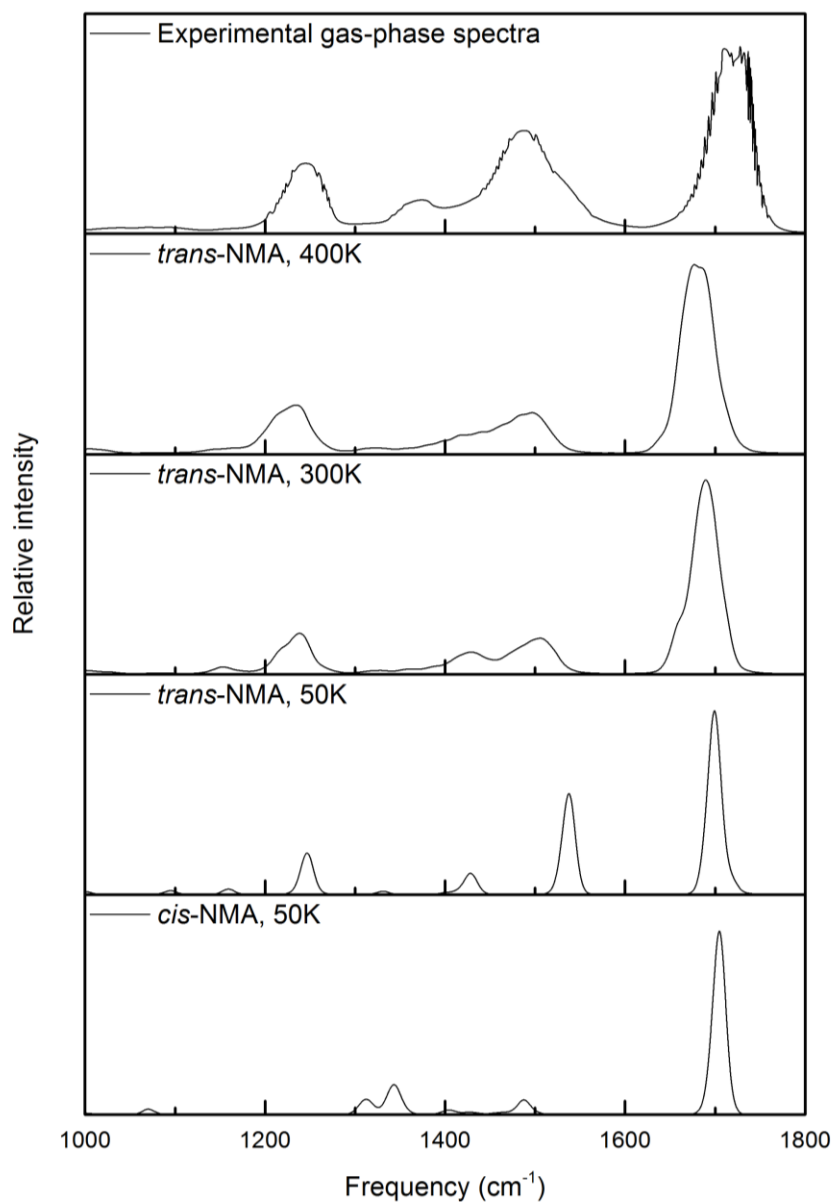


Figure 5.5. Vibrational spectra of NMA in the range 1000-1800 cm^{-1} . **Top panel:** experimental FTIR gas-phase spectrum; **Lower panels:** simulated spectra from molecular dynamics simulation with DFTB3 at various temperature for trans-NMA and cis-NMA.

5.3.5. Vibrational spectra of hydrated NMA complexes

Amide groups are hydrogen binding sites and the band position and shape can be significantly affected by hydrogen bonding.¹¹⁹ From gas-phase to aqueous phase, amide I bands

of *trans*-NMA could down shift by as much as 80 cm^{-1} .⁸ Here we investigate the hydration effects on the amide bands of *trans*-NMA by binding water molecule on N-H group and C=O group, respectively. Temperature of the simulations is 50K. The final averaged spectra are shown in **Figure 5.6**, parallel with the spectra of NMA.

Amide I and II region. Hydration on both sites causes redshift of amide I, by 30 cm^{-1} for hydration on C=O, and 10 cm^{-1} for hydration on N-H, respectively. For amide II, hydration on C=O causes a blueshift by 20 cm^{-1} while hydration on N-H causes negligible effect on band position. This is because the binding energy of water molecule on C=O site is much larger than that on N-H site, i.e. 7.2, 3.8 kcal/mol, respectively. Therefore, hydration on C=O site leads to more electron transfer and cause larger redshift in frequencies.

Amide A region. Hydration on C=O site and N-H site also causes different pattern in amide A bands, as shown in the **right** panel of **Figure 5.6**. In the spectra of NMA-H₂O, the left most weak band is N-H stretch (amide A), the central band is symmetric OH stretch, and the right most band is anti-symmetric OH stretch. It can be seen that upon hydration on C=O group, the OH stretching bands of water molecule split, while upon hydration on N-H group, the O-H stretching bands of water molecule are not significantly affected. This is because in the former case, the water molecule binds the NMA molecule with 3 hydrogen bonds, and cause a symmetry breaking of the water molecule. Also, the hydrogen bonded OH bond is strongly coupled with N-H bond stretching. These effects lead to the redshift and multiple split of symmetric OH stretching mode. In comparison, water molecule bonding to N-H site through the O atom keeps its C_{2v} symmetry. The hydrogen bonding interaction is much weaker. Therefore, the OH stretching bands are not significantly affected. Such a difference can be taken as signature to distinguish the two isomer of NMA-water complex.

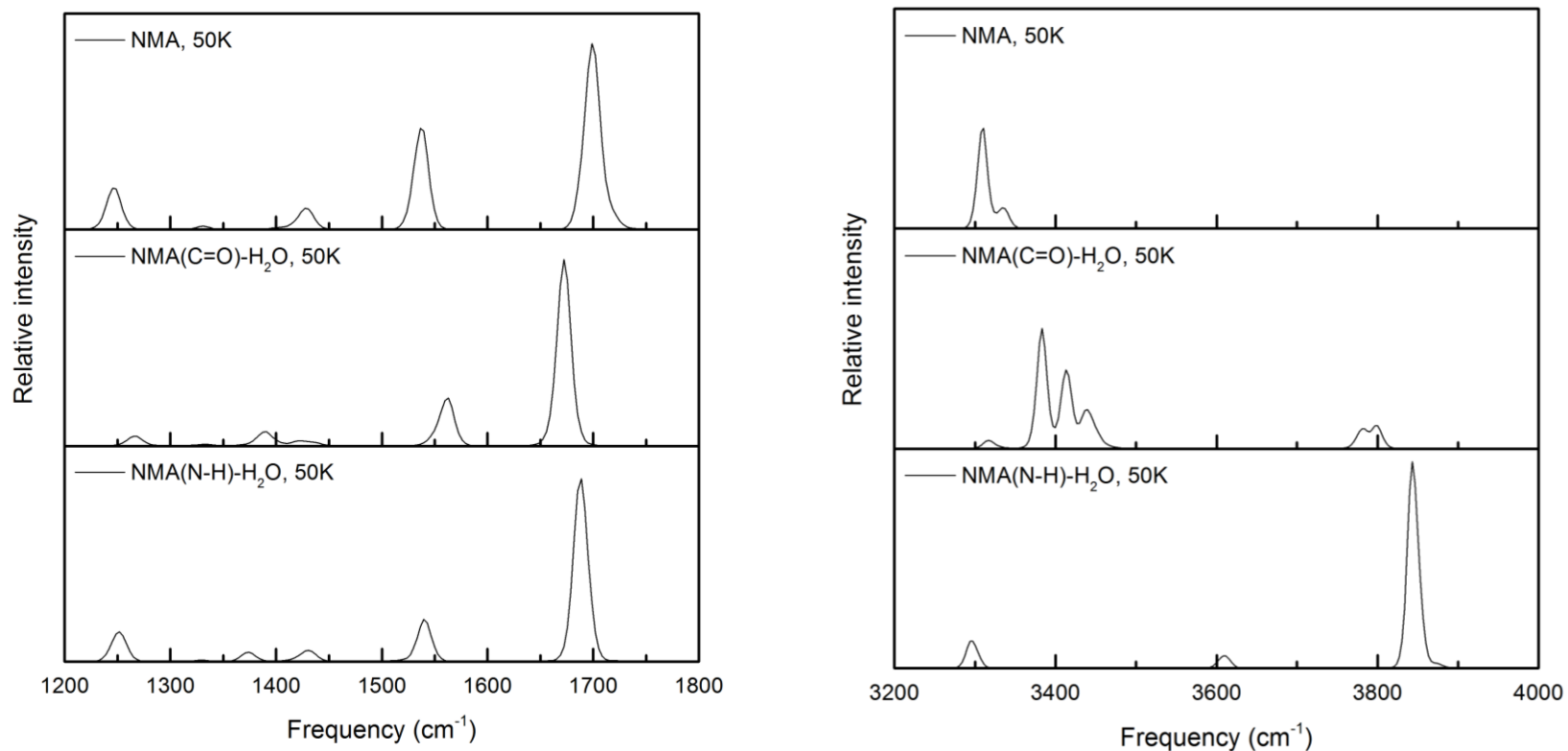


Figure 5.6. Simulated vibrational spectra of *trans*-NMA and *trans*-NMA-water complexes in the range 1200-1800 cm^{-1} (**Left**) and 3200-4000 cm^{-1} (**Right**), respectively. Obtained from molecular dynamics simulation with DFTB3 at 50K. In the NMA(CO)-H₂O complexes the water molecule is hydrogen bonded to the CO group of NMA.

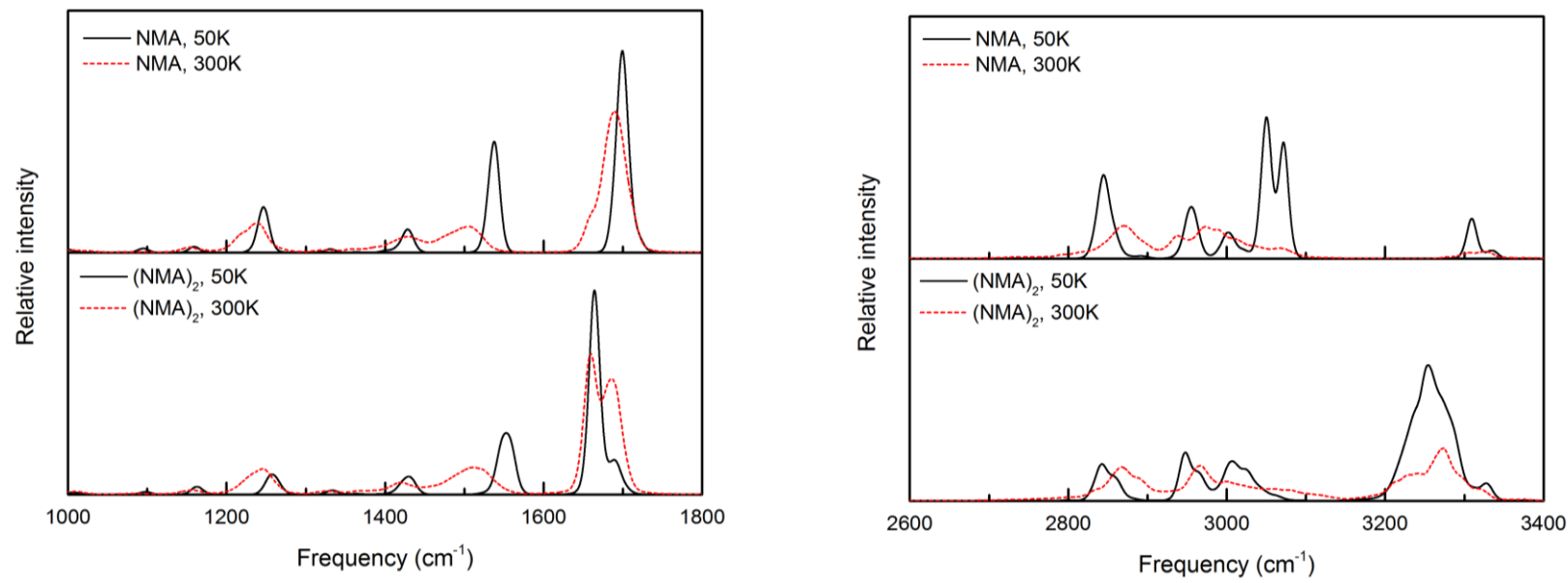


Figure 5.7. Simulated vibrational spectra of *trans*-NMA monomer and *trans*-NMA dimer in the range 1000-1800 cm^{-1} (**Left**) and 2600-3400 cm^{-1} (**Right**), respectively. Obtained from MD simulations with DFTB3 at different temperature.

As a summary of the subsection, we found that DFTB3 model gives reasonable results on the hydration effects on amide bands, in agreement with qualitative conclusion of previous reports.

5.3.6. *Vibrational spectra of NMA dimer*

In α -helix and β -sheets, peptides bind together through hydrogen bonds between amide groups. Such binding has significant effects on the amide bands, and they are usually taken as signature to distinguish the secondary structures. Here, we investigate the effects by examine the NMA dimer. Simulations are performed with temperature setting to 50K and 300K. The final averaged spectra are given in **Figure 5.7**.

Amide I and II region. The dimerization of NMA causes the redshift and split of amide I, and a blueshift of amide II. Other bands in this region are not significantly affected. The redshift of amide I, i.e. C=O stretching, and blueshift of amide II, i.e. N-H wagging, are caused by the hydrogen bonding between C=O and N-H groups. The interaction flattens the potential energy surface of the oscillation of O atom, but sharpens the potential energy surface of the swing of H atom.

Amide A region. In the region of 2600 ~ 3400 cm^{-1} , the bands above 3200 cm^{-1} are N-H stretching, and the others are C-H stretching. In the spectra of the dimer, a significant redshift and broadening of amide A is observed. Its relative intensity to that of C-H stretching is also getting higher, both at low temperature and high temperature. Hydrogen bonding between C=O and N-H leads a flattened potential energy surface of the oscillating of H atom, therefore causes a slower but more intense N-H stretching. The redshift of the amide A band is consistent with an experimental study of the gas phase infrared spectra of monomer and dimer NMA,¹³⁰ in which infrared spectra of NMA monomer and dimer are obtained in N_2 and Ar matrices at ca 200K.

Redshift of amide A is about 115 cm^{-1} . While in our computation, the redshift at 50K and 300K are both around 60 cm^{-1} .

5.3.7. *Vibrational spectra of NMA-Na⁺ complexes and (NMA)₂-Na⁺*

Interaction between peptide and metal ions plays important role in biological studies. The IRMPD spectra of NMA dimer mediated with a Na⁺ had been recorded to determine the frequencies shift resulting from the complexation, as shown in **Figure 5.9**. Here, we computed the vibrational spectra of NMA-Na⁺ and (NMA)-Na⁺, along with NMA, are given in **Figure 5.8** and **5.9**.

Amide I, II and A. Comparison of NMA and NMA-Na⁺ shows a similar effect to that hydrogen bonding to C=O group of NMA, i.e. redshift of amide I and blue shift of amide II, but to a stronger extent. This effect gets even stronger in the case of (NMA)₂-Na⁺. However, no significant effects on amide A bands are found. This is due to the fact that the Na⁺ is bonded to the C=O group, and the potential energy surface of the N-H stretching is not affected sufficiently.

Temperature effects. In **Figure 5.9**, the computed vibrational spectra at 300K and experimental IRMPD spectra¹¹⁹ of (NMA)₂-Na⁺ are compared and an excellent consistence in band shape is found, except a slight underestimate of amide I and slight overestimate of amide II. However, the agreement is much better than the spectra computed with polarizable force field,¹¹⁹ in which the relative intensities of band at 1400 cm^{-1} is somewhat too high, while that of amide I is too low.

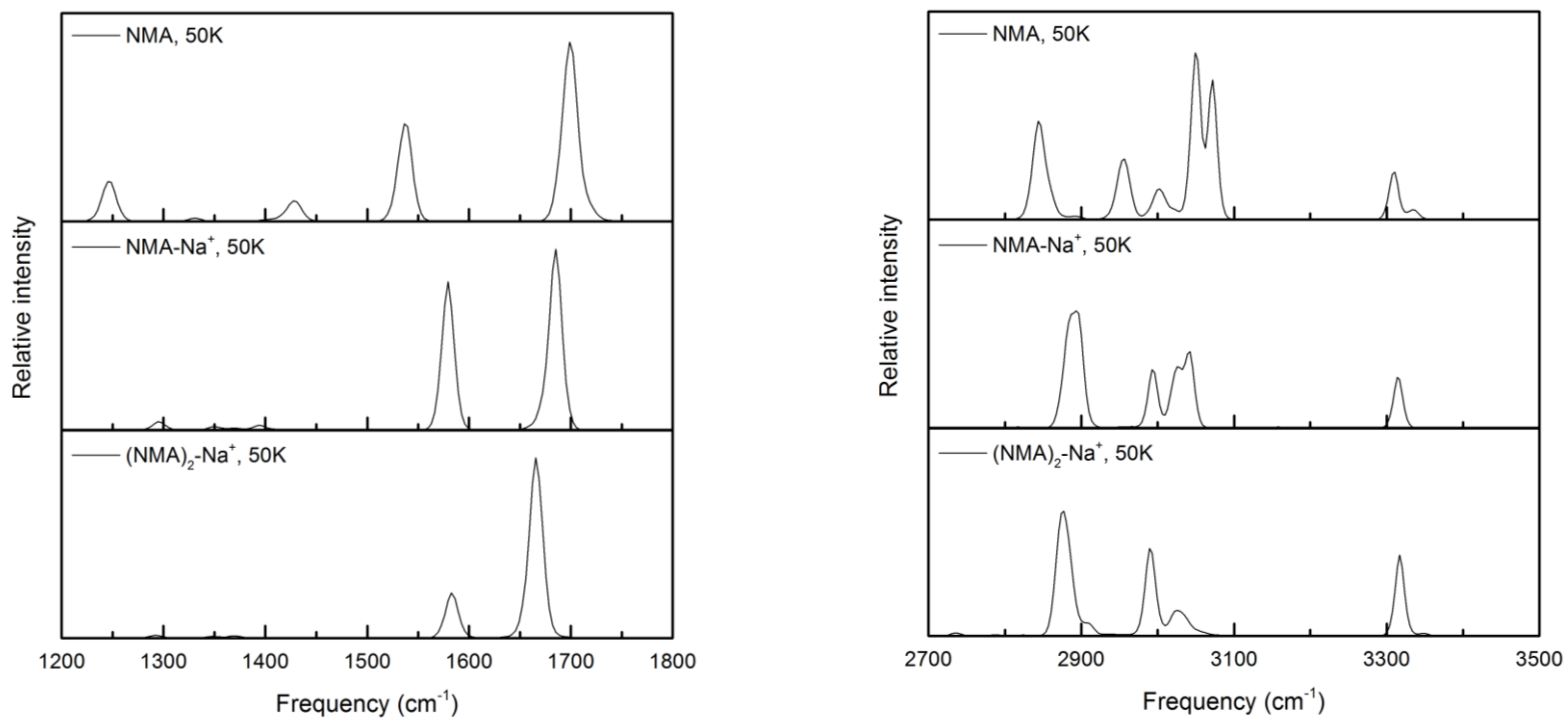


Figure 5.8. Simulated vibrational spectra of *trans*-NMA, *trans*-NMA-Na⁺ complex and *trans*-(NMA)₂-Na⁺ complex in the range 1200-1800 cm⁻¹ (Left) and 2700-3500 cm⁻¹ (Right), respectively. Obtained from MD simulations at 50K with DFTB3 at 50K.

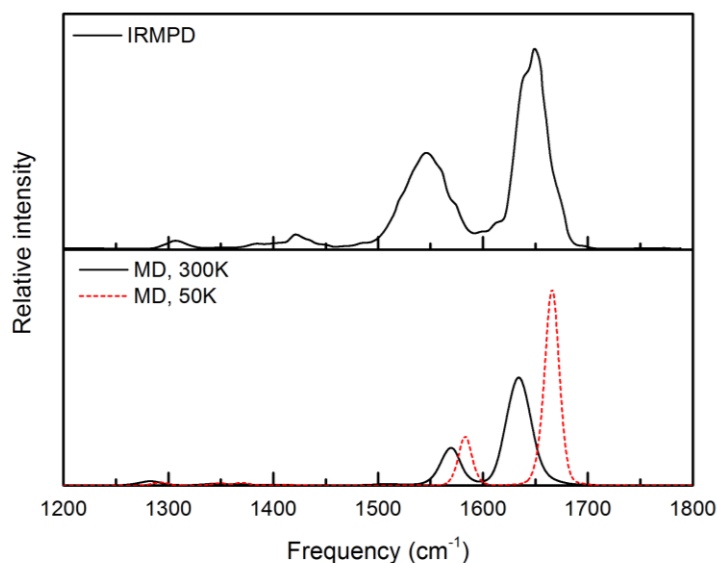


Figure 5.9. Vibrational spectra of $(\text{NMA})_2\text{-Na}^+$ complex in the range 1200-1800 cm^{-1} . **Top:** experimental IRMPD spectra.¹¹⁹ **Bottom:** Simulated spectra from MD simulations with DFTB3 at 50K and 300K. NMA molecules are in the *trans* form.

A significant temperature is found for the complex. With increasing temperature from 50K to 300K, the amide I and II bands red shift by 32 and 13 cm^{-1} , respectively. This finding again confirms the importance of the temperature effects in amide bands as previously reported.

5.4. Summary and conclusions

The present work is the first attempt to examine the performance of the DFTB3 model in computing the effects of hydration, metal ion binding, dimerization on the vibrational spectral signatures of NMA, with the aim to extend DFTB3 applications to computational vibrational spectroscopy of large-size biological systems in aqueous solution. Selected geometric parameters, hydrogen-bonding structural features and interaction energies serve as the basis for the model

validation against high-level quantum chemistry data, and the performance of DFTB3 is found to be far superior to that of other common semiempirical methods. Through comparison with MP2 harmonic vibrational frequencies, DFTB3 is found to reproduce the amide band shift upon typical hydrogen binding interaction. The systematic good performance of DFTB3 brings confidence in the simulated vibrational spectra obtained from MD simulations with the model. The position of the amide I and A bands are underestimated by 100~200 cm^{-1} , an error in frequencies typically encountered in simulated vibrational spectra even with high level quantum chemistry methods.

The simulated vibrational spectra of NMA and its various complexes are in excellent agreement with available experimental results. For example, the splitting of the amide I band is well reproduced for NMA at 400K. For hydrated NMA complexes, binding of water molecule to the C=O and N-H groups leads to different patterns in the N-H stretching and O-H stretching spectral regions, and these differences are suggested to serve as spectral signatures to distinguish between the two types of isomers. NMA dimerization causes a significant redshift of the amide A band by 115 cm^{-1} according to the results of an FTIR experimental study.¹²⁸ In our simulation, the trend is reproduced, but with a smaller redshift of around 60 cm^{-1} . Finally, vibrational spectra of the (NMA)₂-Na⁺ complex at 300K simulated in this work are found to be in much better agreement with experimental IRPD measurement than those obtained with a polarizable force field,¹¹⁹ in particular when it comes to the relative intensities of the amide bands.

In conclusion, the DFTB3 model with its newly published 3OB parameter set developed for organic and biological systems, appears to be promising in modeling the vibrational spectra of peptides and proteins through MD simulations at finite temperature. Finally, the importance of the use of MD simulation and averaging over multiple sufficiently long trajectories in producing robust, converged and smooth spectra for small complexes and clusters in the gas phase, cannot

be stressed enough. Such approaches not only take anharmonic effects into account but also overcome the difficulties in conformational sampling caused by slow internal energy relaxation. They, however, require computationally economical and reliable methods to describe intermolecular interactions such as DFTB3.

Chapter 6.

Conclusions and outlook

The primary objective of this work is to investigate vibrational spectroscopy by computer simulations beyond the harmonic approximation, aiming to aid in the band assignment and explanation of experimental spectra such as IRPD and IRMPD ones. For this purpose, vibrational spectra are computed from the Fourier transform of the autocorrelation function of the dipole moment obtained from MD simulations at finite temperature with ab initio or first-principles based approximate methods. Such methods provide naturally broadened spectral bands by allowing vibrational modes coupling during the simulations. Though the MD simulations are performed in the electronic and vibrational ground states and quantum nuclear effects are neglected, the computational approach is able to provide comparable results to experimental spectra in many cases, confirming that the simulations are performed with an accurate method to describe the potential energy surface and polarization. In this work, we find that the approach is very helpful to aid the understanding of experimental vibrational spectra.

The performance of SCC-DFTB models is of particular interest due to the demand for efficient methods of generating converged spectra for medium to large-size systems. SCC-DFTB models stem from an approximate quantum-chemistry approach based on density functional theory. It has been shown that the latest flavors of DFTB models provide adequate predictions of the molecular structure, energetics and harmonic frequencies of ion water clusters, with a computational cost just a small fraction of that of first-principles methods.

There are 4 prototypical systems investigated in this work, namely the protonated water cluster, sulfate-water clusters, guanidinium water/counter ion clusters, peptide water/ion clusters, covering intermolecular interactions ranging from proton-water, anion-water, cation-water, cation-anion, amide-water and amide-ion interactions.

In chapter 2, the coupling of the proton transfer mode and the temperature effects on vibrational spectra is investigated by studying the protonated water dimer, i.e. the Zundel ion. It is found that computed vibrational spectra from ab initio MD simulations reproduce the main features of the experimental IRMPD and IRPD spectra. The results suggest that temperature effects may play an important role in understanding the discrepancies between various sets of experimental results.

In chapter 3, the sulfate anion-water interaction is investigated using DFTB models. The hypothesis of the spectral signature of “free” water molecules at the surface of the aqueous droplet seeded by the sulfate ion is examined. It is found that computed spectra are in good agreement with experimental spectra in the OH stretch region. Further analysis of the vibrational correlation spectra of the surface water molecules suggest a direct correlation between the surface water molecule vibrations and the small shoulder in the higher-frequency region of the OH stretch bands.

In chapter 4, the guanidinium cation-water interaction is investigated using DFT and DFTB models. It is found that molecular geometries and harmonic frequencies computed with DFTB models are in good agreement with that of hybrid DFT. The vibrational spectra computed from MD simulations with DFTB successfully reproduce the results obtained from more rigorous but computationally more intensive CPMD simulations employing DFT. The results also suggest a redshift of the CN stretch band upon hydration and ion association.

In chapter 5, vibrational spectra of model peptides and their interaction with water molecules and Na⁺ ions are investigated with DFTB models, aiming to extend the approach to studies to larger biologically relevant solutes. The DFTB model is first successfully validated against ab initio calculations of molecular geometries, binding energies and harmonic frequencies. Then computed vibrational spectra from MD simulations show that the DFTB3 model is able to

reproduce all the main features of the amide bands. Though the values of the band positions are slightly underestimated, the band shapes are in excellent agreement with available experimental or theoretical spectra.

In summary, results obtained in this work demonstrate that vibrational spectra computed from MD simulations and the time correlation function of the system dipole moment is a powerful theoretical tool in reproducing and analyzing experimental vibrational spectra. SCC-DFTB models have been shown to be accurate in describing the structure and energetics of ion-water systems. In this work, we further demonstrate that it is a promising approximate method to describe vibrational properties, including band position and relative intensities, within slight and acceptable error bars, at a fraction of the cost of first-principles methods.

It is also noticed that there are some limitations with current work and some more work could be done in the future.

The first issue is the insufficient sampling of the dynamics simulation in the configuration space. In this work, the initial conformations of the large clusters are usually generated randomly and relaxed for hundreds of pico-seconds. However, such clusters feature a rich low-lying conformations. To achieve better consistence with experimental spectra, taking average of the spectra from MD simulations starting from more low-lying conformations would be helpful.

Secondly, the performance of the SCC-DFTB model in simulating vibrational spectra are only validated with a limited number of model systems in this work. It is far not enough to establish a full understanding of its performance. For example, it is found that the simulated vibrational spectra of the small prototype peptides are comparable to the experimental ones, but discrepancies in band positions and relative intensities are noticeable. A more thorough examination with more

model systems or larger systems would be helpful, particularly for cases where experimental vibrational spectra are available.

Finally, nuclear quantum effects are neglected in this work, but they might play a role in modes coupling and absorption intensities for some systems such as protonated water clusters. How these effects affect the simulated spectra is an interesting topic. Further study to include the nuclear quantum effects in the dynamics simulations is suggested.

Bibliography

1. Gaigeot, M.P., *Theoretical spectroscopy of floppy peptides at room temperature. A DFTMD perspective: gas and aqueous phase*. Physical Chemistry Chemical Physics, 2010. **12**(14): p. 3336-3359.
2. Gaigeot, M.P., *DFT-MD simulations for vibrational spectroscopy: A little insight into finite temperature spectroscopy and anharmonicities*. Abstracts of Papers of the American Chemical Society, 2014. **247**.
3. Silvestrelli, P.L., M. Bernasconi, and M. Parrinello, *Ab initio infrared spectrum of liquid water*. Chemical Physics Letters, 1997. **277**(5-6): p. 478-482.
4. Yamada, T. and M. Aida, *Fundamental frequency from classical molecular dynamics*. Physical Chemistry Chemical Physics, 2015. **17**(5): p. 3227-3240.
5. McQuarrie, D.A., *Statistical mechanics*, in *Harper's chemistry series*. 1975, Harper & Row: New York. p. 1 online resource (xiv, 641 pages).
6. Borysow, J., M. Moraldi, and L. Frommhold, *The collision induced spectroscopies: Concerning the desymmetrization of classical line shape*. Molecular Physics, 1985. **56**(4): p. 913-922.
7. Gaigeot, M.P. and M. Sprik, *Ab initio molecular dynamics computation of the infrared spectrum of aqueous uracil*. Journal of Physical Chemistry B, 2003. **107**(38): p. 10344-10358.
8. Gaigeot, M.P., R. Vuilleumier, M. Sprik, and D. Borgis, *Infrared spectroscopy of N-methylacetamide revisited by ab initio molecular dynamics simulations*. Journal of Chemical Theory and Computation, 2005. **1**(5): p. 772-789.
9. Gaigeot, M.P., *Infrared spectroscopy of the alanine dipeptide analog in liquid water with DFT-MD. Direct evidence for P(II)/beta conformations*. Phys Chem Chem Phys, 2010. **12**(35): p. 10198-209.
10. Gaigeot, M.P., *DFT-based molecular dynamics (DFT-MD) simulations: Anharmonic vibrational spectroscopy of polypeptides in the gas phase and immersed in liquid water*. Abstracts of Papers of the American Chemical Society, 2012. **243**.
11. Gaigeot, M.P., M. Martinez, and R. Vuilleumier, *Infrared spectroscopy in the gas and liquid phase from first principle molecular dynamics simulations: application to small peptides*. Molecular Physics, 2007. **105**(19-22): p. 2857-2878.
12. Asmis, K.R., N.L. Pivonka, G. Santambrogio, M. Brummer, C. Kaposta, D.M. Neumark, and L. Woste, *Gas-phase infrared spectrum of the protonated water dimer*. Science, 2003. **299**(5611): p. 1375-7.
13. Marta, R.A., T.B. McMahon, and T.D. Fridgen, *Infrared multiphoton dissociation spectra as a probe of ion molecule reaction mechanism: the formation of the protonated water dimer via sequential bimolecular reactions with 1,1,3,3-tetrafluorodimethyl ether*. Journal of Physical Chemistry A, 2007. **111**(36): p. 8792-8802.

14. Diken, E.G., J.M. Headrick, J.R. Roscioli, J.C. Bopp, M.A. Johnson, and A.B. McCoy, *Fundamental excitations of the shared proton in the H₃O²⁻ and H₅O²⁺ complexes*. Journal of Physical Chemistry A, 2005. **109**(8): p. 1487-1490.
15. Hammer, N.I., E.G. Diken, J.R. Roscioli, M.A. Johnson, E.M. Myshakin, K.D. Jordan, A.B. McCoy, X. Huang, J.M. Bowman, and S. Carter, *The vibrational predissociation spectra of the H₅O²⁺+center dot RG(n)(RG=Ar,Ne) clusters: Correlation of the solvent perturbations in the free OH and shared proton transitions of the Zundel ion*. Journal of Chemical Physics, 2005. **122**(24).
16. Hornicek, J., P. Kapralova, and P. Bour, *Simulations of vibrational spectra from classical trajectories: Calibration with ab initio force fields*. Journal of Chemical Physics, 2007. **127**(8).
17. McQuarrie, D.A., *Statistical mechanics*. Harper's chemistry series. 1975, New York: Harper & Row. xiv, 641 pages.
18. Ramirez, R., T. Lopez-Ciudad, P. Kumar, and D. Marx, *Quantum corrections to classical time-correlation functions: Hydrogen bonding and anharmonic floppy modes*. Journal of Chemical Physics, 2004. **121**(9): p. 3973-3983.
19. Kunz, W., J. Henle, and B.W. Ninham, *'Zur Lehre von der Wirkung der Salze' (about the science of the effect of salts): Franz Hofmeister's historical papers*. Current Opinion in Colloid & Interface Science, 2004. **9**(1-2): p. 19-37.
20. Tobias, D.J. and J.C. Hemminger, *Chemistry. Getting specific about specific ion effects*. Science, 2008. **319**(5867): p. 1197-8.
21. Collins, K.D., G.W. Neilson, and J.E. Enderby, *Ions in water: characterizing the forces that control chemical processes and biological structure*. Biophys Chem, 2007. **128**(2-3): p. 95-104.
22. Marcus, Y., *Effect of ions on the structure of water: structure making and breaking*. Chem Rev, 2009. **109**(3): p. 1346-70.
23. Fridgen, T.D., T.B. McMahon, L. MacAleese, J. Lemaire, and P. Maitre, *infrared spectrum of the protonated water dimer in the gas phase*. Journal of Physical Chemistry A, 2004. **108**(42): p. 9008-9010.
24. Fridgen, T.D., L. MacAleese, T.B. McMahon, J. Lemaire, and P. Maitre, *Gas phase infrared multiple-photon dissociation spectra of methanol, ethanol and propanol proton-bound dimers, protonated propanol and the propanol/water proton-bound dimer*. Physical Chemistry Chemical Physics, 2006. **8**(8): p. 955-966.
25. Kolaski, M., H.M. Lee, Y.C. Choi, K.S. Kim, P. Tarakeshwar, D.J. Miller, and J.M. Lisy, *Structures, energetics, and spectra of aqua-cesium (I) complexes: An ab initio and experimental study*. Journal of Chemical Physics, 2007. **126**(7).
26. Douberly, G.E., A.M. Ricks, B.W. Ticknor, W.C. Mckee, P.V.R. Schleyer, and M.A. Duncan, *Infrared photodissociation spectroscopy of protonated acetylene and its clusters*. Journal of Physical Chemistry A, 2008. **112**(9): p. 1897-1906.
27. Zhou, J., G. Santambrogio, M. Brummer, D.T. Moore, G. Meijer, D.M. Neumark, and K.R. Asmis, *Infrared spectroscopy of hydrated sulfate dianions*. Journal of Chemical Physics, 2006. **125**(11).

28. Bush, M.F., R.J. Saykally, and E.R. Williams, *Evidence for water rings in the hexahydrated sulfate dianion from IR spectroscopy*. J Am Chem Soc, 2007. **129**(8): p. 2220-1.
29. O'Brien, J.T., J.S. Prell, M.F. Bush, and E.R. Williams, *Sulfate Ion Patterns Water at Long Distance*. Journal of the American Chemical Society, 2010. **132**(24): p. 8248-+.
30. Chakraborty, D. and S. Manogaran, *Ground-State Vibrations of Guanidinium and Methylguanidinium Ions - an Ab-Initio Study*. Indian Journal of Chemistry Section a-Inorganic Bio-Inorganic Physical Theoretical & Analytical Chemistry, 1994. **33**(11): p. 969-977.
31. Drozd, M., *Molecular structure and infrared spectra of guanidinium cation - A combined theoretical and spectroscopic study*. Materials Science and Engineering B-Solid State Materials for Advanced Technology, 2007. **136**(1): p. 20-28.
32. Ataka, S., H. Takeuchi, I. Harada, and M. Tasumi, *Infrared Studies of the Cis Form of N-Methylthioacetamide in Low-Temperature Matrices*. Journal of Physical Chemistry, 1984. **88**(3): p. 449-451.
33. Albrecht, M., C.A. Rice, and M.A. Suhm, *Elementary peptide motifs in the gas phase: FTIR aggregation study of formamide, acetamide, N-methylformamide, and N-methylacetamide*. Journal of Physical Chemistry A, 2008. **112**(33): p. 7530-7542.
34. Elstner, M., *DFT and approximate SCC-DFTB methods applied to biological systems: Successes and problems*. Abstracts of Papers of the American Chemical Society, 2006. **231**.
35. Gaus, M., Q.A. Cui, and M. Elstner, *DFTB3: Extension of the Self-Consistent-Charge Density-Functional Tight-Binding Method (SCC-DFTB)*. Journal of Chemical Theory and Computation, 2011. **7**(4): p. 931-948.
36. Elstner, M., K.J. Jalkanen, M. Knapp-Mohammady, T. Frauenheim, and S. Suhai, *Energetics and structure of glycine and alanine based model peptides: Approximate SCC-DFTB, AM1 and PM3 methods in comparison with DFT, HF and MP2 calculations*. Chemical Physics, 2001. **263**(2-3): p. 203-219.
37. Irle, S., G.S. Zheng, H.A. Witek, K. Morokuma, and M. Elstner, *Density functional tight binding (DFTB) method and its application to molecular dynamics simulation of formation of fullerenes and carbon nanotubes*. Abstracts of Papers of the American Chemical Society, 2005. **229**: p. U855-U855.
38. Elstner, M., *The SCC-DFTB method applied to biological systems: Successes, problems and extensions*. Abstracts of Papers of the American Chemical Society, 2006. **232**: p. 125-125.
39. Goyal, P., M. Elstner, and Q. Cui, *Application of the SCC-DFTB Method to Neutral and Protonated Water Clusters and Bulk Water*. Journal of Physical Chemistry B, 2011. **115**(20): p. 6790-6805.
40. Gaus, M., X. Lu, M. Elstner, and Q. Cui, *Parameterization of DFTB3/3OB for Sulfur and Phosphorus for Chemical and Biological Applications*. J Chem Theory Comput, 2014. **10**(4): p. 1518-1537.

41. Jahangiri, S., G. Dolgonos, T. Frauenheim, and G.H. Peslherbe, *Parameterization of Halogens for the Density-Functional Tight-Binding Description of Halide Hydration*. Journal of Chemical Theory and Computation, 2013. **9**(8): p. 3321-3332.
42. Jahangiri, S., L. Cai, and G.H. Peslherbe, *Performance of density-functional tight-binding models in describing hydrogen-bonded anionic-water clusters*. J Comput Chem, 2014. **35**(23): p. 1707-15.
43. Møller, C. and M.S. Plesset, *Note on an Approximation Treatment for Many-Electron Systems*. Physical Review, 1934. **46**(7): p. 618-622.
44. Headgordon, M., J.A. Pople, and M.J. Frisch, *Mp2 Energy Evaluation by Direct Methods*. Chemical Physics Letters, 1988. **153**(6): p. 503-506.
45. Frisch, M.J., M. Headgordon, and J.A. Pople, *A Direct Mp2 Gradient-Method*. Chemical Physics Letters, 1990. **166**(3): p. 275-280.
46. Lee, C.T., W.T. Yang, and R.G. Parr, *Development of the Colle-Salvetti Correlation-Energy Formula into a Functional of the Electron-Density*. Physical Review B, 1988. **37**(2): p. 785-789.
47. Becke, A.D., *A New Mixing of Hartree-Fock and Local Density-Functional Theories*. Journal of Chemical Physics, 1993. **98**(2): p. 1372-1377.
48. Kim, K. and K.D. Jordan, *Comparison of Density-Functional and Mp2 Calculations on the Water Monomer and Dimer*. Journal of Physical Chemistry, 1994. **98**(40): p. 10089-10094.
49. Stephens, P.J., M.B. Cole, and M.V. Jones, *Effect of heating rate on the thermal inactivation of Listeria monocytogenes*. J Appl Bacteriol, 1994. **77**(6): p. 702-8.
50. McCunn, L.R., J.R. Roscioli, M.A. Johnson, and A.B. McCoy, *An H/D isotopic substitution study of the H₂O₂+center dot Ar vibrational predissociation spectra: Exploring the putative role of fermi Resonances in the bridging proton fundamentals*. Journal of Physical Chemistry B, 2008. **112**(2): p. 321-327.
51. Vendrell, O., F. Gatti, and H.D. Meyer, *Full dimensional (15 dimensional) quantum-dynamical simulation of the protonated water-dimer IV: Isotope effects in the infrared spectra of D(D₂O)(₂)(+), H(D₂O)(₂)(+), and D(H₂O)(₂)(+) isotopologues*. Journal of Chemical Physics, 2009. **131**(3).
52. Vendrell, O., M. Brill, F. Gatti, D. Lauvergnat, and H.D. Meyer, *Full dimensional (15-dimensional) quantum-dynamical simulation of the protonated water-dimer III: Mixed Jacobi-valence parametrization and benchmark results for the zero point energy, vibrationally excited states, and infrared spectrum*. Journal of Chemical Physics, 2009. **130**(23).
53. Vendrell, O., F. Gatti, D. Lauvergnat, and H.D. Meyer, *Full-dimensional (15-dimensional) quantum-dynamical simulation of the protonated water dimer. I. Hamiltonian setup and analysis of the ground vibrational state*. Journal of Chemical Physics, 2007. **127**(18).
54. Vendrell, O., F. Gatti, and H.D. Meyer, *Full dimensional (15-dimensional) quantum-dynamical simulation of the protonated water dimer. II. Infrared spectrum and vibrational dynamics*. Journal of Chemical Physics, 2007. **127**(18).

55. Vendrell, O., F. Gatti, and H.D. Meyer, *Dynamics and infrared spectroscopy of the protonated water dimer*. *Angewandte Chemie-International Edition*, 2007. **46**(36): p. 6918-6921.
56. Dai, J., Z. Bacic, X.C. Huang, S. Carter, and J.M. Bowman, *A theoretical study of vibrational mode coupling in H5O2+*. *Journal of Chemical Physics*, 2003. **119**(13): p. 6571-6580.
57. Lammers, S. and M. Meuwly, *Investigating the relationship between infrared spectra of shared protons in different chemical environments: A comparison of protonated diglyme and protonated water dimer*. *Journal of Physical Chemistry A*, 2007. **111**(9): p. 1638-1647.
58. Sauer, J. and J. Dobler, *Gas-phase infrared spectrum of the protonated water dimer: Molecular dynamics simulation and accuracy of the potential energy surface*. *Chemphyschem*, 2005. **6**(9): p. 1706-1710.
59. Agostini, F., R. Vuilleumier, and G. Ciccotti, *Infrared spectroscopy and effective modes analysis of the protonated water dimer H+(H2O)(2) at room temperature under H/D substitution*. *Journal of Chemical Physics*, 2011. **134**(8).
60. Vener, M.V., O. Kuhn, and J. Sauer, *The infrared spectrum of the O center dot center dot center dot H center dot center dot center dot O fragment of H5O2+: Ab initio classical molecular dynamics and quantum 4D model calculations*. *Journal of Chemical Physics*, 2001. **114**(1): p. 240-249.
61. Perdew, J.P., K. Burke, and M. Ernzerhof, *Generalized gradient approximation made simple*. *Physical Review Letters*, 1996. **77**(18): p. 3865-3868.
62. Perdew, J.P., K. Burke, and M. Ernzerhof, *Generalized gradient approximation made simple (vol 77, pg 3865, 1996)*. *Physical Review Letters*, 1997. **78**(7): p. 1396-1396.
63. Perdew, J.P., K. Burke, and M. Ernzerhof, *Comment on "Generalized gradient approximation made simple" - Reply*. *Physical Review Letters*, 1998. **80**(4): p. 891-891.
64. Zhang, Y.K. and W.T. Yang, *Comment on "Generalized gradient approximation made simple"*. *Physical Review Letters*, 1998. **80**(4): p. 890-890.
65. Dunning, T.H., *Gaussian-Basis Sets for Use in Correlated Molecular Calculations .1. The Atoms Boron through Neon and Hydrogen*. *Journal of Chemical Physics*, 1989. **90**(2): p. 1007-1023.
66. Swope, W.C., H.C. Andersen, P.H. Berens, and K.R. Wilson, *A Computer-Simulation Method for the Calculation of Equilibrium-Constants for the Formation of Physical Clusters of Molecules - Application to Small Water Clusters*. *Journal of Chemical Physics*, 1982. **76**(1): p. 637-649.
67. Hangelbroek, T. and A. Ron, *Nonlinear approximation using Gaussian kernels*. *Journal of Functional Analysis*, 2010. **259**(1): p. 203-219.
68. Ninham, B.W. and P. Lo Nostro, *Molecular forces and self assembly : in colloid, nano sciences and biology*. Cambridge molecular science series. 2010, Cambridge: Cambridge University Press. xvi, 365 p.
69. Bakker, H.J., M.F. Kropman, and A.W. Omta, *Effect of ions on the structure and dynamics of liquid water*. *Journal of Physics-Condensed Matter*, 2005. **17**(45): p. S3215-S3224.

70. Omta, A.W., M.F. Kropman, S. Woutersen, and H.J. Bakker, *Influence of ions on the hydrogen-bond structure in liquid water*. Journal of Chemical Physics, 2003. **119**(23): p. 12457-12461.
71. O'Brien, J.T. and E.R. Williams, *Effects of ions on hydrogen-bonding water networks in large aqueous nanodrops*. J Am Chem Soc, 2012. **134**(24): p. 10228-36.
72. Eklund, L., T.S. Hofer, A.B. Pribil, B.M. Rode, and I. Persson, *On the structure and dynamics of the hydrated sulfite ion in aqueous solution--an ab initio QMCF MD simulation and large angle X-ray scattering study*. Dalton Trans, 2012. **41**(17): p. 5209-16.
73. Asmis, K.R. and D.M. Neumark, *Vibrational spectroscopy of microhydrated conjugate base anions*. Acc Chem Res, 2012. **45**(1): p. 43-52.
74. Prell, J.S., J.T. O'Brien, and E.R. Williams, *Structural and electric field effects of ions in aqueous nanodrops*. J Am Chem Soc, 2011. **133**(13): p. 4810-8.
75. Miller, Y., G.M. Chaban, J. Zhou, K.R. Asmis, D.M. Neumark, and R.B. Gerber, *Vibrational spectroscopy of (SO₄(2-))center dot(H₂O)(n) clusters, n=1-5: Harmonic and anharmonic calculations and experiment*. Journal of Chemical Physics, 2007. **127**(9).
76. Gaigeot, M.-P. and R. Spezia, *Theoretical Methods for Vibrational Spectroscopy and Collision Induced Dissociation in the Gas Phase*, in *Gas-Phase IR Spectroscopy and Structure of Biological Molecules*, A.M. Rijs and J. Oomens, Editors. 2015, Springer International Publishing. p. 99-151.
77. Brites, V., J.M. Lisy, and M.P. Gaigeot, *Infrared predissociation vibrational spectroscopy of Li(+)(H₂O)(3-4)Ar(0,1) reanalyzed using density functional theory molecular dynamics*. J Phys Chem A, 2015. **119**(11): p. 2468-74.
78. Gaigeot, M.P., N.A. Besley, and J.D. Hirst, *Modeling the infrared and circular dichroism spectroscopy of a bridged cyclic diamide*. J Phys Chem B, 2011. **115**(18): p. 5526-35.
79. Gregoire, G., M.P. Gaigeot, D.C. Marinica, J. Lemaire, J.P. Schermann, and C. Desfrancois, *Resonant infrared multiphoton dissociation spectroscopy of gas-phase protonated peptides. Experiments and Car-Parrinello dynamics at 300 K*. Phys Chem Chem Phys, 2007. **9**(24): p. 3082-97.
80. Elstner, M., *The SCC-DFTB method and its application to biological systems*. Theoretical Chemistry Accounts, 2006. **116**(1-3): p. 316-325.
81. Elstner, M., D. Porezag, G. Jungnickel, J. Elsner, M. Haugk, T. Frauenheim, S. Suhai, and G. Seifert, *Self-consistent-charge density-functional tight-binding method for simulations of complex materials properties*. Physical Review B, 1998. **58**(11): p. 7260-7268.
82. Kubar, T., Z. Bodrog, M. Gaus, C. Kohler, B. Aradi, T. Frauenheim, and M. Elstner, *Parametrization of the SCC-DFTB Method for Halogens*. Journal of Chemical Theory and Computation, 2013. **9**(7): p. 2939-2949.
83. Gaus, M., A. Goetz, and M. Elstner, *Parametrization and Benchmark of DFTB3 for Organic Molecules*. Journal of Chemical Theory and Computation, 2013. **9**(1): p. 338-354.

84. Andersen, H.C., *Molecular-Dynamics Simulations at Constant Pressure and-or Temperature*. Journal of Chemical Physics, 1980. **72**(4): p. 2384-2393.
85. Aradi, B., B. Hourahine, and T. Frauenheim, *DFTB+, a sparse matrix-based implementation of the DFTB method*. Journal of Physical Chemistry A, 2007. **111**(26): p. 5678-5684.
86. Ledbetter, J.E. and D.A. Mcquarrie, *Statistical-Mechanics of Bolaform Electrolytes*. Journal of Physical Chemistry, 1986. **90**(1): p. 132-136.
87. Burnham, C.J., M.K. Petersen, T.J. Day, S.S. Iyengar, and G.A. Voth, *The properties of ion-water clusters. II. Solvation structures of Na⁺, Cl⁻, and H⁺ clusters as a function of temperature*. J Chem Phys, 2006. **124**(2): p. 024327.
88. Wender, P.A., W.C. Galliher, E.A. Goun, L.R. Jones, and T.H. Pillow, *The design of guanidinium-rich transporters and their internalization mechanisms*. Advanced Drug Delivery Reviews, 2008. **60**(4-5): p. 452-472.
89. Suvitha, A., V. Sathyanarayananmoorthi, and P. Murugakoothan, *Growth, spectroscopy properties and DFT based PCM calculations of guanidinium chlorochromate*. Spectrochimica Acta Part a-Molecular and Biomolecular Spectroscopy, 2013. **110**: p. 255-261.
90. Liu, J.M., F. Wang, Z. Li, J.W. Zhou, J. Chen, and C.G. Xia, *Novel guanidinium zwitterion and derived ionic liquids: physicochemical properties and DFT theoretical studies*. Structural Chemistry, 2011. **22**(5): p. 1119-1130.
91. Todorova, T., O. Krocher, and B. Delley, *DFT study of structural and vibrational properties of guanidinium derivatives*. Journal of Molecular Structure-Theochem, 2009. **907**(1-3): p. 16-21.
92. Drozd, M., *The theoretical calculations of vibrational spectra of guanidine selenate and guanidinium sulphate. Determination of direction of transition dipole moments by two methods: oriented gas model and changes in displacement eigenvectors computed by DFT method*. Journal of Molecular Structure-Theochem, 2005. **756**(1-3): p. 173-184.
93. Vazdar, M., P. Jungwirth, and P.E. Mason, *Aqueous guanidinium-carbonate interactions by molecular dynamics and neutron scattering: relevance to ion-protein interactions*. J Phys Chem B, 2013. **117**(6): p. 1844-8.
94. Mason, P.E., G.W. Neilson, J.E. Enderby, M.L. Saboungi, C.E. Dempsey, A.D. MacKerell, Jr., and J.W. Brady, *The structure of aqueous guanidinium chloride solutions*. J Am Chem Soc, 2004. **126**(37): p. 11462-70.
95. Dempsey, C.E., P.E. Mason, and P. Jungwirth, *Complex ion effects on polypeptide conformational stability: chloride and sulfate salts of guanidinium and tetrapropylammonium*. J Am Chem Soc, 2011. **133**(19): p. 7300-3.
96. Mason, P.E., J.W. Brady, G.W. Neilson, and C.E. Dempsey, *The interaction of guanidinium ions with a model peptide*. Biophys J, 2007. **93**(1): p. L04-6.
97. Jansen, T.L., *Linear absorption and two-dimensional infrared spectra of N-methylacetamide in chloroform revisited: polarizability and multipole effects*. J Phys Chem B, 2014. **118**(28): p. 8162-9.

98. Elstner, M., T. Niehaus, and T. Frauenheim, *DFTB: Recent methodological extensions and challenges*. Abstracts of Papers of the American Chemical Society, 2012. **243**.
99. Helgaker, T., E. Uggerud, and H.J.A. Jensen, *Integration of the Classical Equations of Motion on Abinitio Molecular-Potential Energy Surfaces Using Gradients and Hessians - Application to Translational Energy-Release Upon Fragmentation*. Chemical Physics Letters, 1990. **173**(2-3): p. 145-150.
100. Ditchfield, R., W.J. Hehre, and J.A. Pople, *Self - Consistent Molecular - Orbital Methods. IX. An Extended Gaussian - Type Basis for Molecular - Orbital Studies of Organic Molecules*. The Journal of Chemical Physics, 1971. **54**(2): p. 724-728.
101. Tomasi, J., B. Mennucci, and R. Cammi, *Quantum mechanical continuum solvation models*. Chemical Reviews, 2005. **105**(8): p. 2999-3093.
102. Becke, A.D., *Density-functional exchange-energy approximation with correct asymptotic behavior*. Phys Rev A, 1988. **38**(6): p. 3098-3100.
103. Frisch, M.J., G.W. Trucks, H.B. Schlegel, G.E. Scuseria, M.A. Robb, J.R. Cheeseman, G. Scalmani, V. Barone, B. Mennucci, G.A. Petersson, H. Nakatsuji, M. Caricato, X. Li, H.P. Hratchian, A.F. Izmaylov, J. Bloino, G. Zheng, J.L. Sonnenberg, M. Hada, M. Ehara, K. Toyota, R. Fukuda, J. Hasegawa, M. Ishida, T. Nakajima, Y. Honda, O. Kitao, H. Nakai, T. Vreven, J.A. Montgomery Jr., J.E. Peralta, F. Ogliaro, M.J. Bearpark, J. Heyd, E.N. Brothers, K.N. Kudin, V.N. Staroverov, R. Kobayashi, J. Normand, K. Raghavachari, A.P. Rendell, J.C. Burant, S.S. Iyengar, J. Tomasi, M. Cossi, N. Rega, N.J. Millam, M. Klene, J.E. Knox, J.B. Cross, V. Bakken, C. Adamo, J. Jaramillo, R. Gomperts, R.E. Stratmann, O. Yazyev, A.J. Austin, R. Cammi, C. Pomelli, J.W. Ochterski, R.L. Martin, K. Morokuma, V.G. Zakrzewski, G.A. Voth, P. Salvador, J.J. Dannenberg, S. Dapprich, A.D. Daniels, Ö. Farkas, J.B. Foresman, J.V. Ortiz, J. Cioslowski, and D.J. Fox, *Gaussian 09*. 2009, Gaussian, Inc.: Wallingford, CT, USA.
104. Mulliken, R.S., *Citation Classic - Electronic Population Analysis on Lcao-Mo Molecular Wave-Functions*. Current Contents/Physical Chemical & Earth Sciences, 1985(33): p. 18-18.
105. Box, G.E.P. and M.E. Muller, *A Note on the Generation of Random Normal Deviates*. 1958: p. 610-611.
106. Resta, R., *The quantum-mechanical position operator and the polarization problem*. First-Principles Calculations for Ferroelectrics, 1998(436): p. 174-183.
107. Resta, R., *Topics in polarization theory*. Proceedings of the Vii Italian-Swiss Workshop Advances in Computational Materials Science Ii, 1998. **61**: p. 3-12.
108. Martyna, G.J. and M.E. Tuckerman, *A reciprocal space based method for treating long range interactions in ab initio and force-field-based calculations in clusters*. Journal of Chemical Physics, 1999. **110**(6): p. 2810-2821.
109. CPMD, <http://www.cpmd.org/>. Copyright IBM Corp 1990-2015, Copyright MPI für Festkörperforschung Stuttgart 1997-2001.
110. Borysov, J., M. Moraldi, and L. Frommhold, *The Collision-Induced Spectroscopies Concerning the Desymmetrization of Classical Line-Shape*. Molecular Physics, 1985. **56**(4): p. 913-922.

111. Hollas, J.M., *Modern spectroscopy*. 4th ed. 2004, Chichester ; Hoboken, NJ: J. Wiley. xxvii, 452 p.
112. Jensen, P. and P. Bunker R., *Computational molecular spectroscopy*. Reprint ed. 2003, New York: John Wiley & Sons. xiv, 670 s.
113. Barth, A. and C. Zscherp, *What vibrations tell us about proteins*. Quarterly Reviews of Biophysics, 2002. **35**(4): p. 369-430.
114. Wang, L., *Theoretical vibrational spectroscopy of proteins*. 2012, Madison, Wis.: University of Wisconsin--Madison. xii, 115 leaves.
115. Bush, M.F., R.J. Saykally, and E.R. Williams, *Infrared Action Spectra of $\text{Ca}^{2+}(\text{H}_2\text{O})_{(11-69)}$ Exhibit Spectral Signatures for Condensed-Phase Structures with Increasing Cluster Size*. Journal of the American Chemical Society, 2008. **130**(46): p. 15482-15489.
116. Vaden, T.D., T.S.J.A. de Boer, J.P. Simons, and L.C. Snoek, *Intramolecular interactions in protonated peptides: H^+ PheGlyGly and H^+ GlyGlyPhe*. Physical Chemistry Chemical Physics, 2008. **10**(10): p. 1443-1447.
117. Carnegie, P.D., B. Bandyopadhyay, and M.A. Duncan, *Infrared spectroscopy of $\text{Cr}^+(\text{H}_2\text{O})$ and $\text{Cr}^{2+}(\text{H}_2\text{O})$: The role of charge in cation hydration*. Journal of Physical Chemistry A, 2008. **112**(28): p. 6237-6243.
118. Douberly, G.E., A.M. Ricks, P.V.R. Schleyer, and M.A. Duncan, *Infrared spectroscopy of gas phase benzenium ions: Protonated benzene and protonated toluene, from 750 to 3400 cm^{-1}* . Journal of Physical Chemistry A, 2008. **112**(22): p. 4869-4874.
119. Semrouni, D., A. Sharma, J.P. Dognon, G. Ohanessian, and C. Clavaguera, *Finite Temperature Infrared Spectra from Polarizable Molecular Dynamics Simulations*. Journal of Chemical Theory and Computation, 2014. **10**(8): p. 3190-3199.
120. Sun, J., H. Forbert, D. Bosquet, and D. Marx, *Ab Initio Molecular Dynamics Simulations of Aqueous Glycine Solutions: Solvation Structure and Vibrational Spectra*. High Performance Computing in Science and Engineering, Garching/Munich 2009, 2010: p. 699-708.
121. Wan, Q., L. Spanu, G.A. Galli, and F. Gygi, *Raman Spectra of Liquid Water from Ab Initio Molecular Dynamics: Vibrational Signatures of Charge Fluctuations in the Hydrogen Bond Network*. Journal of Chemical Theory and Computation, 2013. **9**(9): p. 4124-4130.
122. Gaigeot, M.P. and M. Sprik, *Ab initio molecular dynamics study of uracil in aqueous solution*. Journal of Physical Chemistry B, 2004. **108**(22): p. 7458-7467.
123. Baer, M., D. Marx, and G. Mathias, *Assigning Predissociation Infrared Spectra of Microsolvated Hydronium Cations $\text{H}_3\text{O}^+(\text{H}_2\text{O})_n$ ($n=0, 1, 2, 3$) by Ab Initio Molecular Dynamics*. Chemphyschem, 2011. **12**(10): p. 1906-1915.
124. Cimas, A., T.D. Vaden, T.S.J.A. de Boer, L.C. Snoek, and M.P. Gaigeot, *Vibrational Spectra of Small Protonated Peptides from Finite Temperature MD Simulations and IRMPD Spectroscopy*. Journal of Chemical Theory and Computation, 2009. **5**(4): p. 1068-1078.

125. Martinez, M., M.P. Gaigeot, D. Borgis, and R. Vuilleumier, *Extracting effective normal modes from equilibrium dynamics at finite temperature*. Journal of Chemical Physics, 2006. **125**(14).
126. Hornicek, J., P. Kapralova, and P. Bour, *Simulations of vibrational spectra from classical trajectories: calibration with ab initio force fields*. J Chem Phys, 2007. **127**(8): p. 084502.
127. Nose, S., *A Unified Formulation of the Constant Temperature Molecular-Dynamics Methods*. Journal of Chemical Physics, 1984. **81**(1): p. 511-519.
128. NIST Mass Spec Data Center, S.E.S., director, *"Infrared Spectra" in NIST Chemistry WebBook, NIST Standard Reference Database Number 69*. Eds. P.J. Linstrom and W.G. Mallard, National Institute of Standards and Technology: Gaithersburg MD, 20899.
129. Ataka, S., H. Takeuchi, and M. Tasumi, *Infrared Studies of the Less Stable Cis Form of N-Methylformamide and N-Methylacetamide in Low-Temperature Nitrogen Matrices and Vibrational Analyses of the Trans and Cis Forms of These Molecules*. Journal of Molecular Structure, 1984. **113**(Mar): p. 147-160.
130. Albrecht, M., C.A. Rice, and M.A. Suhm, *Elementary peptide motifs in the gas phase: FTIR aggregation study of formamide, acetamide, N-methylformamide, and N-methylacetamide*. J Phys Chem A, 2008. **112**(33): p. 7530-42.